Die approbierte Originalversion dieser Dissertation ist an der Hauptbibliothek der Technischen Universität Wien aufgestellt (http://www.ub.tuwien.ac.at).

The approved original version of this thesis is available at the main library of the Vienna University of Technology (http://www.ub.tuwien.ac.at/englweb/).

DISSERTATION

Characterization of proteins, viruses, nano silica particles, non-covalent complexes and dendrimers by means of Gas Phase Electrophoretic Macromolecule Mobility Analysis (GEMMA) and Parallel Differential Mobility Analysis (PDMA)

ausgeführt zum Zwecke der Erlangung des akademischen Grades eines Doktors der technischen Wissenschaften unter der Leitung von

Prof. Dr. Günter Allmaier
E164, Institut für chemische Technologien und Analytik
der Technischen Univerität Wien
und
Prof. Wladyslaw Szymanski
Fakultät für Physik der Universität Wien

eingereicht an der Technischen Universität Wien
Fakultät für technische Chemie

von

Dipl-Ing. Christian Laschober
e9727028
Untere Hochstrasse 58, 7400 Oberwart

Wien, am 19.2.2007

Name des Kandidaten: Dipl. Ing. Christian Laschober
Name der Prüfer: Univ. Prof. Dr. Günter Allmaier, AO. Prof. Dr. Wlayslaw W. Szymanski
Titel der Dissertation: Characterization of proteins, viruses, nano silica particles, non-covalent complexes and dendrimers by means of Gas Phase Electrophoretic Macromolecule Mobility Analysis (GEMMA) and Parallel Differential Mobility Analysis (PDMA)

Zusammenfassung
Elektrostatische differentielle Mobilitätsanalyse (DMA) ist eine sich in den letzten Jahren stark weiterentwickelnde Methode für die Analyse von geladenen Partikeln/Molekülen im luftgetragenen Zustand. In Kombination mit einer nano-Elektrospray-Aerosol Quelle ist diese Methode geeignet, suspendierte anorganische Partikel und Biopolymere wie Proteine oder DNA ab etwa einer Größe von einem Nanometer zu analysieren. Die Voraussetzung für DMA ist ein definierter Ladungszustand der Partikel. Die Effizienz der konventionellen Methode, welche diesen Zustand mittels Diffusion von mit radioaktive Quellen (z.b. Po^{210}) erzeugten bipolarer Ionen erreicht, ist in diesem Größenbereich sehr gering (<1%).
Es wurde daher ein neuartiges, auf Korona-Entladung basierendes Gerät zum elektrostatischen Aufladen von Nanopartikel implementiert und charakterisiert. Dabei konnte gezeigt werden, dass diese Methode eine bis zu vierfach höhere Effizienz im Erzeugen von einfach geladenen Nanopartikeln besitzt.
Die Anzahl der verfügbaren DMA Instrumente, die im Nanometerbereich einsetzbar sind, steigt stetig. Es wurde daher die Vergleichbarkeit und Reproduzierbarkeit von elektrophoretischen Mobilitätsspektren mehrerer nano-DMA Systeme mittels globulärer Proteine mit Größen unterhalb von 15 nm (Molekulargewicht ca. 1 MegaDa) untersucht. Dabei konnte einerseits eine hohe Präzision (~0,1% Schwankung während einer Messserie auf einem Gerät) auf individuellen Instrumenten, aber auch eine Streuung (bis zu 15% Unterschied zwischen verschiedenen Geräten) beobachtet werden, was die Notwendigkeit einer Kalibration der Messysteme aufzeigt.
Als mögliche Kalibranden wurden Dendrimere (globuläre, durch ihre Herstellungsmethode gut definierte Polymere mit proteinartigen Eigenschaften) von 3 bis 15 nm Größe im DMA untersucht. Die bestimmten Partikelgrößen waren dabei nahezu ident, mit in der Literatur beschriebenen Werten welche mit Elektronenmikroskopie, Atomic Force Mikroskopie, Röntgen- und Neutronenstreuung erhalten wurden.
Es konnte gezeigt werden, dass der verwendete Versuchsaufbau sowohl zerstörungsfreie Messungen von Komplexen mit nicht-kovalenter Bindungen als auch eine Analyse im hohen Massenbereich ermöglicht. Somit konnte eine mit anderen Methoden schwer zugängliche nichtkovalente Bindung von Antikörpern an ein Virususpartikel nachgeweisen werden. Dazu wurde ein humanes Rhinovirus (HRV) in verschiedenen Konzentrationen mit spezifischen Antikörpern inkubiert. Die dabei gemessene Größenänderung des Viruspartikels war Ausgangspunkt der Berechnung der maximalen Anzahl gebundener Antikörpermoleküle, welche 28 ± 4 biospezifisch gebundene Antikörper betragen hat. Dieser Wert ist praktisch identisch mit dem theoretischen Wert, der sich aus der Symmetrie des Virus und der Bindungsstellen des Antikörpers ergibt.
Die Zerstörungsfreiheit der DMA Methode, welche auch noch unter Normaldruck funktioniert, ermöglicht auch ihren mikropräparativen Einsatz um etwa Virusapartikel oder anorganische Nanopartikel aufzutrennen und größenselektiv anzureichern. Ein sogenannter Parallel-DMA (PDMA) kombiniert mit einer elektrostatischen Sammeleinheit wurde für diesen Zweck im Rahmen dieser Dissertation konstruiert und gebaut. Es wurden Nanosilikapartikel bestimmter Größe mit Hilfe dieses Versuchausbaus auf mikroskopischen Gittern gesammelt. Eine elektronenmikroskopische Untersuchung, der so gesammelten Partikelfraktionen, hat die Einsetzbarkeit der PDMA Methode für mikropräparative Zwecke bestätigt.

Abstract

Electrophoretic differential mobility analysis (DMA) is a method for the characterisation of charged, airborne particles/molecules. DMA is suited for the analysis of suspended inorganic particles as well as biopolymers such as DNA and proteins in combination with a electrospray aerosol generation beginning at approximately 1 nanometer in diameter. For DMA, a defined charge state of the nanoparticles is required. The efficiency of the conventional method, which accomplishes this charge state by diffusion of bipolar ions produced by radioactive sources (e.g. Po^{210}) , is very low (>1%). A new, corona discharge based device for their replacement was implemented and characterized and showed a four times higher efficiency in the production of charged nanoparticles compared to conventional charging devices.
The number of available DMA systems designed for the nm size range increases continuously This fact rises question about reproducibility and comparability of electrophoretic size spectra obtained with different nano-DMA systems. For this reason globular proteins in the size range below 15 nm (molecular weight of appr. 1 MegaDa) were applied on various DMA instruments. Results show on one hand a high precision (~0.1% variation within an experimental series) of individual instruments, but also high variation (up to 15%) of the results acquired with different DMA systems, indicating the necessity of harmonized calibration of DMA instruments.
As possible calibrants, dendrimers (synthetic, well defined polymers with protein like properties) in a size range between 3 and 15 nm were investigated. Excellent agreement between DMA obtained particle sizes and values found in literature obtained with Transmission Electron Microscopy (TEM), Atomic Force Microscopy X-Ray scattering and Neutron scattering was observed, suggesting their suitability as size standards.
It could be demonstrated that the used experimental setup offers preservation of non-covalent bonds and analysis of high molecular weights. These characteristics of DMA enabled the observation of the non-covalent attachment of specific binding antibodies to a virus surface, which is difficult to achieve with other analytical methods. For this purpose, a human rhinovirus (HRV) was incubated with varying concentrations of a specific antibody. The observed size shift of the virus particle caused by attaching antibody molecules enabled the calculation of their number, with 28 ± 4 biospecific bound antibodies per virus particle, which is practically identical to the theoretical value which is determined by virus symmetry and position of antibody binding sites.
As DMA operates under atmospheric pressure and particles remain intact after analysis, this method offers opportunity for its micro-preparative application, enabling isolation and size selective sampling of for example Virus particles or inorganic nanoparticles. Based on this reasoning, a Parallel-DMA (PDMA) and an electrostatic sampler were specially designed and constructed within this PhD thesis. For feasibility tests, nanometer sized silica particles were applied this experimental setup and collected on a microscopic grid. Transmission electron microscopic analysis of the sampled nano-silica particle fractions confirmed the selectivity and the feasibility of the PDMA setup for micro-preparative purposes.

An dieser Stelle möchte ich im Besonderen meinen beiden Betreuern der Dissertation, Prof. Günter Allmaier und Prof. Wladyslaw Szymanski danken, die es mir ermöglicht haben, diese Dissertation, im Zuge derer ich mich mit einer völlig neuen Methode und vielen interessanten Fragestellungen beschäftigt habe, durchzuführen.

Des weiteren ist auch herzlich meinen Kollegen – Roland, Jasmin, Martin, Wolfgang, Martina, Ernst und Birgit von der analytischen Chemie der TU Wien und Artur und Anne von der Aerosolphysik der Univerität Wien - die immer Rat bei auftauchenden Problemen gehabt und für ein gutes Arbeitsklima gesorgt haben zu danken.

Auch meine Familie und die engsten Freunde sollen nicht unerwähnt bleiben, ohne deren seelische Stütze und der mit ihnen verbrachten Zeit an einen Abschluss einer so aufwendigen Unternehmung, wie sie die Dissertation darstellt, nicht zu denken gewesen wäre.

Zuletzt danke ich dem Fonds zur Förderung der wissenschaftlichen Forschung für dessen finanzielle Unterstützung im Rahmen des Projektes P16185-N02.

Danke !

The most exciting phrase to hear in science, the one that heralds new discoveries, is not 'Eureka!' (I found it!) but 'That's funny ...'

Isaac Asimov (1920-1996)

Table of Contents

1. General Introduction to Nanoscience and Nanotechnology ---- 1
2. Introduction to nano-electrospray ionization and nano-differenital mobility analysis ---- 6
   - 2.1 Electrospray ---- 6
   - 2.2 Differential Mobility Analysis ---- 14

Aim of this Thesis ---- 29

3. Comparison between an Unipolar Corona Charger and a Polonium-based Bipolar Neutralizer for the Analysis of Nanosized Particles and Biopolymers ---- 31

4. Comparison of various nano-differential mobility analyzers (nDMAs) applying globular proteins ---- 49

5. Determination of molecular weight, particle size and density of high number generation PAMAM dendrimers using MALDI-TOF-MS and nES-GEMMA ---- 63

6. Gas Phase Electrophoretic Molecular Mobility Analysis of Size and Stoichiometry of Complexes of a Common Cold Virus with Antibodies ---- 85

7. Characterization and selective sampling of nano-sized airborne particles with the parallel differential mobility analyzer (PDMA) and comparison with transmission electron microscopy (TEM) ---- 100

Conclusions ---- 110

Curriculum Vitae ---- Appendix

1. General Introduction to Nanoscience and Nanotechnology

Nanotechnology and nanoscience are today viewed as the next big step in technical revolution, with a similar impact on industry and economy as information technology and biotechnology[1]. Nanoscience and Nanotechnology is defined as the field of applied science and technology focused on controlling and exploiting the structure of matter on a scale below 100 nanometers[2]. In difference to bio- and information technology it will not lead to a separate industrial branch, but to next product generations of existing technologies in a large number of industrial branches. The begin of the growing attention towards nanosized structures and devices can be traced back to visionary lectures of Nobel Prize laureate Richard Feynman, “There´s plenty of room at the bottom”[3] 1959 and “Infinitesimal machinery” [4] 1983, in which about unique characteristics of nanosizesd structures and devices was as well as their technical realization and application was speculated. The shift to new technologies and structuring processes becomes even more important, as todays top-down fabrication processes used in the microelectronic industry, which was the driving force of economical development in the last decades reach their physical limit and a shift to completely new technologies and production processes is needed for further development[5].

Nanoscience has a unique position in the scientific field linking virtually all natural sciences and occupying researchers in the fields of Physics, Chemistry, Biology, Electrical Engineering, Mechanical Engineering, Information Technology and Medicine.
The main reason for this view of the benefits and the future impact of nanotechnology is, that structures not only get “smaller” and thus will gain in specific surface, which is beneficial for applications like catalysis[6,7], adsorptive storage of hydrogen or photovoltaic[8], but that in nanometer dimensions materials get completely new properties which cannot be observed in bulk material. This is caused on the fact that the smaller dimension leads to structures and particles which may consist of only one magnetic or topological domain, which as a result leads to phenomena like extreme tensile strengths of nanotubes and nanowires[9,10], the spontaneous emergence of superparamagnetism of iron particles below a certain particle diameter[11], extremely high electrical conductivities[10,12].

Furthermore quantum mechanical effects have large influence at these dimensions, which will especially have impact on the properties of nanosized microelectronical devices, and will theoretically allow the design of reversible (meaning practically current and heat loss-free) electronical switches[4].

The development of Nanotechnology is viewed to happen in several stages which are characterized by a stepwise increase of growing complexity and technical ability of manipulation[13]. This development is now in the beginning with the manufacturing of polydisperse nanoparticles produced from bulk material, which are already commercialized[14] and in use for nanostructured coatings (e.g. Lotus flower effect, surface hardening, toothpaste additives to build up a protective coating) as well as for biological and medical applications[15-18]. The next level of nanotechnological products will most likely consist of nanoparticles and structures, specially designed to fulfil a specific purpose, such as target drug delivery, or the next generation of transistors. The following generation is viewed by experts to be the implementation of 3D structures with hierarchical architecture, using self assembly and biological procedures for structuring. The last step of nanotechnological evolution will be the ability of controlled production of molecular machines and macromolecules “on demand” for specific medical or technological purposes and the achievement of quantum control, which will happen under optimistic estimations within the next 40-50 years.

In the recent decade, first interesting scientific experiments were conducted to reveal possible ways of producing nanoparticles, nanotubes and designed nanoscale structures via different routes. Examples for such nanosized structures are Carbon nanotubes, ZnO nanotubes, nanobelts and nanowires which possess unique mechanical, thermal and electrical properties compared to bulk material[13]. Nanometer sized specific strucures and devices is also the regime of virtually all important biological processes such enzymatic catalysis, cellular recognition, DNA transcription, specific ion transport and electrical switching between nerve branches which have been optimized through millions of years of evolution. Thus it is a logical step to take advantage of these systems for nanotechnological purposes. Some studies already tried to make use of their unique properties and specific binding and recognition mechanisms to create nanosized structures[19]. Promising results were obtained by the coupling of nanoparticles with biological molecules, such as DNA[20,21], proteins and ligands[22,23].

The usage of their specific binding sites and the formation of non-covalent complexes enabled the execution of a self-assembly of nanowires[23] and more complex structures such as grids[22]. Another approach of applying nanosized biological structures such as DNA strings, protein tubes, and protein shells in nanotechnology is to utilize them as templates for the deposition of metallic structures, which was also recently demonstrated[24].
The formation of macromolecular structures from complex organic molecules, which has become a field of growing interest in the recent decade, is another promising way for bottom up synthesis of nanosized structures[25].

From this background, it is clear that besides developing nano applications and -technologies, another focus has to be development and optimization of analytical methods and instruments for the analysis of nanostructured materials and to control ambient and workplace concentrations of possibly hazardous nanoparticles, a view that is also shared in the mission statement of the billion dollar sized National Nanotechnology Initiative (NNI) [2] of the US government. The health risk assessment that is posed by nanoparticles is currently a rapidly developing field [26] due to various ways of incorporation besides inhalation. From first medical studies it is known that nanoparticles are able to penetrate deep into the lung, show the lower clearance the smaller the diameter[27] and are even able to bypass cellular membranes and enter the systemic circulation[28]. The monitoring of nano-aerosol concentrations will become increasingly important with the emergence of an increasing number of nanotechnological products as they can be emitted during production or usage of products containing nanoparticles, nanotubes or nanowires.

Traditional analytical methods to characterize nanosized structures are for example Transmission Electron Microscopy (TEM), which is used for structural and phase characterization at nanometer resolution, Atomic Force Microscopy (AFM), which is used to characterize topology and mechanical surface properties of nanosized structures and Secondary Ion Mass Spectrometry (SIMS) based techniques, which are used to determine elementary and molecular distribution at nanometer scale.

One method recently adapted to characterize nanoparticles according to their size is Differential Mobility Analysis (DMA). This method utilizes a homogenous and well defined electrostatic field to classify charged nanosized objects (particles, biomolecules, clusters) suspended in ambient air. DMA was intentionally designed to characterize aerosol in the micrometer and submicrometer size range[29], but in the recent decade an extension of the accessible size into the single digit nanometer range[30-32] was achieved. The working range of theses new analyzers matches with the kDa to high MDa mass range [31]. Combined with a soft method for aerosol generation from solution, such as nano-Electrospray ionozation this method has already proven to be successful in the characterization of proteins[31], protein complexes[31,33,34], polymers[35-37], bacteriophages[38], viruses[31], virus fragments[39] and inorganic particles[40] from dilute suspensions according to their size.

References

(1) Foster, L. E. *Nanotechnology: Science, Innovation and Opportunity*; Prentice Hall: Upper Saddle River, NJ, 2006.
(2) www.nano.gov.
(3) Feynman, R. *Engineering & Science,* Academic Press, UCLA, Los Angeles, CA **1960**.
(4) Feynman, R. In *Nanotechnology:Science Innovation and Opportunity*; Foster, L. E., Ed.; Prentice Hall: Upper Saddle River, NJ, 2006; 247-268.
(5) Jurvetson, S. In *Nanotechnology: Science, Innovation and Opportunity*; Foster, L. E., Ed.; Prentice Hall: Upper Saddle River, NJ, 2006.
(6) Hu, Z.; Yang, Y.; Shang, X.; Pa, H. *Mater. Lett.* **2005**, *59*, 1373-1377.
(7) Oelerich, W.; Klassen, T.; Bormann, R. *J. Alloys Compd.* **2001**, *315*, 237-242.
(8) O´Regan, B.; Grätzel, M. *Nature* **1991**, *353*, 737-740.
(9) Treacy, M. M. J.; Ebbesen, T. W.; Gibson, J. M. *Nature* **1996**, *381*, 678-680.
(10) Segal, B. In *Nanotechnology: Science, Innovation and Technology*; Foster, L. E., Ed.; Prentice Hall: Upper Saddle River, NJ, 2006; 148-156.
(11) Huber, D. L. *Small* **2005**, *1*, 482-501.
(12) Ebbesen, T. W.; Lezec, H. J.; Hiura, H.; Bennett, J. W.; Ghaemi, H. F.; Thio, T. *Nature* **1996**, *382*, 54.
(13) Reed, M. In *Nanotechnology: Science, Innovation and Opportunities*; Foster, L. E., Ed.; Prentice Hall: Upper Saddle River, NJ, 2006; 141-162.
(14) Salata, O. V. *J. Nanobiotech.* **2004**, *2*.
(15) Mu, L.; MTeo, M.; Z.Ning, H.; Tan, C. S.; Feng, S. S. *J. Control. Release* **2005**, *103*, 565-575.
(16) Gupta, A. K.; Gupta, M. *Biomaterials* **2005**, *26*, 3995-4021.
(17) Li, Z. Z.; Wen, L. X.; Shao, L.; Chen, J. F. *J. Control. Release* **2004**, *98*, 245-254.
(18) Sahoo, S. K.; Labhasetwar, V. *Drug Discov. Today* **2003**, *8*, 1112-1120.

(19) Katz, E.; Willner, I. *Angew. Chem. Int. Ed.* **2004**, *43*, 6042-6108.
(20) Bashir, R. *Superlattices Microstruct.* **2001**, *29*, 1-16.
(21) Niemeyer, C. M. *Appl. Phys. A* **1999**, *68*, 119-124.
(22) Connoly, S.; Cobbe, S.; Fitzmaurice, D. *J. Phys. Chem.* **2001**, *105*, 2222-2226.
(23) Caswell, K. K.; Wilson, J. N.; Bunz, U. H. F.; Murphy, C. J. *J. Am. Chem. Soc.* **2003**, *125*, 13914-13915.
(24) Katz, E.; Willner, I. *J. Am. Chem. Soc.* **2002**, *124*, 10290-10291.
(25) Balzani, V. *Small* **2005**, *1*, 278-283.
(26) Hoet, P. H. M.; Brüske Hohlfeld, I.; Salata, O. V. *J. Nanobiotechn.* **2004**, *2*.
(27) Oberdorster, G.; Ferin, J.; Lehnert, B. E. *Environ. Health Perspect.* **1994**, *102*, 173-179.
(28) Nemmar, A.; Vanbilloen, H.; Hoylaerts, M. F.; Hoet, P. H.; Verbruggen, A.; Nemery, B. *Am. J. Respir. Crit. Care Med.* **2001**, *164*, 1665-1668.
(29) Liu, B. Y. H.; Pui, D. Y. H. *Journal of Colloid and Interface Science* **1974**, *74*, 155-171.
(30) Chen, D.-R.; Pui, D. Y. H.; Hummes, D.; Fissan, H.; Quant, F. R.; Sem, G. J. *J. Aerosol Sci.* **1998**, *29*, 497-509.
(31) Bacher, G.; Szymanski, W. W.; Kaufman, S. L.; Zöllner, P.; Blaas, D.; Allmaier, G. *J. Mass Spectrom.* **2001**, *36*, 1038-1052.
(32) de la Mora, J. F. *Trends in Analytical Chemistry* **1998**, *17*, 328-339.
(33) Loo, J. A.; Berhane, B.; Kaddis, C. S.; Wooding, K. M.; Xie, Y.; Kaufman, S. L.; Chernushevich, I. V. *J. Am. Soc. Mass Spectrom.* **2005**, *16*, 998-1008.
(34) Mouradian, S.; Skogen, J. W.; Dorman, F. D.; Zarrin, F.; Kaufman, S. L.; Smith, L. M. *Anal. Chem.***1997**, *69*, 919-925.
(35) Ku, B. K.; de la Mora, J. F. *Anal. Chem.* **2004**, *76*, 814-822.
(36) Saucy, D. A.; Ude, S.; Lenggoro, I. W.; de la Mora, J. F. *Anal. Chem.***2004**, *76*, 1045-1053.
(37) TSI-Inc. In *http://www.tsi.com/documents/CHEMC-006-Water-solublePEGPolymer.pdf*, **2007**.
(38) Wick, C. H.; McCubbin, P. E. *Toxicol. Meth.* **1999**, *9*, 245-252.
(39) Hogan, C. J.; Kettleson, E. M.; Ramaswami, B.; Chen, D.-R.; Biswas, P. *Anal. Chem.* **2006**, *28*, 844-852.
(40) Laschober, C.; Kaufman, S. L.; Reischl, G.; Allmaier, G.; Szymanski, W. W. *J. Nanosci. Nanotechno.* **2006**, *6*, 1474-1481.

2. Introduction of nano-Electrospray Ionizazion and nano-Differential Mobility Analysis

2.1 Electrospray Ionization:

2.1.1 Historical development

In the beginning mass spectrometry was focused on determining the mass of atomic isotopes and small and gaseous molecules[1]. Further development expanded the analysis to easy vaporable organic molecules of growing complexity. In these first attempts known components were analyzed for molecular mass, stability and fragmentation patterns of the produced ions which lead to a better understanding of ionization and fragmentation processes.

This knowledge lead subsequently to the use of mass spectrometry to determine the structure of unknown molecules by interpretation fragmentation patterns. With the success of mass spectrometry in the analysis of small molecules, and the further development in biochemistry and organic chemistry, the urge to develop mass spectrometric methods for larger molecules, such as synthetic polymers and biopolymers-like DNA and proteins, arose. A first barrier in the analysis of these large molecules with mass spectrometry was that ionization methods developed for small molecules, such as electron impact ionization (EI)[2,3], chemical ionization (CI)[4] and photo-ionization (PI) already require the molecules to be in the gaseous phase.

The thermal energy of vaporizing polymers and biopolymers into the gas phase is rather high and leads usually rather to thermal decay than to vaporization. First attempts and successes in the desorption/ionization of large molecules from solid surfaces were made with field desorption (FD)[5], plasma desorption (PD)[6] and from solution with fast atom bombardment (FAB) and with liquid secondary ion mass spectrometry (L-SIMS). In both methods large molecule ions are produced by converting the energy of a primary atom respectively ion beam which is directed on the surface of the liquid which contains the analyte molecules[7-9]. With these methods, some successes in the analysis of polymers and biopolymers were possible, however, due to high backgrounds and with increasing molecular weight fast decreasing ion currents as well as the emergence of new desorption/ionization methods prevented a broad application.

A major breakthrough in the desorption/ionization of large molecules was made by the introducing the Electro-Spray Ionization (ESI)[10] and the Matrix Assisted Laser Desorption and Ionization (MALDI)[11].

2.1.2 Electrospraying of liquids

The electrostatic spraying of liquids was known since the first decades of the 20th century[12,13] . It was at first investigated in connection with various applications, such as production of coatings[14], ink-jet printing[15], fuel spraying[16,17] and micro-encapsulation[18]. The principle of electrostatic spraying is the application of a high voltage (typically few thousand volts) between a conducting liquid flowing through a capillary and an orifice plate which is mounted perpendicular to the capillary exit. The electrical field induces charge separation at the surface of the liquid and thus a net charging of the droplets. Electro-spraying has been proven to be a rather complex process with various influencing parameters, with a clear distinction of several occurring working modes[19,20] . Most important parameters concerning the spray process are properties of the sprayed liquid, such as viscosity, conductivity and surface tension, followed by operation parameters like the applied flow through the capillary, the capillary diameter as well properties of the sourrounding gas, such as applied sheath gas flow and its dielectric constant temperature which influences evaporation of the liquid.

2.1.3 Main functional modes of the ES-process

Although many parameters influence the electrospray process, a clear distinction between several main functional modes, which are characterized by regular and stable droplet formation (Fig. 2.1) and are separated by regions of unstable droplet formation and pulsation between different modes[20], exists At low electrical fields, the electrospray process forms the so called dripping mode. In this mode, droplets form at the tip of the capillary. When the electrical and gravitational forces are high enough, the droplet is released from the tip of the surface. The frequency in which the droplets form and are released are highly dependent on the applied voltage, with a steep increase with increasing voltage. As the flow of the liquid through the capillary is held stable, the average droplet volume decreases and in the same way the formation frequency of the droplets rises.

The characteristics of this mode are a highly uniform droplet size (0,2-30 µm) and very low charging of the droplets compared to the subsequently discussed cone-jet mode mode. At certain settings, the formation of the main droplets can be accompanied by the formation of secondary droplets when the primary droplets are released from the surface tip.

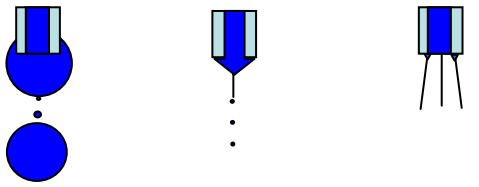

a) Dripping mode b) Cone jet mode c) Multiple jets

Fig. 2.1 ES-Modes

When the voltage and / or the conductivity of the liquid are further increased, the formation of a liquid jet at the tip of the droplets before they leave the capillary tip can occur, a intermediate mode that evolves into the so-called cone jet mode at higher applied voltages. This mode is characterized by very small and uniform droplets which are released from a jet that forms at the tip of a cone produced by the liquid exiting the capillary. Depending on voltage settings, capillary diameter and liquid properties, multiple jets and jets which break up into smaller jets can form at the tip of the capillary. Because of stability, small droplet diameters and high charging, the cone-jet mode is the most important electrospray mode to generate airborne ions from liquid solutions for analytical applications [21].

The cone that forms at the tip of the capillary is a so-called Taylor-cone. Taylor reasoned, that at a certain charge density at the surface of the liquid, the Coulomb forces may equal surface tension, which leads to the formation of a perfect cone[22]. In his considerations, a balanced and static state between surface, gravitational and electrostatic forces was hypothesized. In recent modelling calculations, an applied flow through the capillary as well as liquid properties like viscosity and conductivity were implemented to achieve a more realistic model of the cone[23] which enabled the simulation of the formation of a cone jet, its tip diameter and the occurring current. As theory and experiments have shown, the diameter of the liquid jet at the tip of the cone and thus the diameter of the released primary droplets depend on the applied flow and liquid properties like dielectric constant, conductivity, viscosity and surface tension.

2.1.4 Formation of gaseous analyte ions from aerosol droplets

In experiments the electrospray process has shown its capability to produce gas phase ions from analyte molecules from dilute solutions. As this process is a rather soft desorption/ionization method (e.g. the analyte molecules are exposed to virtually no thermal energy), the production of gas phase ions from large molecules is possible. As the electrospray is, as stated before, a rather complicated process influenced by many parameters, various spray chamber designs were realized to control the spray process, including sheath liquid flow and sheath gas flow to name the most important. This was done to optimize the electrospray ionization as interface between analytical separation techniques and mass spectrometry in terms of ion production rate, reduction of chemical noise, stability and accessible polarity of the solvent systems.

A large number of experiments and theoretical considerations have so far been conducted about the processes leading to analyte molecules after the formation of the highly charged droplets[24] in the electrospray source(Fig. 2.2.). In the first step, evaporation of the solvent from the highly charged droplets takes place. This decrease in surface area leads subsequently to a state where the repulsion of the charges on the surface is equal to the surface tension of the droplet. This leads to a instability, which forms liquid jets from the surface of this droplet and the formation of smaller droplets, with the primary droplet loosing about only 2% of its mass and 15% of its charge[25], a process very similar to the before described formation of a Taylor-cone during the electrospraying itself.
A cascade of this droplet fission follows[24], until only very small droplets with a low number of analyte molecules remain (Fig. 2.2).

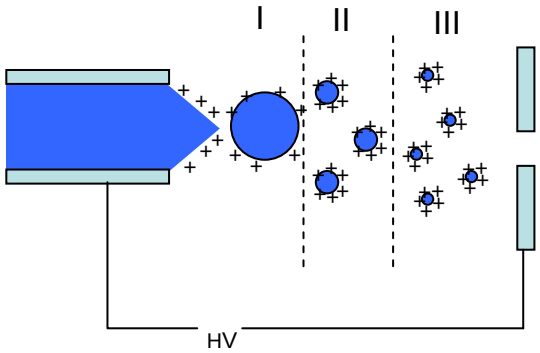

I...Primary droplets, typically 1.5 µm diameter and about 60 000 charges
II..Droplets emitted from primary droplets, typically 0.1 µm diameter and 500 charges
III..Last step of the evaporation/fission step, usually 0.03 µm diameter and 250 charges

Fig. 2.2. Scheme of the droplet fission cascade; charge and diameter values are found in literature[22]

When droplets are too small for a further fission step, the rest of the solvent molecules evaporate until only the analyte molecules remain, taking up the excess charges of their host dropket.. This is the proposition of the so called charged residue model[26,27]. However, a second mechanism of the formation of analyte molecule ions has been proposed. This so called ion evaporation model[28,29] takes into account, that ionic analyte molecules on the surface of the droplet can face enough electrostatic repulsion from the highly charged surface to circumvent the barrier of the solvatisation energy and escape the droplet, a model that is mainly applicable on small ionic molecules.

2.1.5 Analytical characteristics of the ESI – source

As the ion evaporation and the charge residue model already suggest, the electrospray has unique features and properties concerning response and nature of the produced analyte ions. One main difference of the electrospray ionization process compared to other desorption/ionization processes is, that it is known to produce highly charged analyte ions. Even charge states of 20 and more are known to occur in ESI[30,31], especially when used for the ionization of large molecules. One benefit of this phenomenon is that only ions in a certain window of mass to charge ratios (m/z) are produced[30], which means that the m/z limitations of mass spectrometers and their detectors are seldomly reached in ESI-MS. However, the limitation in ESI-MS is not the m/z ratio, but the resolution of the MS to differentiate between molecule ions of adjacent charge states.

According to the charged residue model, the charge state of the ion reflects the charge density at the droplet surface and the tendency of the analyte ions to cover surface area, which is effected by the surface activity and the number of hydrophilic groups of the molecules. Even the same protein in different configurations (e.g. denatured and native) is known to produce ions with a different charge distribution, an effect that is caused by the different positioning of the hydrophilic groups and thus their surface activity.

These considerations also explains differences between signal intensity ratios detected in the mass spectrometer and analyte concentrations in solution, which has been appointed in experiments as result of their different surface activities and in competition of the different analytes for the limited number of charges of the droplet. This effect is so strong, that it can lead to a complete suppression of the ion signal of one analyte by another.

Another cause of this observed enrichment phenomenon is the droplet fission process itself, in which, as described before, small droplets are leaving the surface of larger droplets as they reach the Rayleigh limit, resulting in preferable production of ions from molecules which possess higher surface activity than others.

2.1.6 Introduction and characteristics of the Nano-Electrospray Ionization source

After the development of ESI sources, a modification, the so called nano-Electrospray source, was introduced by Wilm et al[32]. This source, as its name suggests, is characterized by very small capillary diameters and thus a very low liquid flow. This low flow -typically 50-100 nL/min- results in a very small primary droplet size -usually in the order of few hundred nanometers- when operated in the cone-jet mode. This small droplet diameter has further impact on the analytical properties of the nano-ESI source compared to a conventional Electrospray ionization source.

First, primary droplets produced by the liquid jet are much smaller in diameter, which means that less droplet fission steps are necessary (Fig. 2.2) to obtain analyte ions according the charge residue process. This decrease in fission steps leads to less ion suppression effects and preference of the ionization of surface active molecules. Investigations[32,33] have shown that this kind of ESI source is also much more tolerant to high buffer salt concentrations and impurities and that it reduces noise in the mass spectrum. This is likely to be the result of the smaller droplet volume, which decreases the number of ions and molecules which can interact or attach with the analyzed substance during droplet evaporation.

Another characteristic of this nano-Electrospray ionization source compared to conventional Electrospray ionization sources is that the liquid flow, which is usually $1/100^{th}$ of the flow of conventional ESI sources is still charged with ¼ of its current, thus producing a 25 fold higher charging efficiency[32,34]. This higher efficiency has also a beneficial influence on effects like charge-competition between different molecules. The conversion rate, which is the rate of sprayed analyte molecules to in the mass spectrometer detected ions, has been proven to b 500 times higher for nano-ESI compared to conventional ESI sources, which underlines most dramatically the shift of analytical properties in the ESI development[33].

At low concentrations and small droplet sizes, only one analyte molecule is likely to be trapped within one primarily produced droplet, which further increases the quality of the mass spectra. When the sprayed liquid is completely volatile and salt free, the nano-ESI process allows the formation of a highly uniform aerosol consisting of mostly single molecule ions without background residue peaks (Fig. 2.3), thus enabling the analysis of nanoparticles from solution with measurement techniques known from aerosol characterization[35,36], which will be discussed in the chapter 2.2 .

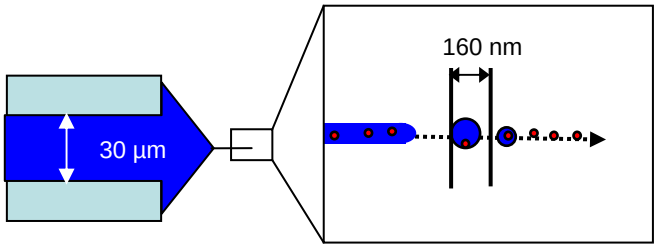

Fig. 2.3 Scheme of the Nano-ESI source used for the production of a monodisperse aerosol

References:

(1) de Laeter, J. R. *Mass Spectrom. Rev.* **1994**, *13*, 3-22.
(2) Dempster, A. J. *Phys. Rev.* **1921**, *18*, 415.
(3) Nier, A. O. *Sci. Instr.* **1947**, *18*, 398.
(4) Munson, M. S. B.; Field, F. H. *J. Am. Chem. Soc* **1966**, *88*, 2621-2630.
(5) Beckey, H.D., *Method. Chim.*, **1974,** 1, 494-504.
(6) Loo, J.A.; Williams, E.R.; Furlong, J.J.P.; Wang, B.H.; Mc Lafferty, F.W.; Chait, B.T.; Field, F.H. *.Int. J. Mass Specr. Ion Proc.* **1986** *40*, 305-313.
(7) Barber, M.; Bordoli, R. S.; Sedgwick, R. D.; Tyler, A. N.; Whalley, E. T. *Biomed. Mass. Spectrom.* **1981**, *8*, 492.
(8) Rinehart, K. L. *Science* **1983**, *218*, 254-260.
(9) Caprioli, R. M. *Anal. Chem.* **1986**, *58*, 2949.
(10) Mann, M.; Meng, C.; Fenn, J. B. In *Proceedings of the 36th Annual Conference of the American Society for Mass Spectrometry,*: San Francisco, 1988; pp 1207-1208.
(11) Tanaka, K.; Waki, H.; Ido, Y.; Akita, S.; Yoshida, Y.; Yohida, T. *Rapid Commun.in Mass Sp.* **1988**, *2*, 151-153.
(12) Zeleny, J. *Prog. Camb. Phil. Soc.* **1915**, *18*, 71-83.
(13) Zeleny, J. *Phys. Rev.* **1917**, *10*, 1-6.
(14) Hines, J. *J. Appl. Phys.* **1966**, *37*, 2730-2736.
(15) Tomita, Y.; Ishibashi, I.; Yokoyama, T. *Jap. Soc. Mech. Eng.* **1986**, *29*, 3737-3743.
(16) Jones, A. R.; Thong, K. C. *Appl. Phys.* **1971**, *4*, 1159-1168.
(17) Kelly, A. J. *J. Inst. Energy* **1984**, *57*, 312-320.
(18) Langer, G.; Yamate, G. *J. Colloid Interface Sci.* **1969**, *29*, 450-455.
(19) Cloupeau, M.; Prunet-Foch, B. *J. Electrostat.* **1989**, *22*, 135-159.

(20) Cloupeau, M.; Prunet-Foch, B. *J. Electrostat.* **1990**, *25*, 165-184.
(21) Fenn, J. B.; Mann, M.; Chin, K. M.; Shek, F. W. *Mass Spectrom. Rev.***1990**, *9*, 37-70.
(22) Taylor, G. I. *Proc. Roy. Soc., Ser. A* **1964**, *280*, 383-397.
(23) Hartman, R. P. A.; Brunner, D. J.; Camelot, D. M. A.; Marijnissen, J. C. M.; Scarlett, B. *J. Aerosol Sci.* **1999**, *30*, 823-849.
(24) Kebarle, P.; Tang, L. *Anal. Chem.* **1993**, *65*, 972.
(25) Gomez, A.; Tang, K. *Phys. Fluids* **1994**, *A6*, 404-414.
(26) Dole, M.; Mack, L. L.; Hines, R. C.; Molbley, L. D.; Ferguson, M. B.; Alice, J. *Chem. Phys.* **1968**, *49*, 2240.
(27) Glenic, J.; Mack, L. L.; Nakamal, K.; Cupta, C.; Cumar, V.; Dole, M. *Biomed. Mass. Spectrom.* **1984**, *11*, 259.
(28) Kebarle, P.; Peschke, M. *Anal. Chim. Acta* **2000**, *11*, 406.
(29) Irbane, I. V.; Thomson, B. A. *J. Chem. Phys.* **1976**, *64*, 2287.
(30) de la Mora, J. F. *Anal. Chim. Acta* **2000**, *406*, 93.
(31) Heck, A. J. R.; Heuvel, R. H. H. v. d. *Mass Spectrom. Rev.* **2004**, *23*, 368-389.
(32) Wilm, M.; Mann, M. *Anal. Chem.* **1996**, *68*, 1-8.
(33) Juraschek, R.; Dülcks, T.; Karas, M. *J. Am. Soc. Mass Spectrom.***1999**, *10*, 300-308.
(34) Schmidt, A.; Kras, M. *J. Am. Soc. Mass Spectrom.* **2003**, *14*, 492-500.
(35) Bacher, G.; Szymanski, W. W.; Kaufman, S. L.; Zöllner, P.; Blaas, D.; Allmaier, G. *J. Mass Spectrom.* **2001**, *36*, 1038-1052.
(36) Chen, D. R.; Pui, D. Y. H.; Kaufman, S. L. *J. Aerosol Sci.* **1995**, *26*, 963-977.

2.2 Electrical Mobility Analysis

Electrical mobility analysis is a method for the classification of charged particles under normal pressure conditions utilizing an electrostatic field. For this purpose, the particles in question have to be suspended in a gas medium, thus forming an aerosol according to the most common definition [1]. The stability of aerosols is dependant on the inertial, gravitational and frictional forces acting on the suspended particles as well as turbulences inside the gas (air) medium, with the viscosity of the medium and the size and density of the particle as most important parameters. Their stability can be ranging from some minutes up to several years dependant on before mentioned parameters.

2.2.1 Particle movement:

When a particle moves with a constant velocity through an uncompressible environment, several forces act on the particle resulting in a resistance of the medium against the particle motion, which means, that a constant force has to be applied on the particle to sustain the constant movement. On one hand, the surrounding medium has to be displaced and neighbouring strata have to be separated, which results in a resistance attributed to the viscosity of the surrounding medium. On the other hand, molecules of the medium take up inertia when they collide with the surface of the particle, which also results in a constant energy loss and adds to the resistance of the surrounding medium on particle movement.

For two extreme cases, where only inertia respectively viscosity acts on the particle, two laws for the resulting resistance on the particle movement exist: Newtons´and Stokes´resistance law. As particles measured by Mobility Analysis are in the sub-µm to nm size range, Reynolds numbers (Re), which are strongly dependant on particle size (D_P), velocities (v) and viscosity (η) and density (ρ_G)of the sourrounding medium (Eq.1) are very small and viscosity forces dominate over inertial forces. For this reason, only Stokes´ resistance law for particle movement has to be considered in Mobility Analysis (Fig. 2.4).

(Eq.1) $$\mathrm{Re} = \frac{\rho_G v D_P}{\eta}$$

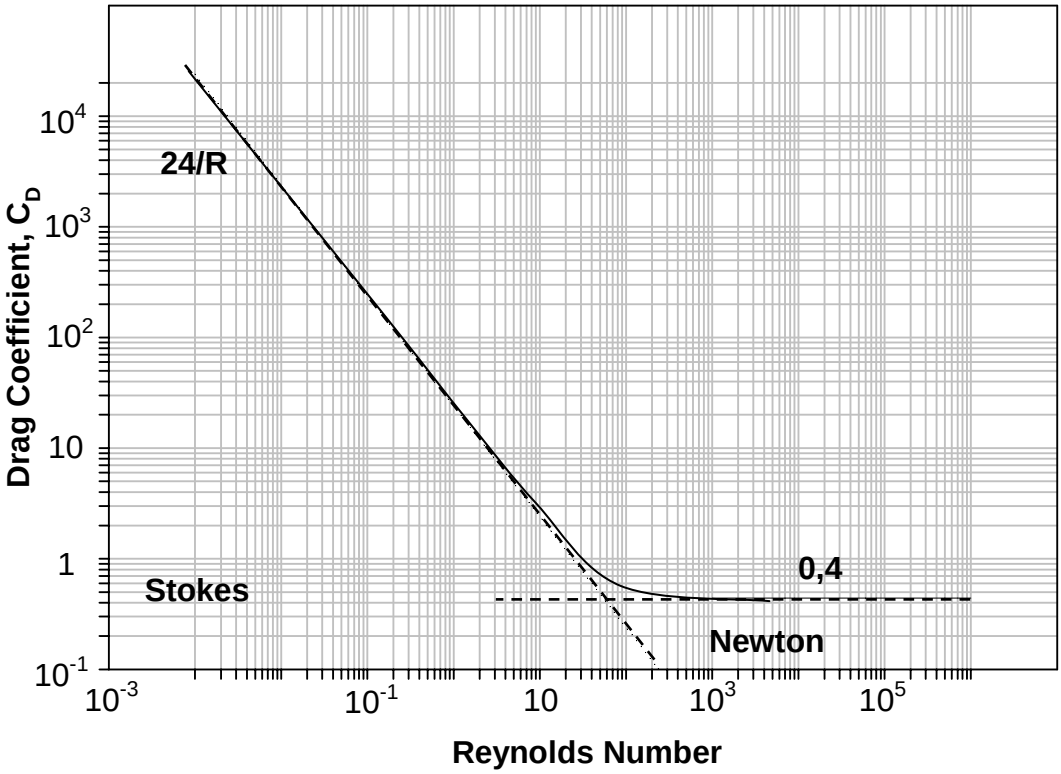

Fig. 2.4 Drag coefficient (C_D) vs. Reynolds number

Stokes´ resistance law:

In Stokes´considerations, inertia forces are completely neglected in order to be able to solve the usually unsolvable Navier-Stokes equations, in which all possible forces acting inside the medium and on the particles are implemented. The solution of this simplification leads to equation (Eq. 2) for the force (F_D) that is faced by a spherical particle with constant velocity v, with η, the viscosity of the medium and D_P, the particle diameter, being the only contributors:

(Eq. 2) $F_D = 3\pi\eta v D_P$

Stokes´ law is valid for Re <1, thus small velocities and particle dimensions. Stokes´ and Newton´s law can be connected through the proportionality factor C_D for small Reynolds numbers, resulting in (Eq. 3) for the drag coefficient (see also Fig. 2.4):

(Eq. 3) $C_D * \rho_g \frac{\pi}{8} {D_P}^2 v^2 = 3\pi\eta v D_P \Rightarrow C_D = \frac{24\eta}{\rho_g v D_p} = \frac{24}{\mathrm{Re}}$

However, Stokes´and Newtons´ resistance laws assume a constant and continuous medium surrounding the particle. When considering, that the mean free path of an average gas molecule under normal conditions (1.013 bar and 24°C) is 66 nm, it is apparent, that another correction has to be made for aerosol particles which have µm dimensions or smaller, especially for nanoaerosols, where particle dimensions are equal or even smaller than the mean free path of the surrounding gas molecules. This correction also called the Cunningham slip correction factor (C_C)[2,3] must be inserted into Stokes´ law to receive the corrected drag force (F_D) for the particle (Eq. 4).

(Eq. 4) $$F_D = \frac{3\pi\eta v D_p}{C_c}$$

This correction factor is mainly dependant on the ratio between the mean free path λ of the gas molecules and the particle diameter D_P (Eq. 5).

(Eq. 5) $$C_c = 1 + \frac{\lambda}{D_P} + \left[2{,}34 + 1{,}05\exp\left(-0{,}39\frac{D_P}{\lambda}\right)\right]$$

As can be seen in Fig 2.5, the slip correction factor is about 1 for particles in the micrometer range, but increases rapidly with decreasing particle dimension, resulting in increasingly smaller forces for aerosol particles in the nanometer size range than predicted without correction.

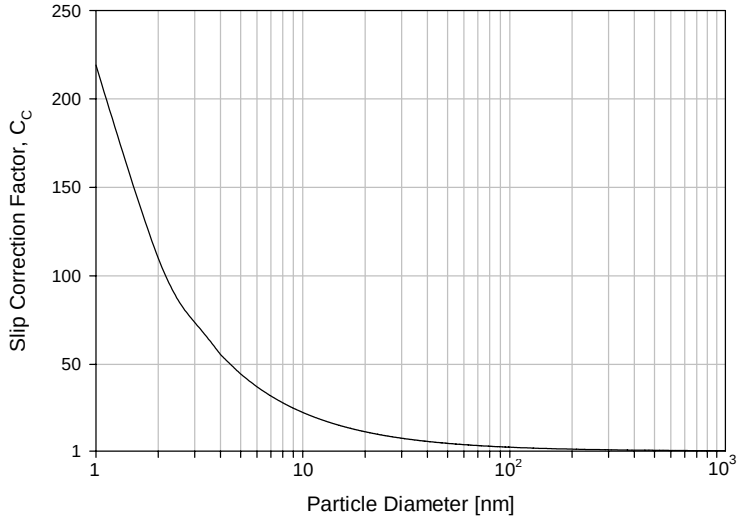

Fig. 2.5 Cunningham slip correction factor vs. particle diameter

2.2.2 Definition of the Particle Electrical Mobility

When particle that carries n elementary charges e ($1.6*10^{-19}$ Coulomb encounters an electrical field with field strength E, a constant electrostatic force F_{el} drags this particle through the gas medium (Eq. 6). As the particle accelerates, frictional forces caused by viscosity and inertia increase. This results consequently in a steady state, where frictional and electrostatic forces are balanced. As aerosol particles are of small dimension, the frictional forces can be described by Stokes´ law containing the Cunningham slip correction factor (Eq. 5). When the frictional force and the electrostatic force that is encountered by the aerosol particle are equalled (Eq. 7), it can be seen, that the terminal velocity v_{TE} of the aerosol particle can be calculated.

(Eq. 6) $F_{el} = neE$

(Eq. 7) $neE = \frac{3\pi\eta v D_P}{C_c}$; $v_{TE} = \frac{neEC_C}{3\pi\eta D_P}$

The electrical mobility Z is now a resulting parameter of a charged aerosol particle linked to equation (Eq. 7), describing the particles terminal velocity due to the electrical field strength (Eq 8).

(Eq. 8) $Z = \frac{v_{TE}}{E} = \frac{neC_c}{3\pi\eta D_P}$

As can be seen in (Eq. 8), the electrical mobility is an important property of aerosol particles, as it offers a way to characterize aerosols with electrical fields. Furthermore it allows the connection between electrical mobility and the particle diameter, consequently enabling the measurement of aerosol size distributions, assuming their charge state and properties of the surrounding gas medium are known.

2.2.3 Electrical Mobility Analysis of particles

Based on the definition of the electrical mobility, aerosol particles have been studied since the beginning of the 20th century. In the first apparatus, developed by Zeleny[4] charged aerosol particles and ion clusters guided through two electrodes were deflected by an electrical field (Scheme: Fig. 2.6).

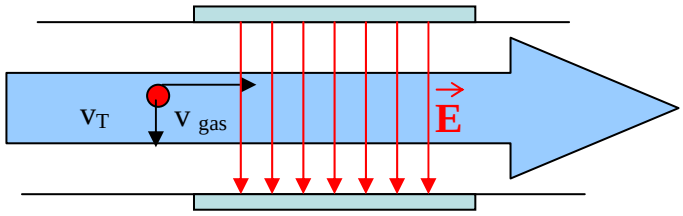

Fig. 2.6 Scheme of Zelenys´experimental setup

Comparing the velocity of the gas stream with the terminal velocity of the aerosol particles with different electrical mobilities, only particles which possessed a certain mobility or lower could pass the way between the deflecting plates in this set-up.

By measuring the voltage and current at an electrode downstream to the deflecting plates, it was possible to determine the amount of particles below a certain electrical mobility. These first experiments were conducted on ions produced with radioactive and X-ray radiation and gave insights into the average mobility of positively and negatively charged ion clusters, which were theorized as molecular clusters consisting of a central ion with attached water molecules[5,6].

Later on, in experiments on atmospheric samples, ions of much higher average mobility were found[7], with decreasing mobility when humidity or average particle concentrations increased[8]. The following findings of different classes of charged particles, as well as their timely variation lead to the need to develop an instrument with which the ion mobility could be measured differentially and not longer as an average value, as well as to establish a way to introduce and control charge of the aerosol particles in order to be able to measure a unbiased size spectrum of abundant aerosol particles.

2.2.4 The Differential Mobility Analyzer (DMA)

Even though the measurement of differential mobility spectra was recognized as being important to understand the nature and reactions of aerosols since the beginning of mobility measurements, the construction of a differential mobility analyzer was delayed until the determination of very small currents or particle concentrations was possible.

In principle, the design of the differential mobility analyzer is strongly related to the design of the mobility analyzer used by Zeleny[4] to determine incremental ion mobilities. The today most common design is the latest development step of various devices used for differential mobility analysis[9-14], which was finally optimized for the use in classification of nano-sized aerosols[15-17]. In this design, a voltage is applied between a cylindrical central electrode and a cylindrical housing. To achieve a selection of only one particle mobility fraction, the aerosol is introduced into the mobility analyzer with a small circular slit, thus narrowing the region from which the aerosol particles start their movement towards the central electrode (Fig. 2.7).

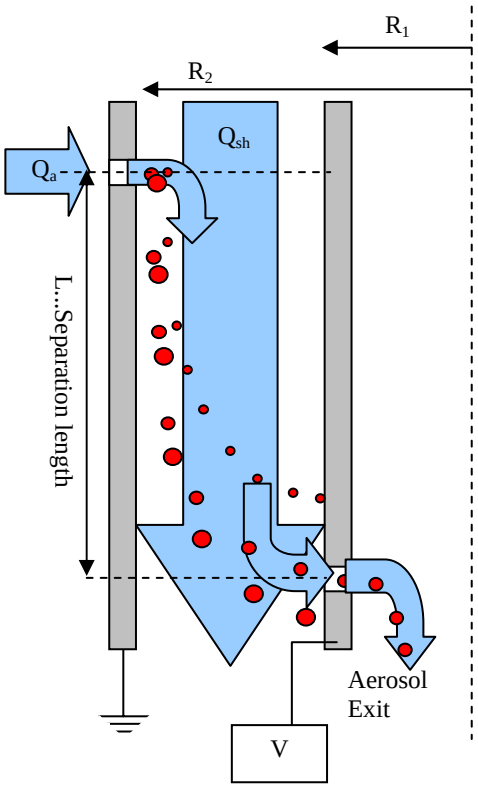

Fig. 2.7 Scheme of Differential Mobility Analysis

V.. Applied Voltage – typically scanned from 0 to 10 kV
R_1... Inner Radius of the central electrode
R_2... Outer Radius of the central electrode
L...Separation length
Q_{sh}...Sheath gas flow
Q_a...Aerosol inlet flow

Further, in their paths, the aerosol particles encounter the electrical field, whose field strength E_r increases due to the cylindrical geometry the lower the distance r to the geometrical centre of the electrode (Eq 9; Fig. 2.7).

(Eq. 9) $$E_r = \frac{V}{r * \ln(\frac{R_2}{R_1})}$$

In contrast to early aerosol measurements, not the total current produced by the particles which collide with the central electrode is measured, but one particle fraction is removed from the sheath gas flow through an exit slit. Particles with a certain and well defined electrical mobility follow a trajectory from the entrance to the exit of the central electrode and are subsequently detected in the flow exiting the central electrode through the slit. This specific electrical mobility can be calculated following the trajectory of the entrance and the exit of the central electrode. As Fig. 2.7 illustrates, aerosol particles with a too small mobility cannot pass the sheath gas in time, whereas aerosol particles with too high mobility collide with the central electrode before they reach the exit slit.

At every point of its trajectory, the aerosol particles have a certain velocity in the direction parallel to the electrode plates v_{II}, which is equal to the velocity of the sheath gas v_{SH} caused by its flow Q_{SH} through the differential mobility analyzer (Eq. 10) and in radial direction v_r, where the velocity of the aerosol particle is equal to the terminal velocity v_{TE} defined by equation (Eq. 7). The time t that it takes for the aerosol particle to pass with the sheath air the length L (Eq. 11) must be equal to the time that is needed for the aerosol particle to traverse the distance between the electrode plates from R_2 to R_1. This time can be calculated by integrating the time ∂t needed for the particle to move the distance ∂r between R_2 and R_1, which is equal to v_{TE} at every point along the trajectory (Eq. 12).

(Eq. 10) $$v_{II} = v_{SH} = \frac{Q_{sh}}{(R_2^2 - R_1^2) * \pi}$$

(Eq. 11) $$t = \frac{L}{v_{SH}} = \frac{L\pi(R_2^2 - R_1^2)}{Q_{SH}}$$

(Eq. 12) $$\frac{\partial r}{\partial t} = v_{TE}(r) = Z * E_r = Z * \frac{1}{r} \frac{V}{\ln(\frac{R_2}{R_1})} \Rightarrow t = \int_{R_2}^{R_1} r * \frac{\ln(\frac{R_2}{R_1})}{Z * V} \partial r = \frac{(R_2^2 - R_1^2)}{2} * \frac{\ln(\frac{R_2}{R_1})}{Z * V}$$

Equalling (Eq. 11) and (Eq. 12) and substituting *Z* from equation (Eq. 8) finally provides the governing equation (Eq. 13) for differential mobility analysis with coaxial cylindrically shaped electrodes.

(Eq. 13) $$Z = \frac{i * e_0}{3 * \pi \eta} * \frac{C_{Dp}}{D_p} = Q_{sh} * \frac{\ln(R_2 / R_1)}{2\pi * L} * \frac{1}{V}$$

As can be derived from (Eq. 13), the mobility spectrum of an aerosol can be obtained by scanning the voltage V of the central electrode and thus changing the mobility that is needed for aerosol particles to pass through the sheath gas and exit the central electrode through the exit slit. The mobility spectrum can be converted to a size spectrum of the analyzed aerosol particles assuming their sphericity, if their charge state is well defined. This is the case when a controlled charging step is conducted before differential mobility analysis.

Details of the charging process which is usually conducted prior to differential mobility analysis can be found in chapter 2.3.

2.2.5 Resolution of the DMA

In a first approach to assess the resolution of different mobility analyzers, particle diffusion and other factors like inhomogenity of the electrical field and the laminar flow are neglected. It is furthermore assumed, that a perfect monodisperse aerosol consisting of particles with the same electrical mobility enter the DMA. Assuming that the aerosol exit and inlet flows are identical, as well as a laminar flow pattern inside the DMA, the width of the aerosol flow in parallel direction to the electrode is equal to the ratio between sheath gas flow Q_{sh} and aerosol flow Q_a. This leads to a variation in the area Δr of the starting point of entering aerosol particles and further to different voltages needed for aerosol particles of the same mobility to pass from R_2 to R_1 in the same time, thus producing a peak and not a step function during a scan of the voltage in the differential mobility analyser (Eq. 14).

(Eq. 14) $$\frac{\Delta r}{R_2 - R_1} = \frac{Q_a}{Q_{sh}}$$

Combining (Eq. 14) with (Eq. 11) and (Eq. 12) leads to the result, that this difference in the starting point produces a triangular peak with a width $\Delta Z/Z$ of Q_a/Q_{sh} along the mobility axis[14,18].

For small particles diffusion effects cannot be ignored. Particle diffusion leads to particle displacement during the mobility analysis, and to an additional broadening and smoothing of the triangular peak into a Gaussian shape. The diffusion coefficient D (Eq. 15) of a particle with the diameter D_P is defined by the thermal energy of the particle kT multiplied with its mobility, which is the reciprocal value of its resistance to movement (Eq. 4).

(Eq. 15) $$D = kT\frac{C_C}{3\pi\eta D_P}$$

The average spatial broadening $\partial\sigma_X$ per time interval ∂t of an aerosol consisting of particles with the same mobility caused by its diffusion is calculated by (Eq. 16).

(Eq. 16) $$\partial\sigma_x = 2D\partial t$$

Implementing diffusion broadening into the transfer function of the DMA results in equation (Eq. 18), firstly provided by Stolzenburg[19] , for the full width half maximum broadness of an aerosol peak for a given DMA design, sheath gas setting and particle mobility.

(Eq. 17) $$\left(\frac{\Delta V}{V_P}\right)^2 = 16 * \ln 2 * \frac{(b + b^{-1}) * G}{Pe} \approx \left(\frac{\Delta D_P}{D_P}\right)^2$$

ΔV ..... Half width of the in Voltage space normalized peak of a monodisperse aerosol

V_P ..... Voltage setting of the peak centre of a monodisperse aerosol

G ..... Constant factor from theory which depends on geometry, usually very close to unity [17]

Pe ..... Peclet number; $Pe = \frac{Q_{sh}}{\pi * D(R_1 + R_2)}$

b ..... geometric factor; $b = \frac{L * G}{R_2 - R_1}$ (compare geometry to Fig. 2.7)

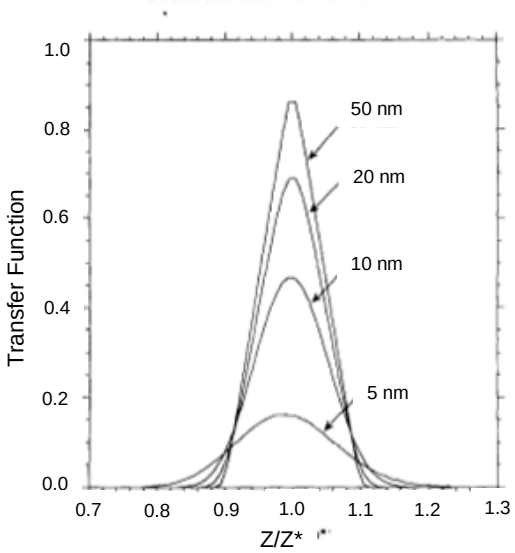

Fig. 2.8 To the average mobility Z* normalized Mobility spectra of particles with varying particle diameter and thus diffusion broadening

The influence on the diffusion of the aerosol particles is illustrated in Fig. 2.8, where the shape of the peak changes from triangular to more Gaussian curve shape with increasing peak width the smaller the particle.

The mobility measurement of nanometer sized particles poses therefore a special challenge on the design of nano-DMAs, since their high mobility and diffusion factor not only leads to substantial broadening, but also to particle losses at the entrance and exit regions of the DMA. The key issue in the design for nano-DMAs is to minimize the time the particles reside in the DMA and consequently to minimize diffusion effects and enhance the resolution. This can be achieved with high sheath gas flows[20] and short separation lengths as well as small distances between the two cylindrical electrode plates in order for the particles to arrive at the exit slit within a small time interval. These high flow rates and small distances pose special problems in maintaining laminar flow inside the DMA. Another unwanted effect of the smaller dimensions is, that inhomogeneities of the electrical field and the aerosol flow at the edges of the exit and entrance slit have far more influence on the quality of the obtained size spectra[21] .

2.3 Charging of aerosol particles

In order obtain a complete aerosol size distribution from a particle mobility spectrum, it is necessary to introduce controlled particle charging over the whole size range. Furthermore, the charging mechanism has to be unbiased concerning chemical composition of the aerosol particles in order for the mobility analysis to cover every sort of particle contributing to the analyzed aerosol.

Since the beginning of mobility analysis, charging was achieved by exposing the aerosol to an ionized gas (air) due to radioactive radiation, corona discharge or X-Rays. In this process, the particles were then subsequently charged by attachment of the produced ions on the particle surface. It was found early, that in order to use mobility analysis in the quantitative determination of aerosol size distributions, an understanding of processes taking place between aerosol particles and ions is necessary. Based on Boltzmann charge equilibrium description Fuchs[22] developed the most widely accepted model of this aerosol charging process.

It was the first theoretical approach able to satisfactorily explain the observed charge formation and its distribution. In his theory, charging of the particles is produced by diffusion of gas ions onto the surface of aerosol particles, where their charge is released.

Given enough interaction time between the aerosol and the ions, a dynamic equilibrium occurs, resulting in a size-dependant charge state of the particles which is theoretically independent of their primary charge state.

For a calculation of this equilibrium charge state, gas properties and mobilities of the positive and negative charge carriers have to be known. Fuchs theorized that the charge carriers in an air environment are not the primary ions produced by the radiation, but more stable clusters consisting of a central ion which is surrounded by water molecules, an assumption that has been confirmed in later conducted experiments.

Experiments have shown, that after about $6*10^{12}$ charging/discharging events between aerosol particle and bipolar ions, an equilibrium charge state independently of the particle´s initial charge state is reached[23,24]. Because of this fact, the bipolar charging step is able to put even highly charged nano-aerosols produced with an electrospray source in a defined reduced charge state suitable for subsequent differential mobility analysis, which is indeed implemented in all systems designed for analyzing nano-aerosols produced by an electrospray process.

The resulting charge distribution calculated for air under ambient conditions is presented in (Fig 2.9) and also confirmed by a number of experiments[23-30]. The charging probability curves for the different numbers of elemental charges *i* show, that for bigger particles, multiply charged particles lead to an overlap of more than one particle size fraction in the mobility spectrum (factor n in eq. 13). Thus their abundance has to be considered in order to calculate the primary size distribution from the mobility spectrum. For small particles with a diameter below 50 nm, the amount of multiply charged particles is practically negligible, justifying the assumption that only singly charged particles are measured by the differential mobility analyzer, simplifying the calculation of a size spectrum from the original mobility data.

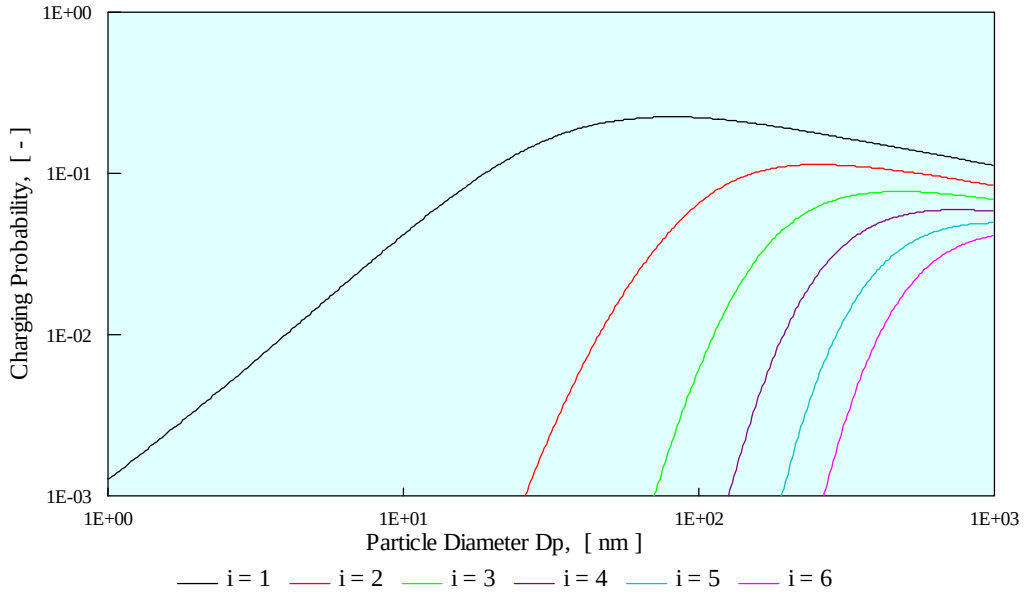

Fig. 2.9 Charging probability for diffusion charging in bipolar ion environment under ambient air conditions for the positively charged aerosol fraction
i: number of attached elementary charges

As can also be derived from the charge distribution, the amount of charged particles decreases rapidly with the diameter of the particle fraction, thus very sensitive detection methods have to be utilized in the analysis of nano-aerosols.

2.4 Particle detection

2.4.1 Condensation Particle Counter (CPC)

One common device used to determine the concentration of particles exiting the DMA is the condensation particle counter (CPC, Fig. 2.10). In this instrument, the aerosol flow entering the system is in a first step saturated with butanol vapour.

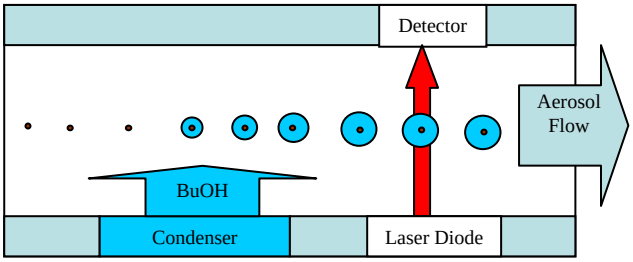

Fig. 2.10 Scheme of a condensation particle counter (CPC)

In a second step, the temperature of the aerosol flow is decreased, producing a supersaturation of the butanol vapour, which, as a consequence, begins to condensate on the particles in the aerosol flow, thus every aerosol particle forms a small butanol droplet, which is however big enough to scatter the light emitted by a laser-diode. Every scattering event and thus every aerosol particle which has been converted into a detectable droplet, can be monitored by this method. The vapour-supersaturations of common butanol-based CPCs (e.g. TSI Mod. 3025) is high enough to activate droplet formation of particles with a diameter of 3 nm or higher.

2.4.2 Faraday Cup (FC)

Another device used frequently for detection of charged particles is the Faraday-Cup arrangement. The Faraday-cup measures the current produced by the charged particles exiting the mobility analyzer[31] (Fig. 2.11). For particles in the nm size range, assuming an equilibrium charge state produced by bipolar diffusion charging[22], it can be assumed that every particle that enters the faraday cup carries one charge, thus contributing $1.6*10^{-19}$ C to the detected current.

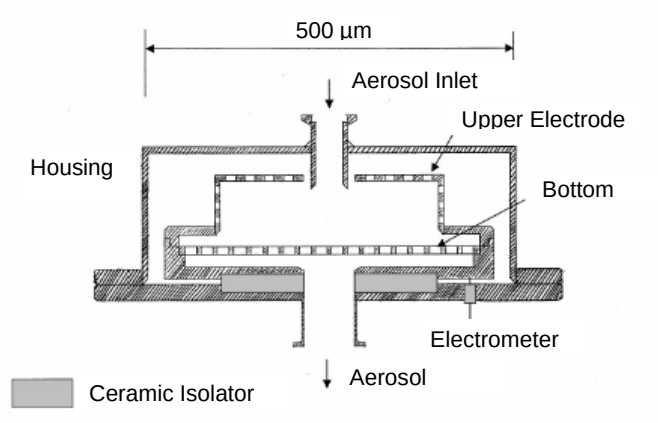

Fig. 2.11 Scheme of a Faraday-Cup electrometer used in differential moblity analysis[31]

Considering that the concentration of aerosol particles is about 10^4-10^6 particles per cm^3, that only around 1% of these particles in the size range of 5-15 nm carries one charge, given an aerosol flow in differential mobility analysis unit of 2 litres per minute, the available FC cup and its electronics are able to detect currents in the order of 10^{-15} A. The advantage of a FC based detection system compared to a CPC is that detection it is not restricted by the particle size.

References

(1) Hinds, W. C. In *Aerosol Technology*; Hinds, W. C., Ed.; John Wiley & Sons: New York, NY, 1999; 1-14.
(2) Cunningham, E. *Proc. Roy. Soc. Ser. A.* **1910**, *83*, 357.
(3) Hinds, W. C. *Aerosol Technology*; John Wiley& Sons: New York, NY, 1999.
(4) Zeleny, J. *Phil. Mag* **1898**, *46*, 120-154.
(5) Nolan, J. *Phys. Rev.* **1924**, *24*, 16-30.
(6) Haines, W. B. *Phil. Mag.* **1915**, *30*, 503-509.
(7) Langevin, P. *Comptes rendus* **1907**, *140*, 232-234.
(8) Langevin, P.; Moulin, M. *Radium* **1907**, *4*, 218-229.
(9) Hewitt, G. W. *Trans. Amer. Inst. Electr. Engr.* **1957**, *76*, 300-306.
(10) Whitby, K. T.; Clark, W. E. *Tellus* **1966**, *18*, 573-586.
(11) Liu, B. Y. H.; Whitby, K. T.; Pui, D. Y. H. *APCAJ* **1974**, *24*, 1067-1072.
(12) Mikasai, M. *Pap. Meteorol. Geophys.* **1950**, *12*, 247-260.
(13) Matisen, R.; Miller, F.; Tammet, H.; Salm, J. *Tartu Ulikooli Toimetised* **1992**, *947*, 60-67.
(14) Knutson, E. O.; Whitby, K. T. *J. Aerosol Sci.* **1975**, *6*, 443-451.
(15) Winklmayr, W.; Reischl, G. P.; Lindner, A. O.; Berner, A. *J. Aerosol Sci.* **1991**, *22*, 289-296.
(16) Chen, D.-R.; Pui, D. Y. H.; Hummes, D.; Fissan, H.; Quant, F. R.; Sem, G. J. *J. Aerosol Sci.* **1998**, *29*, 497-509.
(17) de la Mora, J. F. *Trends Anal. Chem.* **1998**, *17*, 328-339.
(18) Reischl, G. P. *J. Aerosol Sci.* **1991**, *22*, 297-312.

(19) Stolzenburg, M. R.; PhD thesis; University of Minnesota: Minneapolis, MN, 1988.
(20) Rosser, S.; de la Mora, J. F. *Aerosol Sci. Technol.* **2005**, *39*, 1191-1200.
(21) Chen, D.-R.; Pui, D. Y. H. *J. Aerosol Sci.* **1997**, *28*, 985-1004.
(22) Fuchs, N. A. *Geofis. Pura Appl* **1963**, *56*, 185-193.
(23) Reischl, G. P.; Makela, J. M.; Karch, R.; Necid, J. *J. Aerosol Sci.* **1996**, *27*, 931-949.
(24) Alonso, M.; Kousaka, Y.; Nomura, T.; Hashimoto, N.; Hashimoto, T. *J. Aerosol Sci.* **1997**, *28*, 1479-1490.
(25) Adachi, M.; Kousaka, Y.; Okuyama, K. *J.Aerosol Sci.* **1985**, *16*, 109-123.
(26) Wiedensohler, A.; Fissan, H. *Aerosol Sci. Technol.* **1991**, *14*, 358-364.
(27) Hussin, A., Scheibel, H. G., Backer, K. H., & Porstendorfer, J. *J. Aerosol Sci.* **1983**, *14*, 671-677.
(28) Adachi, M.; Okuyama, K.; Kousaka, Y.; Kozuru, H.; Pui, D. Y. H. *J.Appl. Phys.* **1987**, *62*, 350-352.
(29) Kirsch, A. A.; Zagnitko, A. V. *J. Colloid. Interface Sci.* **1981**, *80*, 111-117.
(30) Scheibel, H. G.; Pöstendörfler, J. *J. Aerosol Sci.* **1982**, *14*, 113-126.
(31) Seol, K. S.; Tsutatani, Y.; Camata, R. P.; Yabumoto, J.; Isomura, S.; Okada, Y.; Okuyama, K.; Takeuchi, K. *J. Aerosol Sci.* **2001**, *31*, 1389-1395.

Aim of this Thesis

Differential mobility analysis (DMA) is a method for the analysis of airborne, charged particles as well as molecules and has faced development in the recent decade to reach the single digit nm size range. Low sensitivity and diffusion effects at this size scale pose special problems and allows further optimization of this method. The combination of DMA with electrospray aerosol (ES) generation and its expansion to the nanometer size range also expanded its analytical field of application, leading to a new possibility in the analysis and characterization of nanometer sized biopolymers as proteins, intact viruses and protein complexes, DNA as well as inorganic nanoparticles. The novelty of this method in this size regime makes the estimation of the value of its special qualities compared to other analytical methods still difficult and challenging. For this reasons, experiments within this PhD thesis were conducted to further optimize the ES-DMA method in terms of sensitivity, to determine stability and comparability of results of different DMA instruments, and to apply this method to analytical purposes specially suited for its unique features like high mass range (MDa to GDa), preservation of non-covalent bonds and operation under atmospheric pressure.

The efficiency of conventional Po^{210} chargers for the production of singly charged nanoparticles/molecules, as they are required for DMA, is very low (>1%) and thus limiting its sensitivity. A new, corona discharge based device developed for their replacement was characterized and its efficiency compared to conventional, radioactive charging devices.

As the number of available DMA systems increases steadily, question about reproducibility and stability of different DMA instruments arise. For this reason, globular proteins in the size range of 3 to 14 nm were applied on various ES-DMA instruments, including two instruments identical in construction located in different experienced laboratories. This examination should determine reproducibility and comparability of results obtained with these instruments and may lead to a conclusion about the necessity of implementation of calibration procedures.

Polyamido-amine (PAMAM) dendrimers were investigated for their suitability as calibrants, because they cover a size range between 3 and 15 nm and because of their theoretically uniformity in chemical and spatial terms caused inherently by their synthesis procedure. ES-DMA and MALDI mass spectrometric characterization of PAMAM dendrimers of various generations should determine their uniformity in size and mass and thus confirm or reject their suitability for calibration procedures.

As the used experimental setup also offers preservation of non-covalent bonds/interactions and analysis at ultrahigh molecular weights, the possibility of observing the biospecific attachment of antibodies to an intact virus, which is difficult to obtain with other analytical methods, was investigated. For this purpose, a human rhinovirus was exposed to varying concentrations of a specific binding antibody and analyzed after proper time of incubation.

As ES-DMA operates under atmospheric pressure and particles/molecules remain intact after separation and detection, this method offers opportunity for micropreparative application for enrichment or sampling of virus particles or inorganic nanoparticles. For this reason a “so-called” parallel-DMA (PDMA) with an electrostatic sampler were designed and constructed within this PhD thesis, enabling selective sampling of nanoparticles and subsequent transmission electron microscopic (TEM) characterization of the samples particle fractions. TEM image analysis of the sampled particle fractions should validate the specificity and feasibility of this experimental setup for sampling procedures.

Journal of Nanoscience and Nanotechnology **(2006)**, 6(5), 1474-81

3. Comparison between an Unipolar Corona Charger and a Polonium-based Bipolar Neutralizer for the Analysis of Nanosized Particles and Biopolymers

Christian Laschober[1,3], Stanley L. Kaufman[2], Georg Reischl[1], Günter Allmaier[3]

and Wladyslaw W. Szymanski[1*]

[1] *Institute of Experimental Physics, University of Vienna, A-1090 Vienna, Austria*

[2] *TSI Inc, St. Paul, MN, USA*

[3] *Institute of Chemical Technologies and Analytics, Vienna University of Technology, A-1060 Vienna, Austria*

[*] Author for correspondence.

Address: W. W. Szymanski
Institute of Experimental PhysicsUniversity of Vienna
Boltzmanngasse 5, A - 1090 Vienna, Austria
Tel: +43 1 4277 51109 Fax: +43 1 4277 9511
E-mail: szym@exp.univie.ac.at

Running title: Comparison between Corona Charger and Polonium-based charger

Keywords: Nanoparticles, aerosols, charged particles, biopolymers, electrospray ionization, corona charger, DMA

Abstract

In this work we present results on the charging efficiency of nanoparticles by means of a corona based unipolar charging unit. This device was designed to replace a Po^{210} bipolar charger unit in a commercial electrospray aerosol generator (TSI Mod 3480). The charging efficiency has been investigated for negative and positive charged particles of various chemical composition in the size range between 5 and 18 nm. The corona current has been found to be the most influential operation parameter on the charging efficiency. With a positive electrospray droplet charge and a negatively-biased corona needle, a rapidly decreasing yield of singly positively charged aerosol particles with increasing corona current was found. An increasing yield of negatively charged particles was observed with increasing current of the corona process. Providing appropriate corona settings nanoparticles with charge levels similar to these obtained with a Po^{210} charger were found. At optimal corona settings the yield of singly charged particles was found to be two to four times higher for negative and positive particles compared to bipolar charging. This gain in the charging efficiency increases directly the sensitivity of analysis and enhances all manipulation processes of airborne nanoparticles for which electrical charging is required.

Introduction

Particles and macromolecules of nanometer dimensions (nanoparticles) exhibit special properties compared to bulk of the same materials, such as high specific surfaces, different chemical reactivity, high surface energies and, for nanoparticleand macromolecule aerosols, high mobility. Because of their specific characteristics the monitoring of production and the characterisation of nanoparticles of various chemical compositions have become increasingly important in the last decades. Key applications include the modification of surfaces and surface properties, heterogeneous catalysts[1-3] and local drug delivery[4-8]. Another broad field of application for nanoparticles is their use as starting material for sintering processes, to provide very homogeneous mixtures and a high surface energy which is beneficial for such processes and product properties[9-12]. In the rapidly growing area of biotechnology particles and complexes of nanosized dimension formed from biomacromolecules such as ribosomes, lipoproteins, semisynthetical DNA-protein conjugates, which are used for high affinity immunological recognition agents and which offer properties for the construction of biochips[13] . Furthermore nano-objects of interest are the so called supramolecular complexes, which e.g. are used to generate microelectronical molecular devices [14] nanowires[15] , and functionalised polymer particles, which are also investigated for microelectronic purposes [16]. Adverse health effects and occupational health issues[17-20] of nanosized aerosols increase the importance of investigating the concentration and the physical and chemical properties of the ubiquitous nanoparticles in the ambient air.

The generation of such airborne nanoparticles can be accomplished by an evaporation/condensation technique, from which usually uncharged polydisperse nanoparticles are obtained; or with an electrospray process, from which usually highly charged particles with a broad charge distribution are obtained. Because the charge of these nanoparticles varies over wide limits they cannot easily be analyzed/separated based on their electrical mobility in the gas phase, which is unfortunate because this is otherwise a very convenient method for characterisation and analysis[21-23]. For this reason a controlled charging/neutralisation process of such particles is highly desirable.

One way to influence the charge distribution of nanoparticles under standard conditions is diffusion charging, in which ions in a carrier gas reach the particles by diffusion.

This can be performed either in a bipolar ion environment (in which ions of both charge signs are present), or in a unipolar ion environment (containing ions of one sign). Bipolar ions are easily generated in air by ionising radiation such as α- or β-radiation produced by radioactive materials such as ^{85}Kr, ^{241}Am or ^{210}Po. Primary gaseous ions such as H^+, H_3O^+, N_2^+, O_2^+, NO^+, O^-, O_2^-, and NO_2^-, are formed in this process and interact rapidly to form cluster ions such as $(H_2O)_nH_3O^+$ and $(H_2O)_nX^-$ (n = 1 to 10 and more). Because of their longer lifetime, these cluster ions control the subsequent charge levels of the nanoparticles via their thermal motion thus the term "diffusion charging".

In the bipolar charging environment, collisions with ions change the number of charges of the particles one charge unit at a time, at rates determined by the collision rate and the concentration of ions of their charge sign. This process leads to a steady-state charge distribution which is well described by a model due to Fuchs[24]. This charge distribution is mainly influenced by the diffusion coefficient of ions, physical properties of the gases, and the "active" surface area of the nanoparticles[24]. Because of the small surface area of a nanoparticle only a small fraction of those particles stays finally charged in this process - a result which is supported by experimental work. The probability for single charging of 10 nm in diameter particles amounts 3 % for positive and 4 % for negative charge sign[25-28]; even smaller values of 0.4% for positive and 0.6% for negative charging are found for particles[28] with 2 nm in diameter. The low charging probability for nanoparticles, the limited lifetime of radioactive materials as well as safety and regulatory problems in their use are the main reasons for attempts to replace the widely employed radiation-based bipolar chargers with alternative devices[26,29-33] .

Unipolar ions have been produced in various charger designs using corona discharge [33,34] and the extraction of ions from a bipolar ion environment [29,30,32]. All experimental results found a six times higher extrinsic charging efficiency of unipolar chargers compared to bipolar charging units for positively and a ten times for negatively charged particles with a diameter of 10 nm[29,30,32-34] . Here we present first experimental results of the charging performance for chemically different particles between 5 and 18 nm in electrical mobility diameter generated by an electrospray process (in the cone-jet mode) coupled with a corona charger.

Experimental

Materials

Protein sample solutions.

Protein samples, typically in the concentration range 2–5 μg ml^{-1}, were prepared in 20 mM aqueous ammonium acetate solutions. A solution pH of 5 was chosen , which is below the pI value of the proteins (the pI is defined as the pH value for the isoelectric point – a gross neutral charge state of a given substance in solution), thus ensuring a positive net charge of the proteins in the starting solution. Although this initially promotes attachment of the protein on the negatively charged capillary wall, it is thought that the resulting monolayer of protein subsequently prevent further electrical attraction and thus prevents a progressive decrease in the protein aerosol output. The 20 mM aqueous ammonium acetate buffer system was chosen because it has the required conductivity to generate a stable 'cone jet' electrospray ionisation mode[35]. Furthermore it simulates physiological conditions (pH and ionic strength) and is completely volatile, which prevents residue particle formation and peak broadening as well as size shifts due to non-volatile components remaining on the nanoparticles (e.g. protein molecules).

Streptavidin (Sigma-Aldrich, S4762) forms a very stable complex composed of four identical subunits, thus the peak in the size spectra (Fig. 1a) represents particles formed from the native tetramer complex

Thyroglobulin sample (Calbiochem, 609310) was used for the preparation of the spray solutions It should be noted that the Thyroglobulin solution was partly chemically reduced and thus contained a mixture of free subunits and intact protein molecules resulting in a size spectra with two peaks representing the subunit and the intact protein species.

Furthermore intact Immune Globulin G (Sigma-Aldrich, 56834) was used for the preparation of a sample solution.

Silica nanoparticle suspensions.

The silica nanoparticles are commercially available in a 40% w/w 1% NaOH solution (Sigma-Aldrich; Ludox® HS-40 colloidal silica). This solution was diluted 1/1000 in a 20 mM ammonium acetate buffer solution adjusted to a pH value of 9, to ensure a negative charge of these particles in solution and to prevent these particles from aggregation, which would lead to capillary clogging over time.

The concentrations of proteins and silica particles in the solutions were adjusted according to the average droplet diameter produced by the electrospray process to ensure the dominating abundance of mainly "so called" monomers (one particle per aerosol droplet) and only a negligible number of airborne dimer particles (two particles per aerosol droplet) yielding a highly uniform test aerosol.

Sucrose solution

A 10% v/v sucrose stock solution (0.158g mL^{-1}) was prepared from commercially available sucrose (Sigma-Aldrich Nr.179949). From this solution 1/100 v/v (1.58 mg ml^{-1}); 1/500 v/v (0.31 mg ml^{-1}); 1/2000 v/v (79 µg ml^{-1}) and 1/8000 v/v (17.5 µg ml^{-1}) dilutions in an aqueous 20 mM ammonium acetate buffer were prepared. The electrospray process produces primary droplets whose average diameter depends on the conductivity of the solvent and the flow rate through the capillary[35-37] as well as the inner diameter of the capillary. After the evaporation of the solvent, solid sucrose residue particles with a diameter corresponding to the sucrose concentration and primary droplet size were formed. Under the applied conditions the sucrose solutions formed particles of 15.1, 8.8, 6.3 and 4.6 nm in electrical mobility equivalent diameter[22]. These residue particles were used like the other particles to investigate the charging performance of the corona discharge unit.

The size spectra of the protein and silica nanoparticle aerosol are presented in Fig. 3.1 a, and the size spectra of the electrosprayed and dried sucrose solutions are presented in Fig. 3.1 b. The peak maxima values of measured distributions of each test aerosol were used for the subsequent data analysis in the charging experiments.

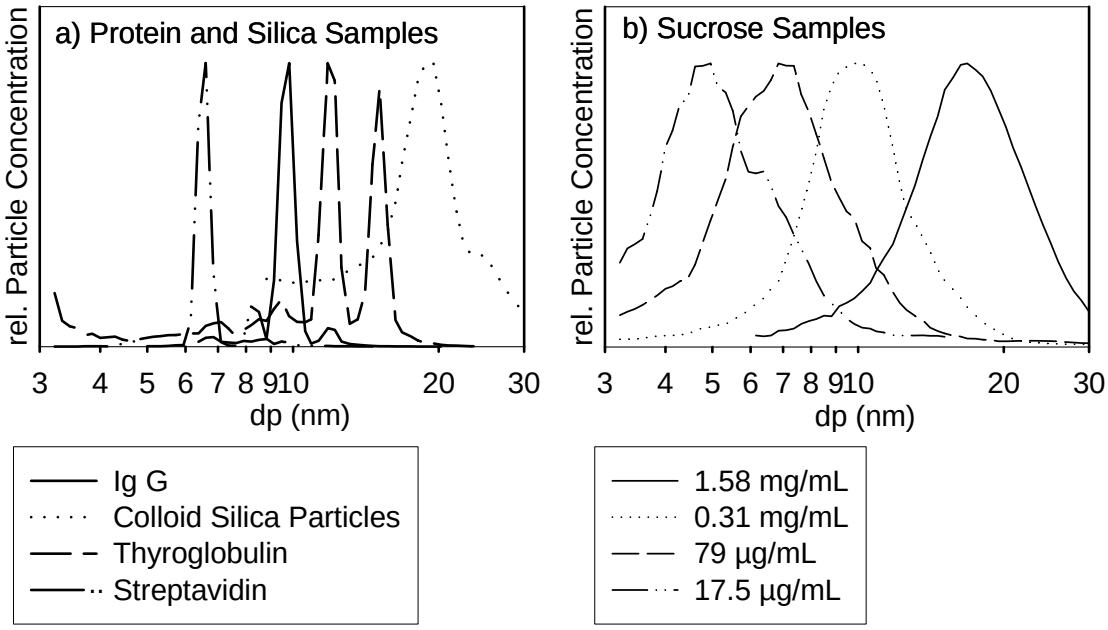

Fig. 3.1 Size spectra of the different types of nanoparticles

Instrumentation

Electrospray-Corona-Jet (ES-C) ***unit***

The ES-C unit consists of three separate chambers, the electrospray ionisation chamber (Fig 3.2, a) and the corona discharge chamber (B), which are separated by the mixing chamber (C). The corona discharge is produced by a platinum needle positioned in approximately 1 mm distance to an orifice plate (durchmesser) (Fig. 3.2 b). The aerosol inlet of the electrospray and the gas inlet from the corona chamber are positioned opposite to each other and perpendicularly to the outlet of the mixing chamber, where the air stream from the corona and the electrospray ionisation chamber unite and the positively charged aerosol with the negatively charged cluster ions interact. This leads to a kind of electrostatic charge titration process yielding an aerosol with an average charge level defined by the operating conditions of the ES-C unit.

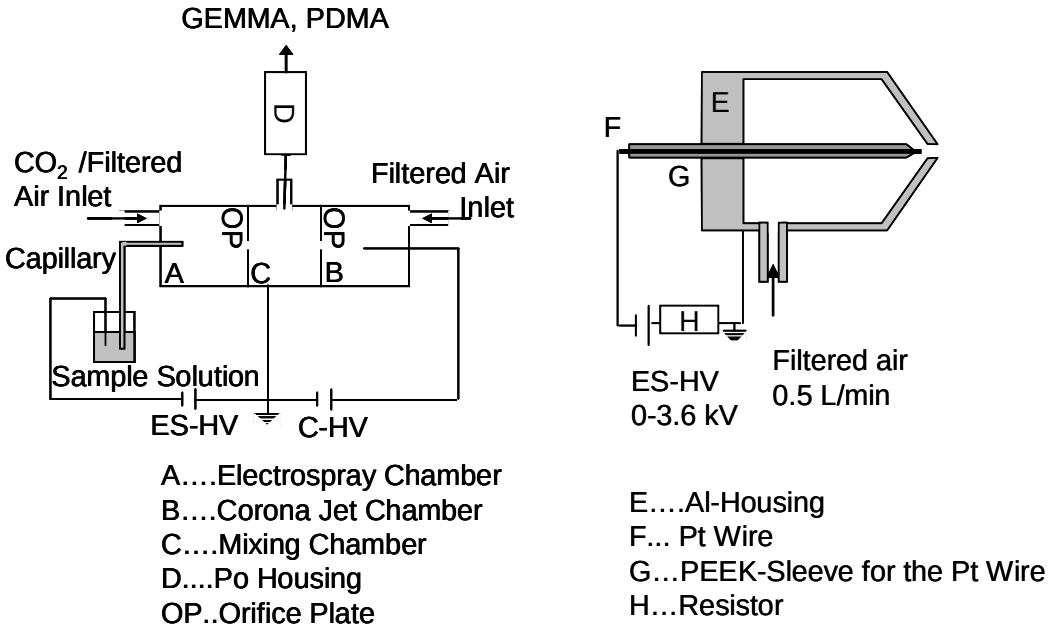

Fig. 3.2 a) Schematic of the Corona Jet unit b) Details of the Corona Jet Chamber

(a) Corona settings

To obtain stable corona operation it was necessary to set the corona chamber air flow slightly above 0.5 l/min. The increasing of the air flow through the corona chamber significantly beyond 0.5 l/min had no influence on the charging outcome, except for dilution effects; therefore during the experiments only the corona high voltage (C-HV) was varied. The C-HV applied between corona needle and orifice plate (OP), determined the amount of negative charges which enters the mixing chamber and interacts with the highly positive charged aerosol from the electrospray ionisation chamber. The corona unit has been operated with C-HV settings between 2.4 and 3.6 kV which resulted in a corona current between 4.5 and 15 µA with linear response between voltage and current, yielding stable experimental conditions.

(b) Electrospray ionization settings

The ES-C was in all cases operated under identical settings, buffer concentrations and solution conductivity. In every case a 20 mM ammonium acetate buffer with a pH of 5 for protein and sucrose solutions and a pH of 9 for silica particle suspensions were electrosprayed.

The optimal operating conditions for this solvent system and spray-chamber design providing a stable cone-jet and a stable aerosol concentration were 2 kV ES-HV, 0.3 L/min CO_2 (Air Liquide N45) and 1L/min compressed air (Air Liquide synth. Air 5.0). A pressure drop of 4 psi between the sample and the spray chamber was applied, which resulted in a sample solution flow of 67 nL/min through the fused silica capillary (25 µm inner diameter, *160 µm outer diameter).*. The primary droplet size, which is determined through the conductivity of the solvent and the sample flow through the capillary as well as the inner diameter of the capillary was 150 nm, thus a flow of 2×10^{11} droplets per minute or about 1.7×10^{8} droplets per cm³ was produced. The electrospray was operated in the positive ion mode, which means that droplets with a high positive initial charge were produced.

Gas Phase Electrophoretic Mobility Macromolecule Analyzer (GEMMA) **.**

The GEMMA system (TSI, 3980) consists of an electrospray unit (TSI 3480), a nano differential mobility analyzer (nDMA) and an ultrafine condensation particle counter (uCPC) as detector. The operating particle size range of the GEMMA is between 3 nm (restricted by the particle detection with the uCPC) and 65 nm (the upper scan limit of the nDMA when using maximum sheath flow for best resolution). In this system the central electrode of the nDMA was operated with negative polarity during these experiments, thus analysing the positively charged fraction of the aerosol in question. The detection limit of the complete GEMMA system in terms of particle number concentration is 1 particle / cm³, however aerosols with concentrations of at least 100 particles / cm³ should be used to obtain good particle count statistics across the whole size range within a reasonable time frame.

Parallel nano- differential mobility analysing system (PDMA)

The PDMA system is an advanced *in-house* development (Institute of Experimental Physics, University of Vienna) of the long existing electrostatic particle separation technology, called differential mobility analyser (DMA)[38] combined with electrical aerosol detection device working on the Faraday cup principle[28]. Parallel with the scanning DMA an identical separation DMA is operated for sampling or enrichment of the selected nanoparticles, hence the acronym PDMA[39].

The most recent engineering solutions (instrument design details will be published elsewhere) extended the lower detection limit of the PDMA system well below 1 nm in terms of the electrical mobility diameter. The prerequisite for this detection method is the necessity of a certain minimum number of charged particles (concentration) needed to achieve measurable electrical signal. The detection limit of this system is currently in the order of 10^2 charged particles per cm^3; however concentrations of 10^3 particles / cm^3 and above are needed to ensure good statistics for a 60 sec scan of the spectrum.

The PDMA was operated under conditions allowing to reach a maximum particle size of 90 nm in particle diameter with high voltage of positive polarity applied to the central electrode of the particle mobility analyzer, thus analysing the negatively charged aerosol fraction.

Both systems (GEMMA and PDMA) function at atmospheric pressure and were operated in the scanning mode yielding a particle size spectrum measured over the complete range of each instrument within two minutes. This cycle time was chosen as compromise between good particle count statistics to obtain satisfying signal-to-noise ratios (above 5:1), and time interval necessary for the completion of correlated measurements concerning one sample and one polarity of charges within the long-term stability period of the experimental setup, especially the electrospray.

Particle neutralization chamber with and without Polonium (Po^{210}) source

The neutralization chamber consist of a brass housing 170 mm long and 30mm inner diameter with a Po^{210} strip (Osmonics, electrostatic eliminator; nominal radioactivity of 500 microcuries = $1.9x10^7$ Bq) mounted on the inner wall without any obstruction of the air flow inside. The neutralization chamber was connected to the exit of the mixing chamber of the ES-C unit. The aerosol flow through the chamber was kept at 1.8 L/min. The residence time of the aerosol inside the neutralization chamber was 5 s under the selected experimental conditions which was sufficient for the aerosol to reach the well defined Fuchs´ charge equilibrium in experiments with the mounted Po^{210} strip. The Polonium strip could be removed from the chamber for comparison measurements as described below.

(a) Po^{210} strip mounted in the chamber:

The Po^{210} strip provides a stable alpha radiation, producing a bipolar ion environment inside the housing. The residence time of 5 s for the aerosol in question inside the neutralisation chamber proved in experiments to be sufficient to reach the Fuchs charge equilibrium[24,40] and thus defining a well known fraction of singly charged nanoparticles. The total particle number concentration of positively or negatively charged particles thus determined was used as reference for the determination of the charging efficiency of the ES-C unit.

(b) Po^{210} strip removed from the chamber

The passage of the aerosol through the empty (without strip) neutralization chamber should simulate diffusion losses which occur inside the neutralisation chamber during the experiments with the Po^{210} strip, too; whereas the charging state of the aerosol produced by the ES-C unit should be unaltered in these experiments. The amount of charged particles determined in these experiments with Po^{210} strip (as example see Fig 3.3 a and b, plot i) and the concentration of charged nanoparticles determined in the experiments with removed Po^{210} strip (as example see Fig 3 a and b, plot ii) will then only differ in the charging efficiency of the processes taking place inside the mixing chamber and the neutralizing chamber, since electrospray ionization settings, test solutions, DMA instrumentation and diffusion losses were practically identical in corresponding measurements.

Five full scan spectra were averaged for each data point (Fig. 3.4) involving one analyte particle, corona current setting, polarity and either mounted or removed Po^{210} strip. The standard deviation of the concentration values of the most abundant nanoparticle species, which was selected for further data analysis of correlated measurements, was typically +/- 1-3%, reflecting a good stability of the ES-C unit, the applied DMA analysers and the different particle detection systems during all experiments.

As stated before the DMA of the GEMMA system was operating with negative voltage at the central electrode, thus all results concerning positive charged aerosol particles were obtained with the GEMMA system; the PDMA was operated with positive voltage at the central electrode, thus detecting the negative charged aerosol fraction.

Results and Discussion

The charged number nanoparticle concentrations obtained in the experiments with the Po^{210} charger concerning one sample was virtually constant and thus largely independent of the corona current. (Fig 3.3 a and b, plot i). This allows the conclusion that the aerosol production by means the electrospray unit and diffusion losses of the highly charged particles inside the mixing chamber were not influenced by the corona current settings. The typical RSD of measured particle concentrations of each analyte averaged over all applied corona currents was 10-15%.

The average value of the concentration of singly charged particles over all corona current settings was used for the normalisation of all experimental data concerning the same analyte and polarity, indicated as dashed line in Fig 3.4 a and b. At corona current settings below 5 µA the corona discharge and the production of the negative ions and thus the corona current ceased and no detectable signal of singly charged particles was observed. The reason for this is the high mobility and the high charge of the nanoparticles after the electrospray ionization process, which leads to high particle losses due to Coulomb repulsion between the particles and to electrostatic forces resulting from isolated charges at the tubing and the inner walls of the device.

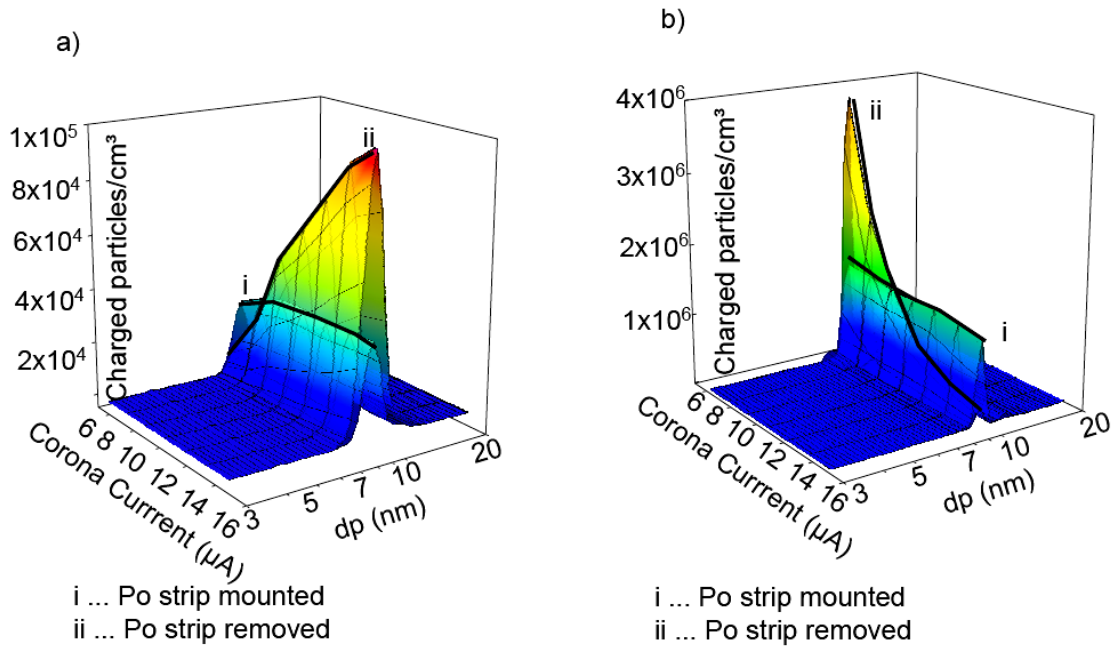

Fig. 3.3 Plot of the charged particle concentration vs. corona current vs. particle size
a) Immune globulin G ,negatively charged particle fraction;
b) positively charged particle fraction

As can be seen in Fig 3.4 a) a clear decrease of the charged particle number concentration with increasing corona current can be observed for all measured analytes and particle diameters. The charged particle number concentrations of all experiments with a given analyte were normalised with the average charged number concentration obtained in the corresponding experimental series with the Po^{210} charger installed in the neutralising chamber housing.

The normalised number concentrations thus obtained reflect the relative charging efficiency of the unipolar neutralisation process compared to the traditional bipolar charging process using the radioactive source.

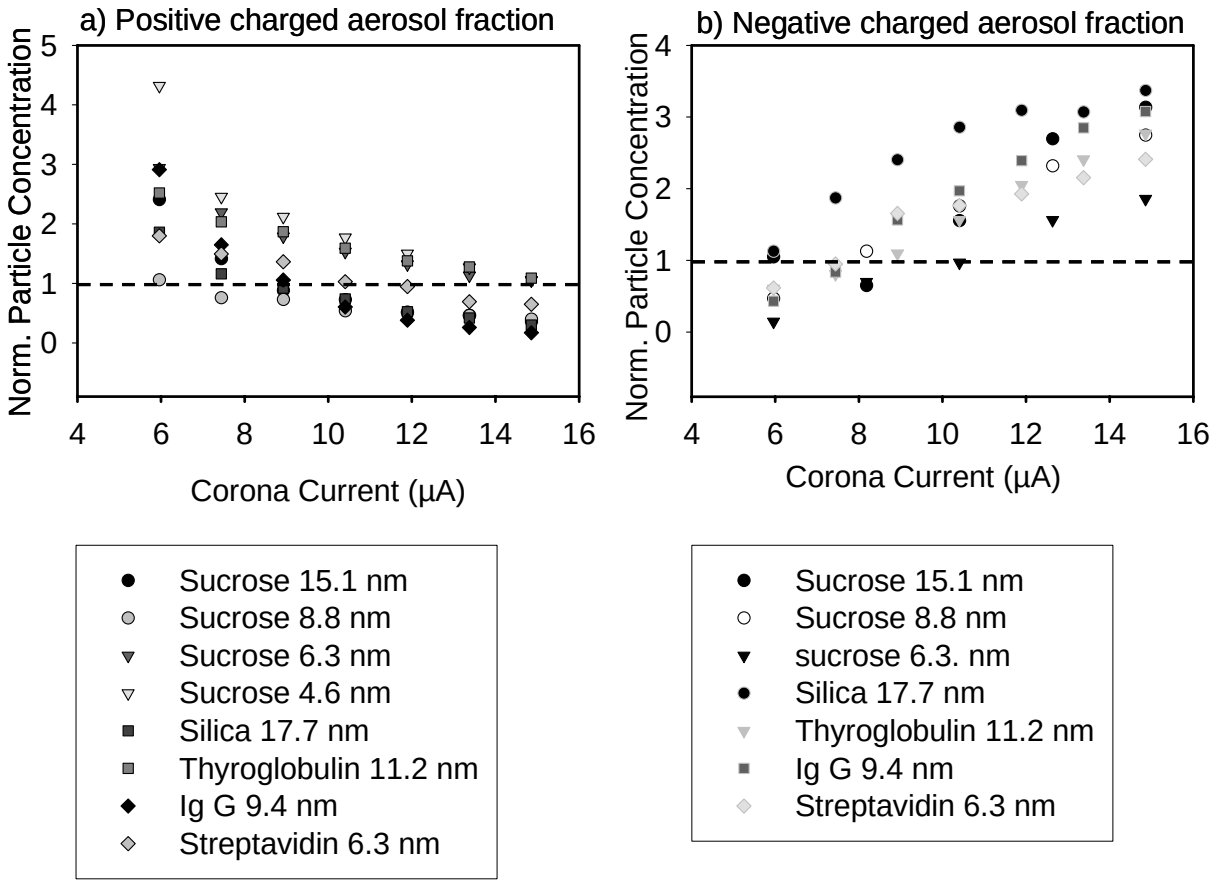

Fig. 3.4 Normalized charged particle concentration

These relative number concentrations are furthermore independent of total analyte particle concentrations and allow the comparison of experiments with different types of analytes; the only remaining influencing parameters are the chemical surface properties of the analytes and their particle size. For high corona currents the measured aerosol fraction is comparable with the yield of the radioactivity based bipolar particle charging.

(a)Positively charged aerosol fraction

With decreasing corona current, and thus less produced negative cluster ions produced, the positively charged aerosol fraction becomes larger, for 6 μA corona current a 2-5 times higher signal can be observed. This trend is understandable since aerosol nanoparticles produced by the electrospray ionisation process are highly positively charged while negative ions are extracted from the corona chamber.

These two streams are, as stated before, subsequently mixed in the mixing chamber, where the positively charged aerosol particles and the negative cluster ions interact, resulting in gradual decrease of the particle charged fraction - a kind of charge titration. The final concentration of singly, positively charged particles is then dependent on a competition between particles being positively charged due to electrospray process and negative cluster ions entering the mixing chamber. Because this process is influenced by the corona current and indeed the yield of a corona driven charger can indeed substantially exceed the yield of a radioactive source charger depending on the corona operating parameters. No obvious correspondence between particle diameter and the enhancement of the yield of singly charged particles compared to bipolar charging was observed.

(b) Negatively charged aerosol fraction

In contrast with the results for positively charged aerosol fraction, an increase of the concentration of negatively charged particles with the increase of the corona current is observed (Fig. 3.4 b). At the maximum of a corona current of 15 μA a significant increase in the yield of negatively, singly charged particles in comparison with the Po^{210} charger can be observed. Moreover, in contrast to the positively charged particle fraction the particle size seems to have a qualitative influence on the augmentation of the charged particles, with a 2 times higher yield of singly charged particles of 5 nm in diameter and 4 times higher yield compared to bipolar charging for particles of 16 nm in diameter.

A by far smaller correlation between particle size and the enhancement of the charged particle fraction of unipolar charging compared to bipolar charging was observed unlike to results found in literature[29,32,33] where a 2 fold yield of charged particles of 3 nm in diameter and a 10 fold yield of singly charged particles 10 nm in diameter of unipolar charging compared to bipolar charging was observed.

This may be caused by several factors. The observed process in our case was not the charging of neutral or singly charged particles as in before mentioned experiments of other authors, but the neutralisation of highly charged nanoparticles produced by the electrospray process, which is known to produce droplets with high initial charge.

Another difference is that the investigated nanoaerosol particles in this work varied not only in size but consisted of different compound classes such as sucrose, various proteins and silica particles, which should reflect the whole variability of analyte groups accessible for the electrospray ionisation and thus relevant for the examination of the charging process of the electrospray-corona unit. The charging process and final charge state of aerosols after the electrospray procedure is known to be strongly dependent on the chemical surface properties of the used test substances. This initial variation in the charge state of investigated aerosols before the unipolar neutralisation step takes place is likely to be large enough to mask size dependant effects of the charging/neutralisation process inside the mixing chamber.

Conclusion

The performance of a newly developed unit combining of a corona discharge - based unipolar particle neutraliser/charger and a nano-electrospray ionisation source was investigated and characterized as well as compared with a broadly used, conventional Po-based bipolar particle neutralizer/charger. The results show that operating corona discharge parameters are critical for control of the neutralisation/charging process. In consequence it is possible to generate using this process positively, as well as negatively singly charged aerosol nanoparticles. A nanoparticle yield increase in comparison with Po-based charging between a factor of about 2 to 4 of the negatively as well as positively charged nanoaerosol fraction was found at the highest respectively lowest operating current of the corona discharge unit. Considering that singly charged nanoparticles are absolutely essential for the functioning of electrostatic sizing devices such as nano-DMAs and that charging processes especially in the size range below 20 nm are still rather inefficient, the obtained results are very promising. Corona discharge seems to be an excellent alternative for charge level control of electrosprayed nanoparticles compared to radioactivity based devices. It is important to note that the yield of such devices can be controlled and that the charge control process results always in singly charged particles with concentrations determined by the corona. For both differential mobility systems used in this study (GEMMA and PDMA) not only better signal to noise ratio was obtained when compared with the radioactive charge manipulator, but thanks to higher concentrations of particles the scanning speed can be increased without the loss of quality of the measured spectra. These results will further strengthen the importance of electrostatic mobility analysis of inorganic and bioparticles in the nanometer size range at atmospheric pressure.

Acknowledgment

This work was supported in part by a grant of the Austrian Science Foundation (FWF, Project P16185-N02 to W.W.S.)

References

(1) Zhongai Hu, Y. Y., Xiuli Shang and Hailong Pa. *Mater. Lett.* **2005**, *59*, 1373-1377.
(2) W.Oelerich; T. Klassen; R. Bormann. *J. Alloys Compd.* **2001**, *315*, 237-242.
(3) J.F.R. de Castro; Yavari, A. R.; LeMoulec, A.; Ishikawaand, T. T.; Botta, W. J. *J. Alloys Compd.* **2005**, *389*, 270-274.
(4) L. Mu; M. MTeo; H. Z.Ning; C. S. Tan; Feng, S. S. *J. Control. Release* **2005**, *103*, 565-575.
(5) Gupta, A. K.; Gupta, M. *Biomaterials* **2005**, *26*, 3995-4021.
(6) Z. Z.Li; L. X. Wen; L.Shao; Chen, J. F. *J. Control. Release* **2004**, *98*, 245-254.
(7) Broska, M.; Langer, K.; Coester, C.; Loitsch, S.; Wagner, T. O. F.; Mallinckrodt, C. V. *Biochem. Biophys. Res. Commun.* **2004**, *318*, 562-570.
(8) Sanjeeb K. Sahoo; Labhasetwar, V. *Drug Discov. Today* **2003**, *8*, 1112-1120.
(9) V. Buscaglia; M. Viviani; M.T. Buscaglia; P. Nanni; L. Mitoseriu; A. Testino; E. Stytsenko; M. Daglish; Zhao, Z.; Nygren, M. *Powder Technol.* **2004**, *148*, 24-27.
(10) Ji-Guang Li , Y. W., Takayasu Ikegami, Toshiyuki Mori, Takamasa Ishigaki. *Mate. Sci. Eng.B* **2005**, *121*, 54-59.
(11) A. Hirvonen; R. Nowaka; Y. Yamamoto; T. Sekino ; Niihara, K. *J. Eur. Ceram. Soc.* **2005**, *Article in press*.
(12) Groza, J. R. *Nanostruct. Mater.* **1999**, *12*, 987-992.
(13) Niemeyer, C. M. *Trends Biotechnol.* **2002**, *20*, 395.
(14) Wei, Y. *Supramol. Sci.* **1998**, *5*, 723.
(15) Franco Cacialli, P. S., Carlos Silva. *Mater. Today* **2004**, 24.
(16) J.L. Hernandez-Lopeza, R. E. B., W.-S. Changa, G. Glassera, D. Grebel-Koehlera,M. Klappera, M. Kreitera, J. Leclaireb, J.-P. Majoralb, S. Mittlera, K. Mullena, K. Vasileva, T. Weila, J. Wua, T. Zhua, W. Knolla. *Mater. Sci. Eng.* **2003**, *23*, 67.
(17) Kittelson, D. B. *J. Aerosol Sci.* **1998**, *29*, 575-588.
(18) K. Donaldson; Li, X. Y.; MacNee, W. *J. Aerosol Sci.* **1998**, *29*, 553-560.
(19) Maynard, R. L. *Atmos. Environ.* **2000**, *34*, 2667-2668.
(20) Roco, M. *J. Nanopart. Res.* **2005**, *7*, 129.
(21) G. Allmaier; G. Bacher; S. Kaufman; Szymanski, W. W. *J. Aerosol Sci.* **1999**, *30*, 303.
(22) Bacher, G.; Szymanski, W. W.; Kaufman, S. L.; Zöllner, P.; Blaas, D.; Allmaier, G. *J. Mass Spectrom.* **2001**, *36*, 1038-1052.
(23) G. Allmaier; Szymanski, W. W. In *Nanostruct. Mater. Appl.*; Szymanski, W., Itho and Odachi, Ed.; Facultas: Vienna, 2004.
(24) Fuchs, N. A. *Geofis. Pura Appl* **1963**, *56*, 185-193.
(25) Hussin, A., Scheibel, H. G., Backer, K. H., & Porstendorfer, J. *J. Aerosol Sci.* **1983**, *14*, 671-677.
(26) Adachi, M.; Kousaka, Y.; Okuyama, K. *J.Aerosol Sci.* **1985**, *16*, 109-123.
(27) Alonso, M.; Kousaka, Y.; Nomura, T.; Hashimoto, N.; Hashimoto, T. *J. Aerosol Sci.* **1997**, *28*, 1479-1490.

(28) Reischl, G. P.; Mäkele, J. M.; Karch, R.; Necid., J. *J. Aerosol Sci.* **1996**, *27*, 931-949.
(29) P. Büscher; A. Schmidt-Ott ; Wiedensohler, A. *J. Aerosol Sci.* **1994**, *25*, 651-633.
(30) A. Wiedensohler; P. Büscher; H.-C. Hansson; B.G. Martinsson; F. Stratmann; G. Ferron ; Busch, B. *J. Aerosol Sci.* **1994**, *25*, 639-649.
(31) F.J. Romay; D.Y.H. Pui; Adachi, M. *Aerosol Sci. Technol.* **1991**, *15*, 60-68.
(32) Da-Ren Chen; Pui, D. Y. H. *J. Nanopart. Res.* **1999**, *1*, 115-126.
(33) Hernandez-Sierra, A.; Alguacil, F. J.; Alonso, M. *J. Aerosol Sci.***2003**, *34*, 733-745.
(34) Kruis, F. E.; Fissan, H. *J. Nanopart. Res.* **2001**, *3*, 39-50.
(35) D.R. Chen; D.Y.H. Pui; Kaufman, S. L. *J. Aerosol Sci.* **1995**, *26*, 963-977.
(36) Prunet-Foch, M. C. a. B. *J. Electrostat.* **1989**, *22*, 135-159.
(37) A. Gomez; Tang, K. *Phys. Fluids* **1994**, *A6*, 404-414.
(38) Liu, B. Y. H.; Pui, D. Y. H. *J. Aerosol Sci.* **1975**, *6*, 249-264.
(39) Allmaier, G.; Laschober, C.; Reischl, G. P.; Szymanski, W. W.: Austrian pat. No A1327 (2005) pending.
(40) W. A. Hoppel; Frick. *Aerosol Sci. Technol.* **1986**, *8*.

Journal of Experimental Nanoscience, to be submitted (2007)

4.Comparison of various nano-differential mobility analyzers (nDMAs) applying globular proteins

C. Laschober[†┼], C. S. Kaddis[‡], G.P. Reischl[┼], J.A. Loo[‡], G. Allmaier[†] and W.W. Szymanski[┼],

[†] Vienna University of Technology, Austria
[┼] University of Vienna, Austria
[‡] University of California, Los Angeles, US

Abstract:

The demand for analysis of nanosized particles and assemblies of organic and inorganic origin has increased in the recent decade together with the growing development of biotechnology and nanotechnology. Recent developments of Electrostatic Differential Mobility Analysis (DMA) managed to provide an excellent characterization tool in the nanometer size range. This method has been successfully applied to the analysis of proteins, protein complexes, viruses, polymers and inorganic particles. With an increasing number of available nDMA systems, a question about comparability and implementation of possible calibration procedures arise. Here we present analysis of proteins in a range between 5.7 kDa (3nm) and 660 kDa (15nm) with five different nDMA systems. Results show differences in the obtained sizes up to 15% between different nDMA system, which consequently leads to the conclusion that a calibration procedure for nDMAs is necessary when applying such systems for the analysis of nanoparticles.

1.Introduction

Mobility analysis is a long established method in aerosol physics[1]designed to characterise ions and charged particles according to their electrostatic mobility, to analyze ambient aerosols and aerosol products of combustion processes and to measure the formation and alteration of atmospheric aerosol particles[1,2]. The working range of DMA for these purposes is typically in the sub-µm to µm range. In the recent decade, mobility analysers were optimised and further developed to expand their working range into the single digit nanometer range, or in terms of mass, into the kDa range[3-5]. This expansion of the working range enabled this technique to be applied in the broad field of chemistry and physics for the analysis of polymers, inorganic nano-sized particles, biopolymers and larger assemblies, such as viruses.

The advantage of this method compared to mass spectrometry is its high dynamic range in terms of mass (kDa to GDa)[4]. Combined with aerosol generation from liquid samples with nano-electrospray sources[6,7] (n-ES) and subsequent neutralisation of the highly charged aerosol [8-10], this method has already been successfully applied in analyzing important biochemical species, such as viruses and virus fragments[4,11], bacteriophages, DNA[12], proteins and protein complexes[4,13], as well as synthetic materials, such as polyethylene glycol polymers [14], polystyrene [15] and nanometer sized silica particles[16].

With increasing importance of this method, a need for determination of important analytical parameters, such as precision and accuracy, arises. Until now, DMAs were mainly characterised in a sequential setup[17-21], in which a first mobility analyser produced monodisperse aerosol from a polydisperse aerosol source, and a second mobility analyser scanned the size distribution produced by the first one. This setup enabled the comparison of the quality of the mobility analysis in terms of resolution and particle diffusion, but opens field for interpretation of results, because both DMAs have influence on the characteristics of the resulting size spectrum.

In investigations reported here we produced a monodisperse test aerosol by using various globular proteins in the size range between 3 and 16 nm. The monodispersivity of the so produced test aerosol is ensured by the inherent uniformity of the protein particles, simplifying the experimental set-up and allowing an independent characterisation of the sizing performance of various DMAs. Size spectra obtained with two Vienna-type nDMAs [17,22], two identical commercially available nDMAs (GEMMA, TSI) and a GEMMA prototype[4]were analysed according to position, spectra quality and stability. Implications for the routinely application of nDMAs in analysis of nanoparticles of biological, inorganic or polymeric nature are discussed.

.

2. Materials and Methods

2.1 Proteins

Protein stock solutions of about 1 mg/mL were prepared from commercial protein powders with a 20 mM ammonium acetate buffer (pH 6). Because of the negligible salt concentration of the protein samples, it was possible to analyse in buffer diluted solutions without further purification. The concentration of the different proteins was adjusted to give only negligible $2M^+$ signals, which was about 20 µg/mL for proteins > 20 kDA and 5 µg/mL for proteins < 20 kDA. Insulin (5734 Da), ubiquitin (8565 Da), cytochrome C (12.3 kDa), myoglobin (17.6 kDa), carbonic anhydrase (29.0 kDa), ovalbumin (44.6 kDa), avidin (64.0 kDa), bovine serum albumin (66.4 kDa), enolase (93.4 kDa), fibrinogen (339 kDa), ferritin (483 kDa) and thyroglobulin (660 kDa) solutions were used for the production of monodisperse aerosol in this study.

2.2 Nano-Electrospray (N-ES)

The N-ES instrument (Mod. 3480, TSI Inc.) was used for the aerosolization of the protein samples which were electrosprayed in a 20 mM ammonium acetate buffer. For this instrument and solvent system we found that a stable cone-jet mode operation was obtained at 2 kV and 0.3 L/min CO_2 (99.995%, Air Liquide N) and 1 L/min compressed air (99.999% synthetic air, Air Liquide)[16]. A pressure difference of 4 psi between sample and spray chamber was applied, which resulted in a sample solution flow of 67 nL/min through the fused silica capillary (25 µm inner diameter and 160 µm outer diameter, uncoated; supplied by TSI Inc).

The primary generated droplet size, which is determined by the conductivity of the solvent system and the sample flow through the capillary as well as the inner diameter of the capillary was 150 nm, corresponding to a flow of 2×10^{11} droplets per minute or about 1.7×10^{8} droplets per cm³. The nano-ES generator generates highly positively charged droplets, which are then subsequently neutralised in bipolar ion environment obtained with a Po-210 α-radiation source. This process results in mainly singly negatively and positively charged airborne molecules and nanoparticles [8,9]. N-ES settings, buffer concentrations, and solution conductivity were identical for all presented experiments.

2.3 Differential Mobility Analyzers

Gas phase electrophoretic macromolecule mobility analyzer (GEMMA)

The GEMMA system consists of a nano-electrospray (nES) unit, a nano-differential mobility analyzer (nDMA) and an ultrafine condensation particle counter (uCPC) as detector. The operating particle size range of this instrument combination is between 3 nm (limited by the particle detection with the uCPC) and 65 nm (the upper scan limit of the nDMA when using maximum sheath flow for maximum nDMA resolution). The GEMMAs were operated with negative high voltage, thus separating the positively charged fraction of the generated molecules/aerosol particles. The detection limit of the GEMMA system in terms of particle concentration is in the order of one singly charged particle/cm³. However, due to the limited charging efficiency, concentrations of at least 10000 protein particles/cm³ are necessary to obtain appropriate particle count statistics across the whole adjusted sizing range within a reasonable time (120 s per scan). Ten scans were averaged for each final GEMMA spectrum presented in this paper. Both GEMMA systems (Vienna and Los Angeles) were operated under identical settings concerning sheath gas, scan time and size range of the acquired size spectra. Details of the GEMMA prototype and in this paper included results can be found in literature [4].

Parallel nano- differential mobility analysing system (PDMA)

The PDMA system is an advanced in-house development (Faculty of Experimental Physics, University of Vienna) combined with electrical aerosol detection device working on the Faraday cup principle [23]. Parallel to the scanning DMA an identical separation DMA is simultaneously operated for sampling or enrichment of the selected nanoparticles, hence the acronym PDMA.

Recent development extended the lower detection limit of the PDMA system well below 1 nm in terms of the electrical mobility diameter with a length of the central electrode of only 15 mm (Fig. 4.1) The applied detection method needs a certain minimum number of charged particles (concentration) in order to achieve measurable electrical signal.
The detection limit of this system is currently in the order of 10^2 charged particles per cm³; however concentrations of 10³ particles/cm³ and above are needed to ensure good statistics for a 120s scan of the spectrum.

The PDMA was operated under conditions allowing to reach a maximum particle diameter of 50 nm. High voltage of positive polarity was applied to the central elecrtode, thus analysing the negatively charged aerosol fraction. The PDMA was operated under scanning conditions to yield a particle size spectrum within two minutes. Ten spectra were averaged for the presented data of each protein sample.

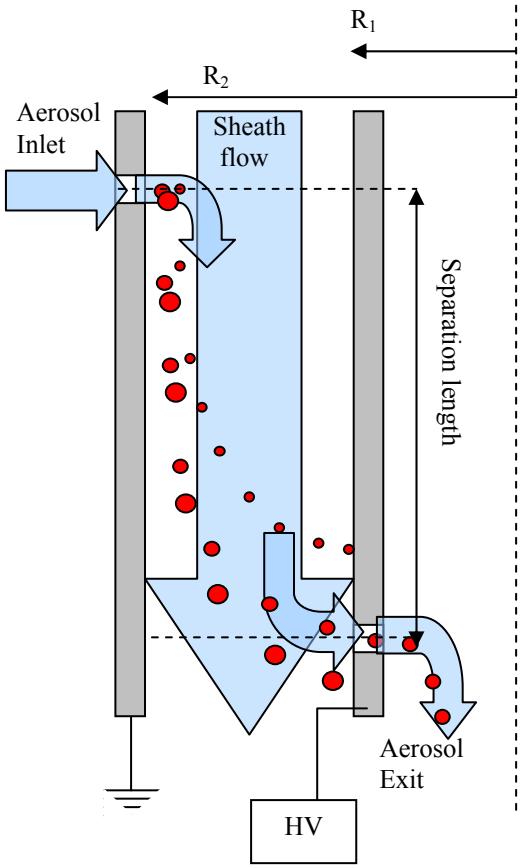

Fig. 4.1 scheme of differential mobility analysis

HV.. High Voltage
R_1... Inner Radius of the central electrode
R_2... Outer Radius of the central electrode

Long nano-differential mobility analyzer (L-nDMA)

The L-nDMA is as the PDMA an in-house constructed DMA. Its difference to the the PDMA is the longer separation path (150 mm) of the central electrode (Fig.4.1), which results in a different sizing range, starting from 2 nm up to 200 nm. The detection system of the L-nDMA is also based on the Faraday-cup principle. This system was used with identical scanning rate (2 sec per channel) as the PDMA and the GEMMA, and thus possesses similar characteristics concerning sensitivity and dynamic signal range.

Properties and settings of all investigated DMAs important for the subsequent comparison and discussion of results are presented in Tab. 4.1

	GEMMA (UCLA,Vienna)	L-nDMA	PDMA	Gemma Prototype
Sheath gas flow	15 lpm	14 lpm	20 lpm	18 lpm
Aerosol flow to sheath gas flow ratio (%)	8.7	9.3	6.5	7.2
Polarity of the Central electrode	Negative	Positive	Positive	negative
Working range	3-65 nm	2-200 nm	0.7-50 nm	3-65 nm
Scan range set in presented experiments	3-25 nm	2-20 nm	1-20 nm	3-65 nm
No. of channels	60	47	68	90
Scan direction	up	down	down	up
Scan rate	2 sec / channel	2 sec/channel	2 sec/channel	2 sec/channel
Detector	CPC	FC	FC	CPC

Tab. 4.1 operating parameters of the n-DMAs

3. Particle diameter determination and resolution in DMA

The DMA has been described extensively in literature[1,3,5,22], so here only key aspects of this technique are summarized. Electrical ion mobility is defined by equation (1) and is the ratio between electrostatic forces and friction that leads to constant particle movement when facing a certain electrical field. The electrical mobility can also be expressed in terms of design and operation parameters of the DMA (Fig.4.1) and leads as a consequence to only one particular size fraction of particles that is analyzed by the DMA at certain sheath gas and voltage settings (Equation 2).

As the number of charges of the analyzed particles is determined by a neutralisation step[8,9], a size spectrum can be obtained by scanning through all size fractions by varying the voltage of the central electrode and by incorporating the charging probability of the analyzed size fractions.

$$Z = \frac{i * e_o}{3\pi\eta} * \frac{C_{(D_P)}}{D_P} \tag{1}$$

$$\frac{i * e_0}{3 * \pi\eta} * \frac{C_{(D_P)}}{D_p} = Q_{sh} * \frac{\ln(R_2 / R_1)}{2\pi * L} * \frac{1}{V} \tag{2}$$

i.....Number of Charges

Z... Electrical Mobility Diameter

R_1,R_2..Inner and outer radius of the DMA electrode

D_P…particle diameter, exiting the DMA for a given voltage

Q_{sh}...Sheath gas flow

L... Separation length of the DMA

$C(D_P)$...Cunningham slip correction factor , equation (3)

$$C_{(D_P)} = 1.0 + 2.492 \cdot \left(\frac{\lambda}{D_P}\right) + 0.84 \cdot \left(\frac{\lambda}{D_P}\right) \cdot \exp\left(-0.43 \cdot \left(\frac{D_P}{\lambda}\right)\right) \tag{3}$$

λ mean free path of the surrounding gas molecules, 65.3 nm at 20 °C and 1 bar

The resolution of a DMA is influenced by the DMA geometry, particle diffusion and physical properties of the sheath gas. Equations (4)-(6) describe the relationship between the resolution of a DMA and conditions in the separation path and particle properties. A detailed discussion about the DMA transfer function can be found in literature[5,22,24,25]

$$\left(\frac{\Delta V}{Vp}\right)^2 = 16 * \ln 2 * \frac{(b + b^{-1}) * G}{Pe} \approx \left(\frac{\Delta Dp}{Dp}\right)^2 \quad (4)$$

ΔV Half width of the in Voltage space normalized peak of a monodisperse aerosol

Vp Voltage setting of the peak center of a monodisperse aerosol

G constant factor from theory [5] which depends on geometry, usually very close to unity

Pe Peclet number (5)

b device parameter (6)

$$Pe = \frac{Q_{sh}}{\pi * D(R_1 + R_2)} \quad (5)$$

D Diffusion coefficient of the ion in question

$$b = \frac{L * G}{R_2 - R_1} \quad (6)$$

As can be seen from equations (4)-(6), several parameters contribute to a DMA performance. Due to particle diffusion, which decreases the resolution and leads to particle losses, transit time through the DMA has to be minimized, which is especially important for particles below 30 nm. This leads to the conclusion that a DMA should be operated with highest possible sheath gas flow (equation 5). To decrease the separation path, the separation length L of the central electrode has to be minimized which also leads to a narrower width (R_2-R_1) within the DMA to minimize the term $b+b^{-1}$ in equation (5) and results in high voltages which have to be applied to the DMA (Fig 4.1).

In practice, engineering of DMAs has shown, that the minimization of the separation length and the increase of the sheath gas flow has its limit, as both leads to too high flow velocities and thus turbulence, which corrupts mobility analysis. Chen et al. [26] found from simulations that the geometry of aerosol inlet and outlet slits has also a substantial influence on establishing a homogenous electrical field and a turbulence free zone behind the inlet and outlet slits. A comparative study of the of the broadening of the transfer function of three identical DMAs [27]showed, that even small differences in the mesh that distributes the sheath flow can lead to a different performance of the DMAs concerning resolution.

The complexity of mobility analysis of such small particles lead to further DMA prototypes in which attempts are made to optimize the transfer function of the DMA in producing turbulence free flows even with extremely high sheath flow rates[28], or, for example, to scan the sheath flow instead of the voltage of the central electrode or to even a DMA with variable separation length[29] [30].

4. Calculation of size spectra values for comparison

The obtained raw size data was first normalized to the maximum height of the analyte peak, which is in the case of the presented size spectra ovalbumine, determined with the PDMA and the GEMMA Vienna (Fig.4.2). The full width at half maximum (FWHM) was determined by measuring the width of the peak at a relative signal intensity of 0.5. The peak midpoint was calculated according to equation (7) for all ten size spectra obtained from one protein sample with a specific instrument. Subsequently all peak midpoints regarding to one protein sample and one DMA instrument were averaged to give a data point at Fig. 4.3. The standard deviation of each peak midpoint was calculated to receive a value that reflects the stability of the DMA analysis on each instrument.

$$M(nm) = \frac{\sum_{i=b}^{e} I_i * D_i}{\sum_{i=b}^{e} I_i} \qquad (7)$$

M ------ Midpoint of the peak

b,e ----- integration borders of the Peak

I_i ------ Signal intensity at the size channel i

D_i ------ Mobility Diameter of the size channel i

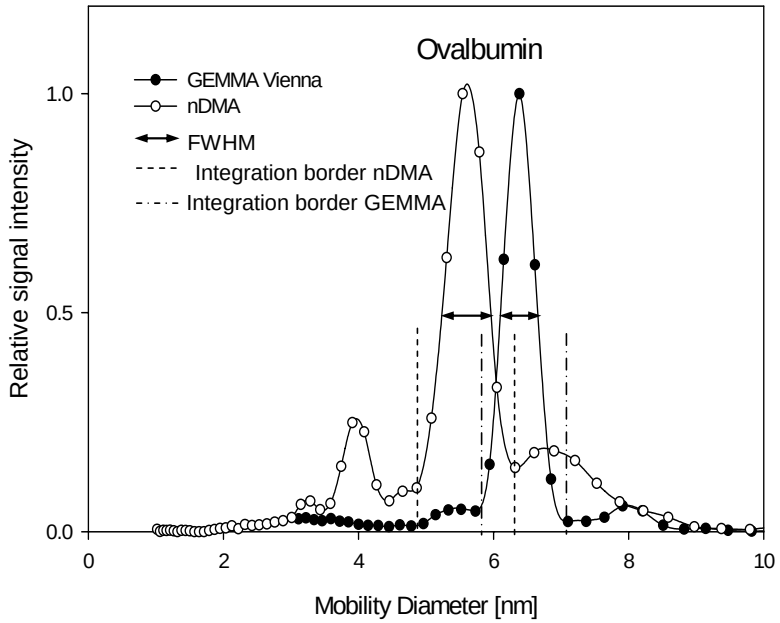

Fig. 4.2 Size spectra of ovalbumin obtained with two different n-DMAs

5. Results and Discussion

The size spectra of ovalbumin obtained with two different nano-DMAs are shown in Fig. 4.2. As can be observed, the two size spectra differ in peak position. As was described in the theoretical section, all parameters necessary to calculate a size spectrum from the raw data, such as gas properties, charging probability of the particles, geometrical parameters, sheath flow rate, are precisely known and implemented in the analyzer software (TSI Inc, University of Vienna[3,17,22]). As both DMA systems whose spectra are compared in Fig.4.2 represent the last developments the observed differences in the resulting size spectra of identical protein particles is rather surprising. The so obtained peak midpoints obtained with different DMA systems are summarized in Fig. 4.3, which shows the position of the peak vs. molecular weight (MW) of with each DMA measured protein samples. As can be seen, the obtained particle diameters are within a certain size interval, with a difference of up to 15%. Also noticeable is the fact the relationship between molecular mass and the particle diameter of the analyzed globular proteins does not follow a certain gradient of the slope. The difference between the investigated nano-DMAs becomes even more significant, as the standard deviation of the peak midpoint for each protein particle was in the order of 0.1% within a series of ten size spectra obtained with one DMA, which is about 100 times smaller than its spread caused by differences between the DMAs.

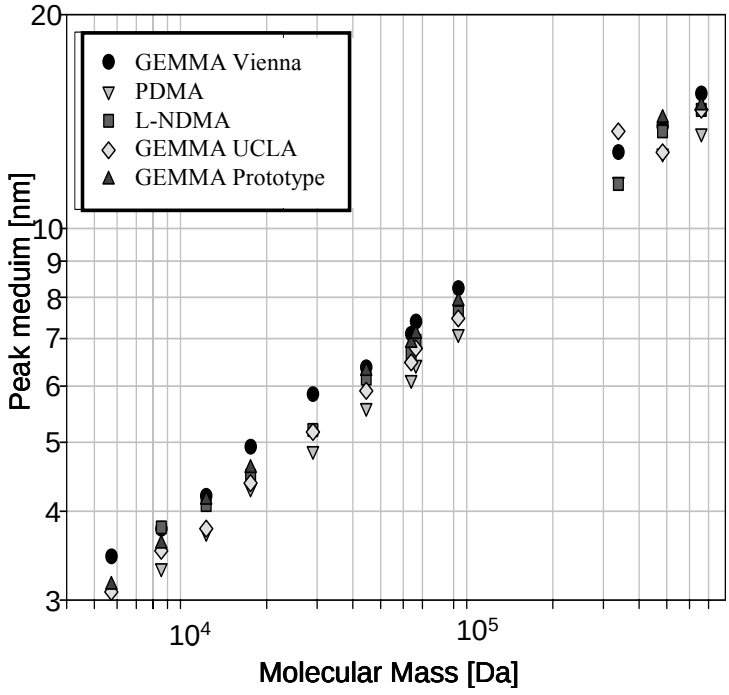

Fig. 4.3 Peak medium obtained with different n-DMAs

The relative FWHM of the measured size spectra is similar for all investigated instruments and typically below 0.06 for proteins with a MW >30 kD except for the L-nDMA showing the relative width in this mass range of about 0.08, which is presumably a result of the longer separation distance which results in increased diffusion broadening[22]. The latter effect becomes a dominating factor for measurements of species <30 kDa, where the diffusion broadening leads to relative widths in the order of 0.1 for smallest investigated proteins for all DMAs but the L-nDMA , where values of about 0.15 were found.

The observed differences between the investigated instruments may result from differences in particle detection method, as well as the voltage scanning direction and consequently the involved algorithm which recovers the actual size distribution from raw data (TSI, Reischl et al.[17]). The Vienna .type DMAs use for particle detection a Faraday cup, thus they measure directly and for practical reasons instantaneously the presence of a charged nanoparticle. The GEMMA systems use a CPC for the particle detection. This method is known to deliver somewhat varying peak positions depending on the operating conditions if the time-delay between DMA voltage setting and the detection event, which is an inherent occurrence of this detection method, is not completely corrected [31].

Whatever the reasons for the differences of the peak position found in this study might be, it is obvious that the use of calibrants of known size, mass and high homogeneity, such as proteins, polymers or inorganic particle, is necessary for the precise performance of any DMA system; especially for analysis in which a DMA is used as mass spectrometer at ambient pressure[4,15]or in which conclusions about size, changes of size caused by alteration, agglomeration, denaturation, degradation or the formation of complexes of certain analytes have to be drawn.

6. Conclusions

The stability (0,1 % variation) of the measured diameter values in one series of 10 size spectra with each DMA shows evidently the ability of these instruments for the characterisation and analysis of nano-sized biological, inorganic and polymeric material. But the fact, that all DMA systems even though operated under optimal and nearly identical working conditions show consistently a sizing disagreement displays, that not all parameters which influence the size analysis can be controlled to a level at which differences between various DMAs would be below 5%.

Wherever these differences root – in the exact value of the of the sheath gas flow, in discrepancies between geometrical and effective separation length or in an not completely corrected time delay between setting of the DMA and particle detection- the result clearly lead to the conclusion that for qualitative analysis of nanoparticles, macromolecules, proteins and polymers, a calibration of such systems with size or mass standards is inevitable.

Acknowledgments. JAL acknowledges support from the W. M. Keck Foundation, UCLA Jonsson Comprehensive Cancer Center, the U. S. Department of Energy for funding of the UCLA-DOE Institute for Genomics and Proteomics, and the U. S. National Institutes of Health (RR 20004). This work was further supported in part by a grant of the Austrian Science Foundation (FWF, Project P16185-N02 to W.W.S.)

References

(1) Flagan, R. C. *Aerosol Sci. Technol.* **1998**, *28*, 301-380.
(2) Kittelson, D. B. *J. Aerosol Sci.* **1998**, *29*, 575-588.
(3) Chen, D.-R.; Pui, D. Y. H.; Hummes, D.; Fissan, H.; Quant, F. R.; Sem, G. J. *J. Aerosol Sci.* **1998**, *29*, 497-509.
(4) Bacher, G.; Szymanski, W. W.; Kaufman, S. L.; Zöllner, P.; Blaas, D.; Allmaier, G. *J. Mass Spectrom.* **2001**, *36*, 1038-1052.
(5) de la Mora, J. F. *Trends Anal. Chem.* **1998**, *17*, 328-339.
(6) Wilm, M.; Mann, M. *Anal. Chem.* **1996**, *68*, 1-8.
(7) Juraschek, R.; Dülcks, T.; Karas, M. *J. Am. Soc. Mass Spectrom.* **1999**, *10*, 300-308.
(8) Reischl, G. P.; Makela, J. M.; Karch, R.; Necid, J. *J. Aerosol Sci.* **1996**, *27*, 931-949.
(9) Fuchs, N. A. *Geofis. Pura Appl* **1963**, *56*, 185-193.
(10) Hussin, A., Scheibel, H. G., Backer, K. H., & Porstendorfer, J. *J. Aerosol Sci.* **1983**, *14*, 671-677.
(11) Hogan, C. J.; Kettleson, E. M.; Ramaswami, B.; Chen, D.-R.; Biswas, P. *Anal. Chem.* **2006**, *28*, 844-852.
(12) Mouradian, S.; Skogen, J. W.; Dorman, F. D.; Zarrin, F.; Kaufman, S. L.; Smith, L. M. *Anal. Chem.* **1997**, *69*, 919-925.
(13) Loo, J. A.; Berhane, B.; Kaddis, C. S.; Wooding, K. M.; Xie, Y.; Kaufman, S. L.; Chernushevich, I. V. *J. Am. Soc. Mass Spectrom.* **2005**, *16*, 998-1008.
(14) Saucy, D. A.; Ude, S.; Lenggoro, I. W.; de la Mora, J. F. *Anal. Chem.* **2004**, *76*, 1045-1053.
(15) Ku, B. K.; de la Mora, J. F. *Anal. Chem.* **2004**, *76*, 814-822.
(16) Laschober, C.; Kaufman, S. L.; Reischl, G.; Allmaier, G.; Szymanski, W. W. *J. Nanosci. Nanotechnol.* **2006**, *6*, 1474-1481.
(17) Reischl, G. P.; Makela, J. M.; Necid, J. *Aerosol Sci. Technol.* **1997**, *27*, 651-672.
(18) Brimili, W.; Stratmann, F.; Wiedensohler, A.; Covert, D.; Russell, L. M.; Berg, O. *Aerosol Sci. Technol.* **1998**, *27*, 215-233.
(19) Fissan, H.; Hummes, D.; Stratmann, F.; Buscher, P.; Neumann, S.; Pui, D. Y. H.; Chen, D.-R. *Aerosol Sci. Technol.* **1996**, *24*, 1-13.
(20) Fissan, H.; Pöcher, A.; Neumann, S.; Boulaud, D.; Pourpix, M. *J. Aerosol Sci.* **1998**, *29*, 289-293.
(21) Hummes, D.; Stratmann, F.; Neumann, S.; Fissan, H. *Part. Part. Sys. Char.* **1996**, *13*, 327-332.
(22) Reischl, G. P. *Aerosol Sci. Technol.* **1991**, *14*, 5-24.
(23) Laschober, C.; Szymanski, W. W.; Allmaier, G.; Reischl, G. P. *Manuscript in preparation* **2007**.
(24) Stolzenburg, M. R.; University of Minnesota: Minneapolis, MN, 1988.
(25) Reischl, G. P. *J. Aerosol Sci.* **1991**, *22*, 297-312.
(26) Chen, D.-R.; Pui, D. Y. H. *J. Aerosol Sci.* **1997**, *28*, 985-1004.
(27) Karlsson, M. N. A.; Martinsson, B. G. *J. Aerosol Sci.* **2003**, *34*, 603-625.
(28) Rosser, S.; de la Mora, J. F. *Aerosol Sci. Technol.* **2005**, *39*, 1191-1200.
(29) Seol, K. S.; Yaburnoto, J.; . Takeuchi, K. *J. Aerosol Sci.* **2002**, *33*, 1481-1492.
(30) Collins, D. R.; Nenes, A.; Flagan, R. C.; Seinfeld, J. H. *J. Aerosol Sci.* **2000**, *31*, 1129-1144.
(31) Russell, L. M.; Flagan, R. C.; Seinfeld, J. H. *Aerosol Sci. Technol.* **1995**, *23*, 491-510.

Macromolecules in press (2007)

5. Determination of molecular weight, particle size and density of high number generation PAMAM dendrimers using MALDI-TOF-MS and nES-GEMMA

Roland Müller[1+], Christian Laschober[1,2+], Wladyslaw W. Szymanski[2] and Günter Allmaier[1*]

[+]Both have contributed equally to the work.

[1]Institute of Chemical Technologies and Analytics, Vienna University of Technology, A-1060 Vienna, Austria

[2]Institute of Experimental Physics, University of Vienna, A-1090 Vienna, Austria

Corresponding author: Günter Allmaier, Institute of Chemical Technologies and Analytics, Vienna University of Technology, Getreidemarkt 9/164, A-1060 Vienna, Austria Tel: +43 1 58801 15160 Fax: +43 1 58801 15199 E-mail: guenter.allmaier@tuwien.ac.at

Running title: MALDI-MS and nES-GEMMA of PAMAM dendrimers

ABSTRACT

In this work we present the characterization of PAMAM dendrimers (nanosized particles) from generation two (G2) up to ten (G10) with a focus on the G5 to G10 with matrix-assisted laser desorption/ionization linear time-of-flight mass spectrometry (MALDI-TOF-MS) and nano-electrospray gas-phase electrophoretic mobility molecular analysis (nES-GEMMA). For the first time the molecular masses of real large dendrimers G8-G10 were determined by MALDI-MS and by nES-GEMMA, techniques which are based on different physico-chemical principles. Obtained experimental data allowed the determination of the molecular mass (up to 580 kDa with a precision below ± 0,9%), of the spherical size (from 3.3 - 14.0 nm with a precision of ± 0.02 nm) and the calculation of the density. Amounts in the nano-gramm range were sufficient for analysis and measurements could be performed within several minutes. The results based on these methods for high generation dendrimers exhibited an excellent correlation and were compared with published data using techniques based on different principles.

Introduction

Dendritic (branch like) architecture has been recognized as complete new building scheme for polymers as early as 1926 by Herman Staudinger within his macromolecular hypothesis[1]. This kind of architecture lead to polymeric molecules[2,3], called dendrimers, which faced a rapidly increasing importance in the recent decade[4-8], since they are recognized as a whole new type of well defined functionalised building blocs for a bottom-up synthesis of nanoscale objects with designable properties[9-12]. Unlike other polymers, dendrimers possess a well defined globular size in the low nm range and structure, with a clear distinction between core and surface, which makes them suitable for applications like catalysis and as delivery vehicles[7] for small drug molecules[13]. Various interesting molecular architectures using dendrimers have already been realised, such as self assembly macromolecule structures between different types of dendrimers[14,15], dendrimers coupled with various polymers in different arrangements[16-19], dendrimers with hydrophobic core and hydrophilic surface, which may be used as artificial liposomes, and dendrimers coupled to peptides, antibodies, DNA and carbohydrates for example. The goal of these architectures is to create a whole set of new macromolecular properties which could not have been realised otherwise.

To be able to create desired dendrimer products and structures, dendrimer properties (e.g. molecular weight, hydrophobic vs. hydrophilic character, number and type of free reaction groups, average diameter and density) have to be sufficiently characterised during macromolecular synthesis steps and before their use in the above mentioned applications. Despite this fact, analysis seems to be a step behind their importance and as was already stated by Caminade et. al.[20]. The main reason for this fact is that dendrimers pose a new challenge to all analytical techniques as they exhibit exponentional growth of surface and mass during their stepwise synthesis (producing the next higher generation) as well as covering a mass range from a few kDa in the case of generation one (G1) to one MDa for generation ten (G10).

A special, very important subclass of the dendrimers, namely poly(amido-)amine (PAMAM) dendrimers, will be the focus of this work. PAMAM dendrimers resemble proteins in their size and particular chemical structure (a huge number of peptide bonds). But while proteins can fold oddly or change their shape, dendrimers are more or less cemented structures with strong and rigid bonds. Due to these attributes they are already used to replace proteins in immunodiagnostics[21,22] and *in vitro* gene expression applications[23], for example. Therefore it is not surprising that PAMAM dendrimers are the first class of dendrimers which have been successfully commercialised[3], which makes their detailed characterisation even more important. A scheme of the structure of PAMAM dendrimers of different generation is presented in Fig. 5.1.

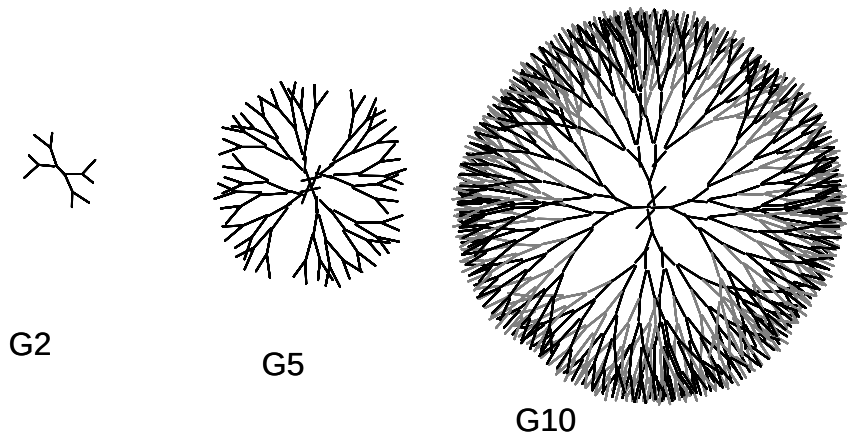

Fig. 5.1 Structure of PAMAM dendrimers of different generation (G)

Until now size exclusion chromatography (SEC)[24-28], slab gel electrophoresis (SDS-PAGE)[29], capillary electrophoresis (CE)[29,30], small angle x-ray scattering (SAXS)[31,32], and small angle neutron scattering (SANS)[33,34] atomic force microscopy (AFM)[35-38], transmission electron microscopy (TEM)[39] and mass spectrometry[40,41], have been applied to determine the molecular mass, diameter and shape of PAMAM dendrimers. Other techniques that focus on a chemical characterisation such as the characterisation of surface groups or the abundance of certain structure elements will not be discussed in this work, since the presented experimental data are solely focused on molecular mass, size and density determination. In the following section we give a brief overview of the before mentioned techniques as well as their advantages and disadvantages. A detailed description of other analytical techniques applied to dendrimers can be found in following reviews [20,42-44].

SEC is a widely and routinely used separation technique which allows the separation of analytes according to their size in solution. The main advantages of SEC are easy handling and a high dynamic range concerning molecular weight determination. When this method was applied to determine the molecular mass of dendrimers, a systematic error between expected and with SEC determined molecular mass values was found[24]. This error could be linked to the different shape of the commonly used calibrants, which are linear polystyrol polymers, and the spherically shaped dendrimers. This shape dependency of the molecular weight determination is a general phenomenon of SEC and thus makes this method somehow problematic in the use of molecular weight determination of dendrimers particularly for higher generations.

CE and SDS-PAGE are analytical techniques widely used for the analysis of biopolymers. Both techniques separate analytes according to their electrophoretic migration behaviour, which strongly depends the number of charged surface groups, the pH of the buffer solution and the cross section of the molecule. For molecular weight determination, as it is carried out with proteins, denaturation and the attachment of sodium dodecyl sulphate (SDS) molecules to the polypeptide backbone is inevitable as it levels the charging differences between different types of proteins and leads to a direct relationship between migration behaviour and molecular weight.

Applying these techniques to analyse dendrimers, it is possible to differentiate between different generations of one particular dendrimer species and between dendrimer particles of one generation with different surface modification.

Both techniques lack the ability to determine the size or molecular mass of the dendrimers[30]. However, a qualitative analysis of the change of dendrimer populations during synthesis and modification steps has been possible with these methods[20].

SAXS and SANS are both scattering techniques which allow the determination of the radius of gyration of the dendrimer molecules as well as the electron density distribution inside the dendrimer particles in solution. With these techniques it was possible to prove that PAMAM dendrimers change their characteristic shape from star like (varying electron density to radius function) to rigid sphere like (constant electron density along the outer radius of the particle). The advantage of both techniques is that the determined value is an average of a vast amount of scattering events on many dendrimer particles, and that measurements are made with dendrimers in solution. However, both techniques also have their disadvantage, as considerable experimental expense as well as high expertise in interpreting the experimental data is required [31-34].

AFM is a microscopic technique that allows investigation of shape as well as mechanical properties of single dendrimer particles. The strongest limitation of AFM in the determination of dendrimers is the softness of these organic molecules, which limits the resolution and hampers the analysis of dendrimers smaller than G5 [35-38]. Another observed effect is the deformation and losing of the spherical shape of dendrimers during adsorption on substrate surfaces, which poses problems in the size determination. With scanning the whole dendrimer particle it was possible to circumvent this problem and determine the volume and calculate a spherical–equivalent diameter[35,36,38].

TEM is an additional microscopic method whose resolution depends on the energy of the primary electron beam. For samples which provide enough contrast and regularity even atomic resolution is possible. This method was used to determine the diameter of G5 up to G10 PAMAM dendrimers in vacuum[39]. However, as dendrimers are organic molecules with a weak contrast, a staining step must be carried out before analysis, which may lead to a systematic error in the determined particle dimensions, but as TEM can be carried out at low temperature, the loosing-shape effect as described for AFM can be avoided[39].

Mass spectrometry is an analytical technique preliminary used for the exact molecular weight determination of various high-mass biopolymers. The MALDI-TOF-MS technique was a major break-through for the mass spectrometric analysis of molecules with molecular weights higher than 2 kDa and was first presented in 1988 by Hillenkamp, Karas and Tanaka [45,46,47]. Whereas today most MALDI-MS experiments are performed with proteins, carbohydrates and oligonucleotides, the analysis of dendrimers with this technique is also already described in literature up to G4 [40,41,48-51]. Observed imperfections and deviations from the calculated molecular weights of the dendrimer samples were attributed to chemical defects. Additionally fragmentation of dendrimers was observed for dendrimers absorbing at a similar wavelength of the applied laser wavelength used for desorption/ionization [49,50]. Like in the case of proteins or DNA fragments post-source decay (PSD) fragmentation of PAMAM dendrimers of small size (up to G4) was also observed with MALDI-TOF-MS [51]. Beside MALDI-MS, electrospray ionization (ESI)-MS is another mass spectrometric technique for the exact molecular weight determination already applied to dendrimers [52,53].

Advantages of MALDI-TOF-MS (in the linear mode) are its high molecular weight range, sensitivity and mass accuracy [54]. The main disadvantages of this technique are the rather high instrumentation cost and the search for an optimal matrix and a proper sample preparation method for a given analyte. ESI-MS has the advantage of generating highly charged molecular ions which reduces the mass-to-charge ratio and makes molecules with higher mass accessible to mass analysers other than TOF systems. But for the determination of the actual molecular mass, the exact charge states of the multiply charged ions are required. For this purpose peaks representing adjacent charge states have to be resolved, which is difficult for many high mass molecules[55] and was not possible for e.g. a PAMAM G6 dendrimer (for higher generation dendrimer it is even more difficult) despite combining ESI with a Fourier-transform ion cyclotron analyzer[40].

The nano-ES-GEMMA (electrospray gas phase electrophoretic mobility molecular analyser), which is used in this study, is a relatively new technique that combines the benefits of the low charge levels (one or two charges per molecule) of the MALDI with the process of desorption/ionisation from the bulk solution by the nano-ES process.

It uses a differential mobility analyser (DMA) for the separation of the singly charged particle by their electrophoretic mobility diameter (EMD) at atmospheric pressure.

Such devices have been in use since a long time in aerosol physics for the analysis of submicrometer to micrometer particle aerosols[56]; their design was recently adapted to extend the measurable size range into the low single digit nanometer region, or in terms of molecular mass, into the low kDa mass range. A condensation particle counter (CPC) is used for the detection of the separated singly charged particles (ions), offering single particle detection allowing high sensitivity (10^3 particles or ions / cm^3). Furthermore a direct relationship between molecular mass and diameter has already been demonstrated for globular proteins[57] and small DNA fragments[58], allowing the use of the nES-GEMMA to determine the molecular mass of high molecular weight proteins and non-covalent protein complexes. Also the size analysis of bacteriphages[59], viruses and virus fragments[60], high mass protein complexes hinzu[56 61] and polyethylene-glycol polymer mixtures[62] as well as small (≤ G4) PAMAM dendrimers[63] was demonstrated with this method.

In this work we present now the characterisation (molecular mass, size and average density) of PAMAM dendrimers up to G10 with the two independent techniques MALDI-TOF-MS and nES-GEMMA as well as the comparison with other techniques as SAXS, SANS, AFM, TEM and data provided by the manufacturer as well as theoretical values based on molecular dynamics calculations.

Material and Methods

Chemicals

All amine-terminated PAMAM dendrimers with an ethylenediamine core were obtained as 5-20% solutions in methanol (G2 to 7 from Sigma-Aldrich, G9 and 10 from Dendritech). Ammonium acetate and acetonitrile (ACN) of analytical grade were acquired from Merck. Trifluoroacetic acid (TFA, 99%) was purchased from Riedel-de-Haen and 2,4,6-trihydroxyacetophenon monohydrate (THAP) from Fluka, both analytical grade. Ammonium acetate and TFA solutions were made by means of analytical grade water from Merck. For MALDI-TOF-MS calibration bovine insulin (Sigma-Aldrich) and the Invitromass HMW Calibrant Kit (Invitrogen) were applied.

MALDI-TOF-MS instrument.

MALDI mass spectrometry was carried out on an Axima TOF^2 tandem instrument from Shimadzu Biotech Kratos Analytical. The device is a high resolution, floor-standing instrument equipped with a pulsed nitrogen laser (wavelength: 337 nm, pulse width: 4 ns), an integrated 2 GHz transient recorder, a curved field reflector and a differential pumped collision gas cell. The instrument was operated in the positive ion linear (flight path 1,2 m) mode applying an accelerating voltage of 20 kV without delayed extraction.

Calibration for PAMAM dendrimers from G4 to G10 was performed externally by using the Invitromass HMW Calibrant Kit, which contained various recombinant standard proteins with given molecular weights in the mass range from 30 kDa to 160 kDa. The calibration kit was applied according to the manufacturer's instructions, but in contrast to the instruction manual THAP as MALDI matrix solution was applied for external calibration. Calibration for PAMAM dendrimer G2 was performed externally using the singly and doubly protonated molecule of bovine insulin. All mass spectra were acquired by averaging 50 to 200 unselected and consecutive laser shots on the same preparation by automatic rastering. In order to calculate relative standard deviations (RSDs) for molecular weight determination each PAMAM dendrimer sample was analyzed ten times using different sample spots on the same MALDI target. All mass spectra were smoothed using the company-supplied Savitzky-Golay algorithm [64]. The applied peak (m/z determination) detection method was threshold-centroid at 50% height of the peak maximum.

Sample preparation for MALDI MS analysis.

Prior to analysis, THAP was dissolved in 1/1 (v/v) 0,1% TFA/ACN mixture to give a final MALDI matrix concentration of 10 mg/mL. Prior to use the all day freshly prepared matrix solution was vortexed thoroughly. For MALDI-TOF-MS analysis 1 uL PAMAM dendrimer stock solution was vacuum dried at RT in order to remove all solvents. Afterwards, the residue was dissolved completely in a 9/1 (v/v) 0,1% TFA/ACN solvent mixture to give a final PAMAM dendrimer concentration of 10 nmol (assuming an ideal molecular weight)/mL which was equivalent to the following mass concentrations: 0,03 mg/mL (G2), 0,14 mg/mL (G4), 0,29 mg/mL (G5), 0,58 mg/mL (G6), 1,16 mg/mL (G7), 4,67 mg/mL (G9) and 9,34 mg/mL (G10). One part of the resulting PAMAM dendrimer solution was mixed with two parts of THAP matrix solution in an Eppendorf tube.

0,5 uL aliquots of this matrix/sample mixture were deposited on several different spots on a stainless steel microtiter format MALDI target and dried under a gentle stream of air at RT forming smooth crystalline layers.

nES-GEMMA instrument.

The GEMMA system consists of a nano-electrospray (nES) unit, a nano-differential mobility analyzer (nDMA) and an ultrafine condensation particle counter (uCPC) as detector (all parts from TSI Inc). The nano-ES generated multiple charged particles are charge reduced in a bipolar air environment produced by α-radiation from a Po-210 radioactive source (NRD). This charge-reduction process results in neutral and only singly charged molecules/nanoparticles. The operating particle size range of the instrument combination is between 3 nm (limited by the particle detection with the uCPC) and 65 nm (the upper scan limit of the nDMA when using maximum sheath flow for maximum nDMA resolution). The nDMA was operated with negative high voltage polarity on the central electrode, thus separating and detecting the positively charged fraction of the generated molecules/nanoparticles. The detection limit of the complete GEMMA system in terms of particle concentration is 1 singly charged nanoparticle/cm³. However, due to the limited efficiency of charge manipulation process concentration of airborne dendrimer particles of at least 10000 particles (equivalent to approx. 4 pg for G5 molecules)/cm³ are necessary to obtain appropriate particle count statistics across the whole sizing (3 nm to 30 nm)/scanning range within a reasonable time frame (120 s per scan). Ten scans were averaged for each final size spectrum presented in this paper.

Nano electrospray conditions.

For all measurements, the settings of the nano-ES source, buffer concentrations, and solution conductivity were identical. Samples in 20 mM ammonium acetate buffer (pH 7.4) were electrosprayed. For this solvent system and spray-chamber design we found that a stable cone-jet mode operation was obtained at 2 kV and 0.3 L/min CO_2 (99.995%, Air Liquide)/1L/min compressed air (99.999% synthetic air, Air Liquide). A pressure difference of 4 psi between sample and spray chamber was applied, which resulted in a sample solution flow of 67 nL/min through the fused silica capillary (25 µm inner diameter and 160 µm outer diameter, length 25 cm uncoated; supplied by TSI Inc).

The primary generated droplet size, which is determined by the conductivity of the solvent system and the sample flow through the capillary as well as the inner diameter of the capillary was 150 nm, corresponding to a flow of 2×10^{11} droplets/minute or about 1.7×10^{8} droplets/cm³. The electrospray process was operated in the positive ion mode, which means that droplets with a high initial number of positive charges were produced.

Sample preparation for nES-GEMMA analysis. For the nES-GEMMA all PAMAM stock solutions (commercially available from 1-10% w/w in methanol) were diluted directly with a 20 mM aqueous ammonium acetate buffer (pH 7.4) to a concentration avoiding the formation of PAMAM cluster ions ($[nM]^+$, $n \geq 2$) consisting of 2 and more dendrimer molecules through the ES process. This concentration was 20 µg/mL for G5, G6, G7, G9 and G10 and 2 µg/mL for G2 and G4.

Results and Discussion

Exact molecular weight determination with MALDI mass spectrometry

The MALDI-TOF mass spectra of PAMAM dendrimers G2 to G10 are shown in Fig. 5.2 a-g. Most mass spectra exhibit mainly singly charged molecular ions and to a lesser degree doubly charged molecular ions (see Fig. 5.2 a-e). Sometimes the mass spectra show additionally (e.g. in case of G5 and G6, Fig. 5.2 c and d) singly charged dimeric molecular ions. Beside the singly charged molecular ion peak the doubly charged molecular ion peak was found as well. The mass spectrum of PAMAM dendrimer G9 showed beneath singly and doubly charged molecular ions also an abundant signal at m/z ~94000 (Fig. 5.2 f).The peak observed at this m/z ratio was not a triply charged molecular ion peak of PAMAM G9 but either a fragment ion of the analyte molecule or with a much higher probability an impurity. Since no comparable molecular ion peaks (or fragment ions) were observed in the mass spectra of PAMAMs with generations lower than 9, it is most likely that this peak derived from an impurity within the original sample. Possible impurities are precursors of earlier synthesis steps, like G7 or G8, which were not completely removed or converted. Given a similar chemical structure of analytes, molecules with lower molecular weight tend to show more intense peaks in MALDI mass spectrometry due to better desorption/ionization yield.

Thus, the impurity can actually be present in the sample solution in a much lower concentration than the PAMAM dendrimer G9. In the case of PAMAM G10 only the doubly and triply charged molecular ions, but no singly charged molecular ion was observable (Fig. 5.2 g) despite the instrument can handle a m/z range up to 600000. Concerning the full peak widths at half maximum (FWHM) of the singly charged molecular ion analyte peaks it was interesting to notice, that well-defined proteins of similar molecular weight had several times lower FWHMs than dendrimers. The high FWHM values of the PAMAM dendrimer analyte peaks could be explained by incomplete synthesis and non-optimized purification after synthesis. In the case of PAMAM dendrimer G2 to G7 the singly charged molecular ion peaks were used for molecular weight determination (Table 5.1).

PAMAM Generation	Theoretical number of NH_2 groups [67]	Theoretical MW [kDa] [67]	MALDI-TOF-MS derived MW [kDa]	RSD [%]	MW difference [%]
2	16	3,256	3,233	0,0	-0,6
4	64	14,21	13,32	0,2	-6,3
5	128	28,82	25,92	0,4	-10,1
6	256	58,05	50,16	0,3	-13,6
7	512	116,49	90,97	0,9	-21,9
9	2048	467,14	323,30	-	-30,8
10	4096	934,69	~580	-	-37,9

Tab. 5.1 Summary of the average molecular weights determined with MALDI-TOF mass spectrometry and the calculated molecular weights of various generations of PAMAM dendrimers. The differences (given in percents) shown in the right column refer to the measured molecular weights compared with the calculated molecular weights

Because molecular weight calibration was limited to 160 kDa for PAMAM G9 the doubly charged and for PAMAM G10 the triply charged molecular ion peak was applied for molecular weight determination. Nevertheless the molecular weight of the triply charged molecular ion peak of PAMAM G10 was slightly out of external calibration range, which was limited with a m/z ratio of 159081. The molecular weights of all PAMAM dendrimer samples determined with MALDI-TOF-MS were below the calculated molecular weight for ideal synthesis (Table 5.1). This difference between measured and calculated molecular weight increased continuously with increasing generation of the PAMAM dendrimers and was already surprisingly high for lower PAMAM dendrimer generations (G4: minus 6,3%, G5: minus 10,1%). This observation was corroborated by nES-GEMMA data shown below.

Most likely the synthesis of PAMAM dendrimers was not complete and as a consequence the difference between the calculated and actual molecular weight increased with every synthesis step. It has to be stated in this context that the MALDI mass spectrometric derived molecular weight in the linear mode is independent of 3-dimensional structure of the dendrimer molecule and that under our MALDI conditions no considerable metastable decay was observed [50,51]. The obtained precision of molecular weight determination with MALDI-TOF-MS in the linear mode across all analytes was ± 0,4%.

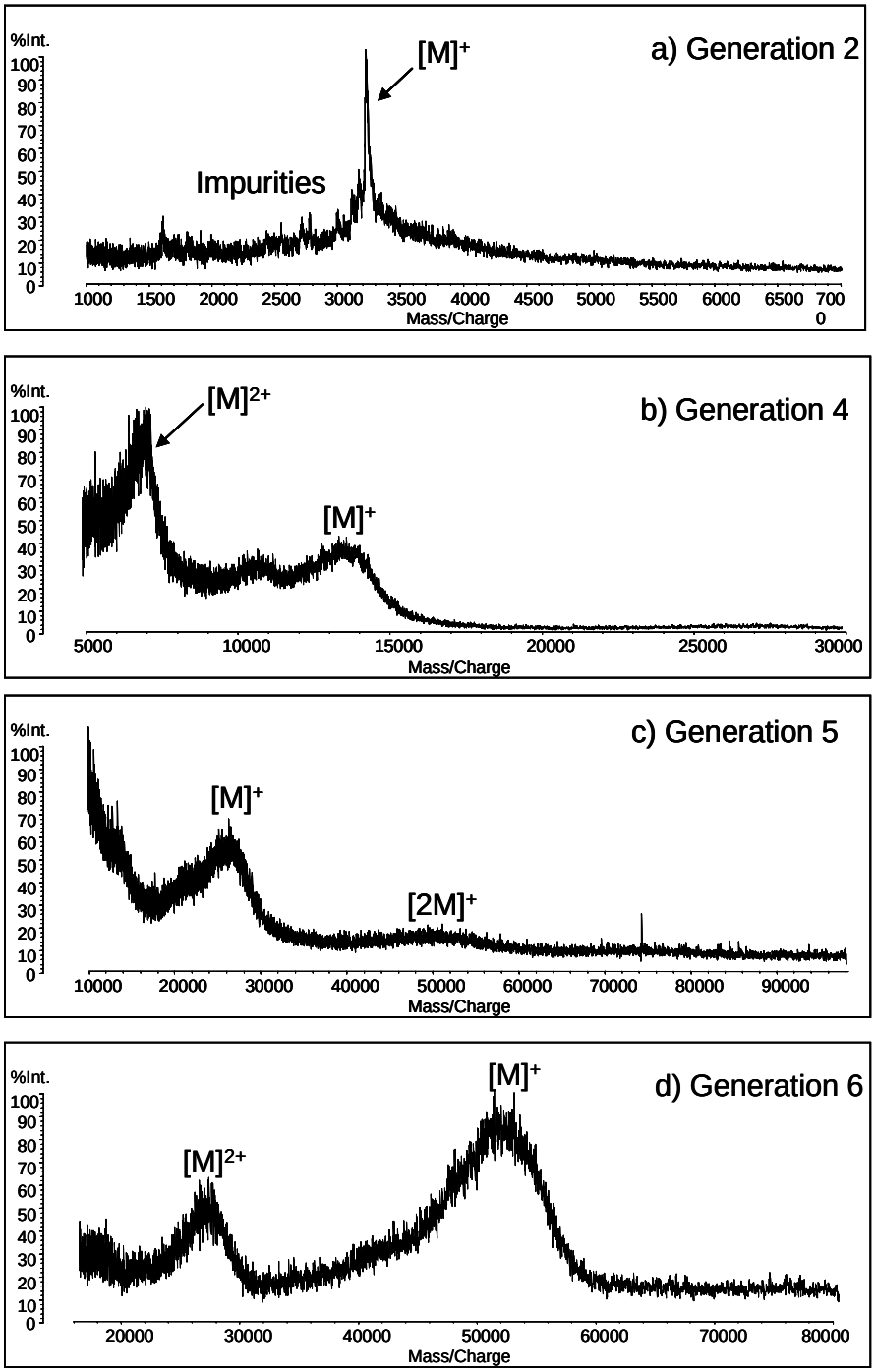

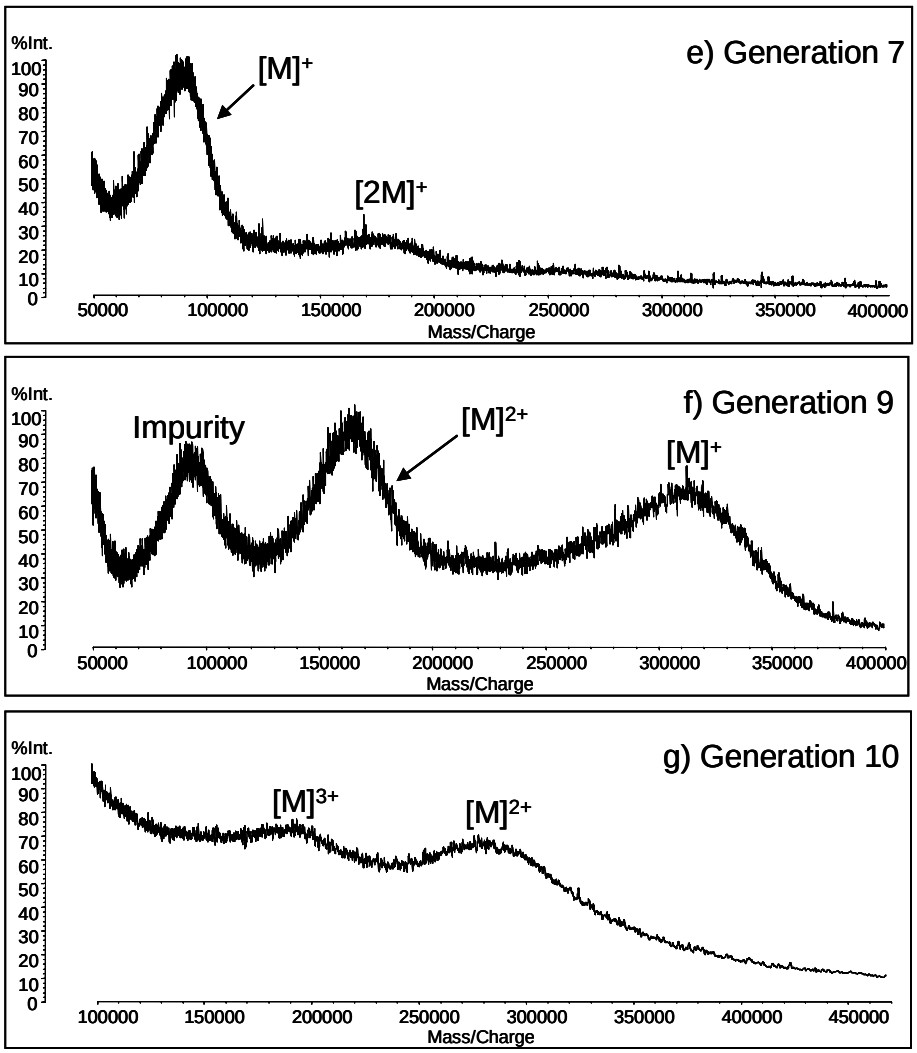

Fig. 5.2 positive ion MALDI mass spectra in the linear mode of PAMAM dendrimers of generation a) G2, b) g4, c) G5, d) G6, e) G7, f) G9, g) G10

Size determination with nES-GEMMA. Fig. 5.3 shows the GEMMA size spectra of PAMAM dendrimers G4, G6, G9 (Fig. 4.3 a) and G2, G5, G7, G10 (Fig. 4.3 b). The typical amount of particles being characterised within one spectrum is between 10^4-10^7, thus characterising bulk and not single particle properties as it is done in TEM, AFM, SAXS and SANS. As can be seen, the $[M]^+$ peak maximum increases steadily with the number of the generation.

The size growth from generation to generation is nearly constant especially above G4, where dendrimer particle characteristics change to rigid sphere like as SAXS[31,32], SANS[33,34] and AFM[35-38] results suggest . For G7, G9 and G10 cluster dimers ($[2M]^+$ ion) could be observed (Fig. 5.3).

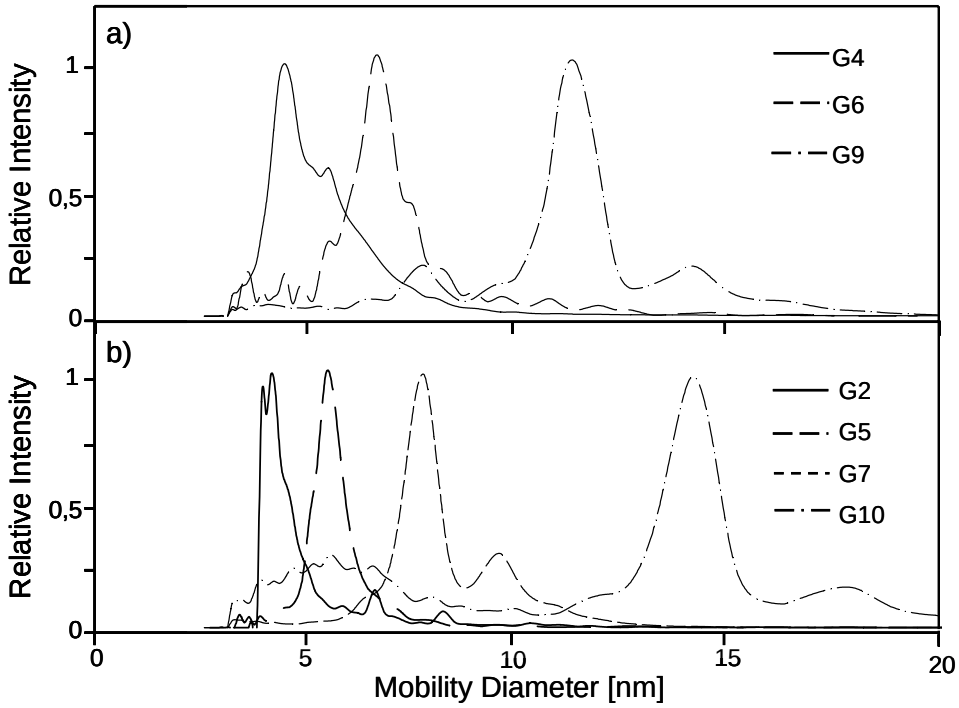

Fig. 5.2 nES-GEMMA spectra of PAMAM dendrimers
a) G4, G6, G9 and b) G2, G5, G7, G10

Furthermore, in the GEMMA spectrum of PAMAM dendrimer G9 and G10 some impurities (particles of smaller size) could be detected (Fig. 5.3). As these impurities are also high molecular weight components, which is also confirmed by MALDI-MS, it can be assumed that they are either incomplete products of the G9 and G10 dendrimer synthesis, or dendrimers of smaller generation which were not successfully removed after the synthesis. For G9 and G10 a FWHM of 7 and 8%, respectively was found, which is significantly higher than the instrumental resolution of the GEMMA and values found for proteins in the same size range[57]. This increase of the peak width with increasing number of generation is probably the result of statistically incomplete attachment of the next dendrimer shell, an error that propagates in dendrimer synthesis as every dendrimer generation is the starting material of the synthesis of the succeeding generation.

As can be seen in Table 5.2, the diameters determined by nES-GEMMA measurements agree excellent with volume equivalent diameters derived from AFM measurements of different origin [35,36,38], the average particle diameter found for dendrimer particles in vitrified solutions by TEM[39], and the diameter of gyration found in SAXS[31,32] and SANS[33,34] studies.

PAMAM Generation	GEMMA	AFM[35]	AFM[36]	AFM[38]	TEM[39]	SAXS[31]	SAXS[32]	SANS[33]	SANS[34]	Manufacturer [a, 68]
	Average particle diameter (nm)									
G2	3,3	-	-	-	-	-	-	-	-	2,9
G3	n.d.	-	-	-	-	3,2	2,9	3,3	-	3,6
G4	4,3	-	-	-	-	3,4	3,6	3,9	-	4,5
G5	5,1	4,5	-	4,9	4,3	4,8	4,4	4,9	4,4	5,4
G6	6,4	5,6	5,9	5,9	6,9	5,3	5,7	6,1	-	6,7
G7	7,6	7,2	7,1	7,1	8,0	6,4	6,5	7,2	-	8,1
G8	n.d.	9,2	9,0	8,9	10,2	8,1	7,8	-	8,4	9,7
G9	11,2	12,5	10,5	10,5	12,4	9,8	9,2	-	-	11,4
G10	14,0	15,6	-	-	14,7	11,5	10,8	-	-	13,5

Tab. 5.2 Average particle diameter found in this work with nES-GEMMA and in literature. SAXS, SANS, TEM and AFM. AFM diameters were calculated from determined particle volumes, assuming sphere like shape.
n.d., not determined; -, not available.
[a] according to manufacturer medium diameter derived with viscosimetry, SAXS and SANS

The differences in size between the different studies are well within there described standard deviations resulting from the experimental method uncertainties and the polydispersity of the dendrimers themselves. The only exception are the two SAXS studies, whose results for generations smaller than 7 agree with TEM, AFM and GEMMA measurements, but which found significantly smaller diameters than the other methods for PAMAM dendrimers G7 and higher. This phenomenon is discussed in literature[31,32] and can be attributed to higher order scattering events inside the particle, which distort the scatter angle and results subsequently in an underestimation of the particle diameter.

Molecular weight and density determination based on nES-GEMMA.

As mentioned before, the nES-GEMMA data can not only be used for the determination of the average particle diameter, but also, with appropriate calibration, for the determination of the molecular weight. For this reason, the GEMMA system was calibrated with common globular proteins, which are all of spherical shape according to Bacher et al.[57].

Another approach to estimate the molecular mass of a dendrimer particle is the calculation of the average particle volume and the calculation of its mass with an assumed density. As was found by molecular dynamics caculations of dendrimers [65] a density of about 50 atoms/nm³, or, when multiplied with the average atom mass of the PAMAM dendrimers, 0.52 kg/L can be assumed for the bulk volume of the dendrimer particle. Both approaches were used for the calculation and determination of the molecular mass from GEMMA derived particle diameters (Tab. 5.3).

PAMAM generation	MALDI MS [a]	nESI-GEMMA [b]	Molecular dynamics [c]
	Molecular Mass (kDa)		
G2	3,24	5,17	5,68
G4	13,32	12,3	13,1
G5	25,92	20,5	21,5
G6	50,16	41,6	42,6
G7	90,97	71,0	71,4
G9	323,3	239	231
G10	580	482	454

Tab. 5.3 Molecular mass determination on MALDI-TOF-MS, nES-GEMMA and Miolecular dynamics

[a] external Protein calibration

[b] calibration function: molecular mass (Da) = 131.77*D_P(nm)^(3.106), R^2=0.9943 derived from measurements of well definded protein standards

[c] assuming particle density of 0.52 kg/l which was found by molecular dynamics calculations

As can be seen in Table 5.3, both approaches clearly overestimate the molecular mass of the PAMAM G2 dendrimer particle. This result can be explained by the fact that such small dendrimers cannot be viewed as rigid spheres, but more as star-like branched molecules (disk-like), with a significant distance between its branches, thus neither possessing spherical shape, which is known to bias the determined electrophoretic mobility diameter, nor the assumed bulk density. For higher generation PAMAM dendrimers, where spherical shape, rigidity and bulk properties of the dendrimer particle can be assumed, both approaches do not over- but underestimate the molecular weight of the dendrimers by ~18% but agree very well with each other.

The reason for this difference can either be rooted in the determined particle diameter, or in the explicitly (derived from molecular dynamics) or implicitly (as in case of the protein calibration curve) set particle density. As particle diameters between different analytical methods showed good agreement (as discussed in the paragraph before), particle densities were calculated from molecular dynamics for ideal structures (data received from the manufacturer[62]) and from MALDI mass spectrometric and nES-GEMMA data (Fig 5.4).

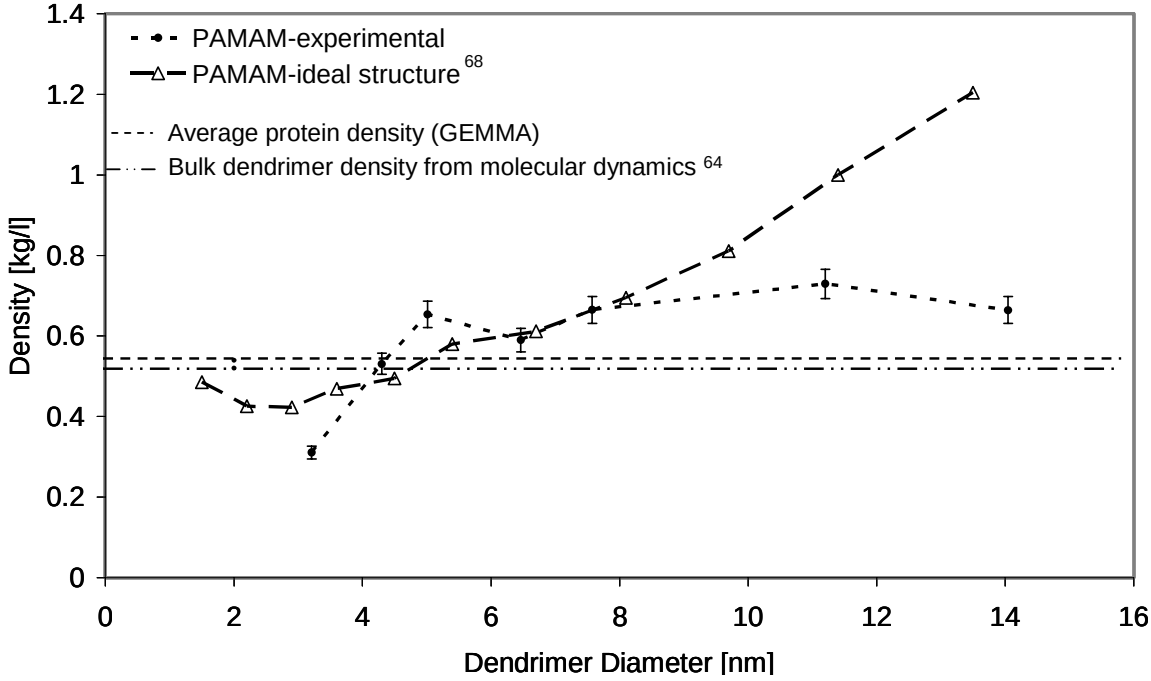

Fig. 5.4 Plot of theoretical and experimental PAMAM dendrimer particle densities vs. particle diameter

As can be seen in Figure 5.4 the by means of nES-GEMMA determined average protein density (~0,54 kg/L) is nearly identical to the average dendrimer density found in molecular dynamics calculations, thus explaining the good agreement between the molecular mass derived from protein calibrations and calculated from the determined particle volume and the theoretical density. The series representing the density values derived from MALDI-TOF_MS and nES-GEMMA data shows an increase of the particle density from 0.31 (G2) to 0.65 (G5). PAMAM generations above G5 show constant density, thus confirming the change from star-like branching to rigid spheres with bulk properties as was found by SAXS[31,32], SANS[33,34] and AFM[35,36,38] studies.

However, the density difference between proteins and with molecular dynamics calculated values for dendrimers[65] to experimental data leads directly to the observed differences between the molecular masses derived from MALDI-MS and the protein calibration and via density calculated values from the nES-GEMMA experiments. One reason for this difference to theory might be that the dendrimer particles are not surrounded by solvent environment as in the molecular dynamics simulation. This amplifies intramolecular forces and might lead to a more dense packing inside the particle and a higher average bulk density. Proteins, as used in the calibration, are not branch like, but linear in their primary structure, which also might lead to differences in particle density, even when the elemental distribution is roughly the same.

The theory of ideal dendrimer growth behaviour postulates a nearly constant growth of the diameter of dendrimers, especially for generations above 4, where globular particle shape can be assumed, but an exponentional molecular mass growth (values derived from manufacturer[62]). This leads to a steady increase of the postulated dendrimer density (dashed line in Fig. 5.4) with every generation above 4; for smaller generations a slight decrease of density is postulated, since there the star like branching leads to an increase of the distance between the different branches (dashed line with triangles in Fig. 5.4). Theory and determined densities agree very well until G7. However, the density of G9 and G10 PAMAM dendrimers is significantly below theoretical values according to our MALDI-MS and nESI-GEMMA data. The reason for this difference from our experimental values and values calculated for ideal dendrimer structures is probably a congestion-induced *De Gennes dense packing*[9,66,67] , as was postulated for high generation dendrimers in literature, which leads to incomplete saturation of free branching spots during the synthesis of the next generation.

Conclusions

In this work we have shown, that molecular mass determination of PAMAM dendrimers up to G10 was generally possible with MALDI-TOF-MS analysis. The observed average precision was ±0.4%. An increasing difference between the theoretical molecular masses for ideal dendrimer growth/synthesis and molecular masses determined with MALDI-TOF-MS with increasing number of generation was found. Analysis with MALDI-TOF-MS provided molecular weights up to 40% below the calculated theoretical molecular weight.

nESI-GEMMA analysis of the electrophoretic mobility diameter of dendrimer particles of all generations was possible with a precision of 0.2 nm and a relative FWHM of 5%. All diameter values were in excellent agreement with values found by various other analytical techniques such as SAXS, SANS, TEM and AFM. The polydispersity of the molecular mass and the distribution of diameters of the analysed dendrimer generations was found to be significantly higher than for proteins in the same molecular mass and size range. It was attempted to calculate the molecular mass of PAMAM dendrimers via their particle diameter with different approaches, but all resulted in a significant discrepancy to the MALDI-MS data. The calculated density of the dendrimer particles based on the MALDI-MS and nES-GEMMA data showed a significant difference to protein densities (0.54 kg/L), densities calculated from molecular dynamic results (0.52 kg/L) as well as to densities derived from dendrimer growth theory (up to 1.2 kg/L). Our results indicate that PAMAM dendrimer particles of G4 or higher possess a constant average density of 0.65 kg/L, which is determined by tight packing of the branches inside the particle.

Acknowledgements. This research was partially supported by the Austrian Science Foundation grants P15008 (to G.A.) and P16185 (to W.W. S.).

References

(1) Staudinger, H. *From organic chemistry to macromolecules*; Wiley-Interscience: New York,US, 1970.
(2) Frechet, J. M. J.; Tomalia, D. A. *Dendrimers and other dendritic polymers*; Wiley: Chichester,UK, 2001.
(3) Tomalia, D. A.; Baker, H.; Dewald, J. R.; Hall, M. J.; Kallos, G.; Matrin, S. *Polymer J. (Tokyo)* **1985**, *17*, 117-132.
(4) Tomalia, D. A.; Hedstrand, D. M.; Ferrito, M. S. *Macromolecules* **1991**, *24*, 1435-1438.
(5) Tomalia, D. A. *Macromolecular Symposium* **1996**, *101*, 243-255.
(6) Naj, A. K. *Wall Street Journal* **1996**, *B1*.
(7) Hecht, S.; Frechet, J. M. J. *Angew. Chem. Int. Ed.***2001**, *40*, 74-91.
(8) Gauthier, M.; Moller, M. *Macromolecules* **1991**, *24*, 4548.
(9) Tomalia, D. A.; Naylor, A. M.; W.A. Goddard, I. *Angew. Chem. Int. Ed* **1990**, *29*, 138-175.
(10) Frechet, J. M. J.; Hawker, C. J.; Gitsov, I.; Leon, J. W. *JMS Pure Appl. Chem.* **1999**, *A33*, 1399.
(11) Voit, B. I. *Acta Polym* **1995**, *46*, 87-99.
(12) Fischer, M.; Vögtle, F. *Angew. Chem. Int. Ed* **1999**, *38*, 884-905.
(13) Boas, U.; Heegaard, P. M. H. *Chem. Soc. Rev.* **2004**, *33*, 43-63.
(14) Tomalia, D. A.; Uppuluri, S.; Swanson, D. R.; Li, J. *Pure Appl. Chem.* **2000**, *72*, 2343-2358.
(15) Tomalia, D. A.; Swanson, D. R. In *Dendrimers and other dendritic polymers*; Frechet, J. M. J.; Tomalia, D. A., Eds.; Wiley: Chichester, UK 2001; 617-629.
(16) van Heerbeek, R.; Kamer, P. C. J.; van Leeuwin, P. W. N. M.; Reek, J. N. H. *Chem. Rev.* **2002**, *102*, 3717-3756.
(17) Hedrick, J. L.; Magbitang, T.; Conner, E. F.; Glauser, T.; Volksen, W.; Hawker, C. J.; Lee, V. Y.; Miller, R. D. *Chem. Eur. J.* **2002**, *8*, 3308-3319.
(18) Jenkins, A. D.; Kratochvil, P.; Stepto, R. F. T.; Sutter, U. W. *Pure Appl. Chem.* **1996**, *68*, 2287-2311.
(19) Schlüter, A. D. *Topics Curr. Chem.* **1998**, *197*, 165-191.
(20) Caminade, A.-M.; Laurent, R.; Majoral, J.-P. *Adv. Drug Deliver. Rev.* **2005**, *57*, 2130-2146.
(21) Singh, P.; Moll, F. I.; Lin, S. H.; Ferzli, C. *Clinical Chemistry* **1996**, *42*, 1567-1569.
(22) Singh, P. In *Dendrimers and dendritic polymers*; Tomalia, D. A.; Frechet, J. M. J., Eds.; Wiley: Chichester, UK 2001; 463-484.
(23) Bieniarz, C. In *Enceclopedia of pharmaceutical chemistry*; Marcel Dekker: New York, 1998; pp 55-89.
(24) Hawker, C. J.; Frechet, J. M. J. *J. Am. Chem. Soc* **1990**, *112*, 7638-7647.
(25) Zeng, F.; Zimmerman, S. C.; Kolotuchin, S. V.; Reichert, D. E. C.; Ma, Y. *Tetrahedron* **2002**, *58*, 825-843.
(26) Maraval, V.; Laurent, R.; Donnadieu, B.; Mauzac, M.; Caminade, A.-M.; Majoral, J.-P. *J. Am. Chem. Soc* **2000**, *122*, 2499-2511.
(27) Padias, A. B.; Hall, H. K.; Tomalia, D. A.; McConnell, J. R. *J. Org. Chem.* **1987**, *52*, 5305-5312.

(28) Newkome, G. R.; Young, J. K.; Baker, G. R.; Potter, R. L.; Audoly, L.; Copper, D.; Weis, C. G. *Macromolecules* **1993**, *26*, 2394-2396.
(29) Shi, X.; Patri, A. K.; Lesniak, W.; Islam, M. T.; Zhang, C.; Jr., J. R. B.; Balogh, L. P. *Electrophroesis* **2005**, *26*, 2960-2967.
(30) Brothers, H. M.; Phieler, L. T.; Tomalia, D. A. *J. Chromatogr. A* **1998**, *814*, 233-246.
(31) Prosa, T. J.; Bauer, B. J.; Amis, E. J.; Tomalia, D. A.; Scherrenberg, R. *J. Polym. Sci.* **1997**, *35*, 2913-2924.
(32) Prosa, T. J.; Bauer, B. J.; Amis, E. J. *Macromolecules* **2001**, *34*, 4897-4906.
(33) Amis, E. J.; Topp, A.; Bauer, B. J. In *29th ACS Central Regional Meeting*: Midland, MI, 1997.
(34) Topp, A.; Bauer, B. J.; Tomalia, D. A.; Amis, E. J. *Macromolecules* **1999**, *32*, 7323-7237.
(35) Li, J.; Piehler, L. T.; Qin, D.; Jr., J. R. B.; Tomalia, D. A.; Meier, D. J. *Langmuir* **2000**, *16*, 5613-5616.
(36) Betley, T. A.; Holl, M. M. B.; Orr, B. G.; Swanson, D. R.; Tomalia, D. A.; jr., J. R. B. *Langmuir* **2001**, *17*, 2768-2773.
(37) Li, J.; Qin, D.; jr., J. R. B.; Tomalia, D. A. *Macromol. Symp.* **2001**, *166*, 257-269.
(38) Betley, T. A.; Hessler, J. A.; Mecke, A.; Holl, M. M. B.; Orr, B. G.; Uppuluri, S.; Tomalia, D. A.; jr., J. R. B. *Langmuir* **2002**, *18*, 3127-3133.
(39) Jackson, C. L.; Chanzy, H. D.; Booy, F. P.; Drake, B. J.; Tomalia, D. A.; Bauer, B. J.; Amis, E. J. *Macromolecules* **1998**, *91*, 6259-6265.
(40) Tolic, L. P.; Anderson, G. A.; Smith, R. D.; II, H. M. B.; Spindler, R.; Tomalia, D. A. *Int. J. Mass Spectrom. Ion Proc.* **1997**, *165*, 405-418.
(41) Zhou, L.; Russel, D. H.; Zhao, M.; Crooks, R. M. *Macromolecules* **2001**, *34*, 3567-3573.
(42) Esfand, R.; Tomalia, D. A. *Drug Discov. Today* **2001**, *6*, 427-436.
(43) Frauenrath, H. *Prog. Polym. Sci.* **2005**, *30*, 325-384.
(44) Tomalia, D. A. *Prog. Polym. Sci* **2005**, *30*, 294-324.
(45) Karas, M.; Hillenkamp, F. *Anal.l Chem.y* **1988**, *60*, 2299-2301.
(46) Tanaka, K.; Waki, H.; Ido, Y.; Akita, S.; Yoshida, Y.; Yohida, T. *Rapid Comm. Mass Sp.* **1988**, *2*, 151-153.
(47) Berkenkamp, S.; Kirpekar, F.; Hillenkamp, F. *Science Reports* **1998**, *281*, 260-262.
(48) Hood, R.; Watson, J. T.; A.D.Jones. In *Proceedings of the 54th Annual conference in Mass Spectrometry, ASMS*: Seattle, WA, 2006.
(49) Felder, T.; Schalley, C. A.; Fakhrnabavi, H.; Lukin, O. *Chem-Eur J* **2005**, *11*, 5625-5636.
(50) Baytekin, B.; Werner, N.; Luppertz, F.; Engeser, M.; Brüggemann, J.; Bitter, S.; Henkel, R.; Felder, T.; Shalley, C. A. *Int.l J. Mass Spectrom.* **2006**, *249-250*, 138-148.
(51) Subbi, J.; Aguraiuja, R.; Tanner, R.; Allikmaa, V.; Lopp, M. *Eur. Polym.r J.l* **2005**, *41*, 2552-2558.
(52) Schwartz, B. L.; Rocwood, A. L.; Smith, R. D.; Tomalia, D. A.; Spindler, R. *Rapid Commun. Mass Sp.* **1995**, *9*, 1552-1555.
(53) Kallos, G. J.; Tomalia, D. A.; Hedstand, D. M.; Lewis, S.; Zhou, J. *Rapid Commun. Mass Sp.***1991**, *5*, 383-386.
(54) Covey, T. R.; Huang, E. C.; Henion, J. D. *Anal. Chem.* **1991**, *63*, 1193-1200.

(55) Thomas, J. J.; Bothner, B.; Traina, J.; Benner, W. H.; Siuzdak, G. *Spectroscopy* **2004**, *18*, 31-36.
(56) Liu, B. Y. H.; Pui, D. Y. H. *J. Colloid Interface Sci.* **1974**, *74*, 155-171.
(57) Bacher, G.; Szymanski, W. W.; Kaufman, S. L.; Zöllner, P.; Blaas, D.; Allmaier, G. *J. Mass Spectrom.* **2001**, *36*, 1038-1052.
(58) Mouradian, S.; J.W., S.; F.D., D.; Zarrin, F.; Kaufman, S.L.; Smith, L. M., *Anal. Chem.* **1997**, *69*, 919-925.
(59) Wick, C. H.; McCubbin, P. E. *Toxicol. Meth.* **1999**, *9*, 245-252.
(60) Hogan, C. J.; Kettleson, E. M.; Ramaswami, B.; Chen, D.-R.; Biswas, P. *Anal. Chem.* **2006**, *28*, 844-852.
(61) Loo, J. A.; Berhane, B.; Kaddis, C. S.; Wooding, K. M.; Xie, Y.; Kaufman, S. L.; Chernushevich, I. V. *J. Am. Soc. Mass Spectrom.* **2005**, *16*, 998-1008.
(62) In *http://www.tsi.com/documents/CHEMC-006-Water-solublePEGPolymer.pdf*; TSI Inc.: Minneapolis, MN.
(63) In *http://www.tsi.com/appnotes/images/gemma-starburst.gif*; TSI Inc.: Minneapolis, MI.
(64) Savitzky, A.; Golay, M. J. E. *Analytical Chemistry* **1964**, *36*, 1627-1639.
(65) Han, M.; Chen, P.; Yang, X. *Polymer* **2005**, *46*, 3481-3488.
(66) Tomalia, D. A.; Mardel, K.; Henderon, S. A.; Holan, G.; Esfand, R. In *Handbook of nanoscience, engeneering and technology*; W.A. Goddard, I., Ed.; CRC Press: Boca Raton, FL, 2003; pp 1-34.
(67) Tomalia, D. A.; Frechet, J. M. J. In *Dendrimers and other dendritic polymers*; Tomalia, D. A.; Frechet, J. M. J., Eds.; Wiley: Chichester, UK, 2001; 3-44.
(68) In http://www.dendritech.com/pamam.html , Dendritech Inc., Midland, MI, USA

BioTechniques submitted (2006)

6. Gas Phase Electrophoretic Molecular Mobility Analysis of Size and Stoichiometry of Complexes of a Common Cold Virus with Antibodies

Christian Laschober[1, 3], Juergen Wruss[2], Dieter Blaas[2], Wladyslaw W. Szymanski[3] and Günter Allmaier[1]

[1]Institute of Chemical Technologies and Analytics, Vienna University of Technology, A-1060 Vienna, Austria
[2]Max F. Perutz Laboratories, Department of Medical Biochemistry, Medical University of Vienna, A-1030 Vienna, Austria
[3]Institute of Experimental Physics, University of Vienna, A-1090 Vienna, Austria

Abstract

Attachment of a non-aggregating monoclonal antibody (Ig G) and of a recombinant soluble receptor molecule to the icosahedral non-enveloped human rhinovirus serotype 2 was studied with a nano-electrospray ionization gas-phase electrophoretic molecular mobility analyzer (nESI-GEMMA). The virus mass, as determined via nESI-GEMMA was within instrument accuracy (±6%) close to the theoretical value ($8*10^6$ Da) calculated from the sum of all constituents of one virus particle (60 copies of each of the four viral capside proteins, the RNA genome and one copy of the RNA-linked protein VpG). The formation of virus-antibody complexes of different stoichiometry (with up to $12.5*10^6$ Da corresponding to 30 attached antibodies) and virus-receptor complexes (up to $8.8*10^6$ Da corresponding to 12 attached receptor molecules) was monitored. Considering these complexes as nanoparticles of given electrophoretic mobility diameter (EMD) the stoichiometry of of the components inside the complex was determined. The accuracy of the EMD was within ± 0.5 nm which corresponds to ± 4 antibodies and ± 5 receptor molecules in the respective complexes. For the first time, we here demonstrate the use of nESI-GEMMA for the analysis of the stoichiometry of biomolecules in high-order complexes in real time under normal pressure conditions. The method exhibits high sensitivity and delivers a complete size spectrum requiring only about 10^4 particles within typically 60 s.

Introduction

The analysis of stoichiometric complexes of various types of biomolecules has become increasingly important in the recent decade. Such assemblies are frequently found in nature and exhibit a variety of biological functions such as recognition of vesicles [1], neutralisation of viruses and bacteria by the immune system, expression and repairing of the genetic information [2,3], formation of tissues and blood coagulation [4], to name just a few. Furthermore reduces the oligomerisation of identical protein chains the size of the required coding information and increases the avidity towards its cognate partner [5].

The analysis of such complexes as well as of the dynamics of their formation and decomposition is hampered by the non-covalent character of the bonds that result in limited physico-chemical stability [6]. Only few techniques have so far been successfully applied for the detection of such complexes using small amounts of sample. Amongst them the most important are capillary electrophoresis (CE) and the two mass spectrometric "soft ionisation" techniques, namely electrospray ionisation (ESI) [7] and matrix-assisted laser desorption and ionisation (MALDI)[8] as well as atomic force microscopy (AFM) and cryo-electron microscopy (cryo-EM). AFM and cryo-EM have undergone a rapid development in the recent decade; both are now well suited to investigate the three dimensional structure of viruses and other large molecular assemblies [9,10]. In contrast to the other techniques they are used to investigate individual specimens. AFM can operate with the sample held under physiological conditions; it was shown recently that it enables real-time detection of protein complex formation [11]. On the other hand, cryo-EM is better suited for structure reconstruction as it offers better spacial resolution. Nevertheless, both methods do not allow the characterization of the kinetics of formation and disassembly of complexes and the stoichiometry can only be derived via complex image analysis.

CE can detect and quantify the formation of biological assemblies. Even entire bacteria and viruses, alone or complexed, were resolved [12]. The separation parameter of the CE is the electrophoretic mobility of the analytes in the liquid phase. Although its value depends on the cross section of the analyte [12,13], which correlates with the mass, it is strongly influenced by solvent and buffer properties, such as pH, viscosity and ionic strength, as well as by parameters of the analyte itself, such as the number of surface groups and the isoelectric point. Furthermore, highly concentrated solutions are necessary for analysis, which might result in non-specific aggregation and adsorption.

Additionally, at high separation voltages, orientation effects of non-spherically shaped analytes might occur, which results in an alteration of the electrophoretic mobility [14]. The high resolution and low amount of sample needed for the measurement makes CE extremely suitable for this type of analysis but it fails if the electric mobilities of the constituents and their complexes are too similar. Furthermore, migration in the capillary is not correlated with the mass of the analyte and thus the stoichiometry of the components present in the complexes can only be derived in those rare cases in which a strong shift in the electrophoretic mobility between complexes with different stoichiometry is observed[15].

MALDI can preserve the non-covalent bonding of protein complexes [16,17]. However, this requires compromises in the sample preparation and analysis to avoid denaturation and degradation during the solvation and matrix mixing as well as in the laser desorption and ionisation. Usually salts and/or organic solvents are added and low laser intensities are being used to preserve non-covalent bonds; the latter often disadvantageously affects the performance. Since the MALDI process produces mainly single or double charged ions the analysis is limited to a mass to charge ratio that can be handled by the mass spectrometer; the current maximum measurable value amounts to 335 kDa (for aerolysin), a protein complex assembled from seven identical subunits [18].

Electrospray ionisation (ESI) is likely the most established desorption/ionisation technique for the analysis of non-covalent complexes [19,20]. The advantage of ESI compared to MALDI is that the samples are desorbed/ionised from bulk solution and not via a solid/gas phase transition. This decreases the risk of destroying the complex prior to ionisation. The second benefit of the electrospray ionisation is that the proteins are endowed with high charge, which lessens the m/z ratio of the produced ions and therefore allows for the analysis of protein complexes of higher mass as compared to MALDI. Here, the mass of detectable protein complexes is not limited by the m/z ratio itself but by the resolution of the mass spectrometer and the determination of the charge state of the molecular ions; recently even the detection of intact viruses was possible with this method coupled to an ion mobility device[21]. Furthermore, Ruotolo *et al.* [7] found evidence that the conformation of protein complexes is unaffected by the ESI process.

The measuring technique utilized in this work - the nano-ESI-GEMMA (gas phase electrophoretic molecular mobility analysis, schematic see Fig.6.1) - is relatively new; it combines the benefits of the low charge levels of the MALDI (one or two charges of both polarities) with the process of desorption/ionisation from the bulk solution by the nano-ESI process. It uses a differential mobility analyser (DMA) for the separation of the protein ions at atmospheric pressure, a device that has been in use since a long time in aerosol physics for the analysis of submicrometer to micrometer particle aerosols [22]. This technique was recently extended into the single digit nanometer region, or in terms of mass, into the low kDa mass range. It has been successfully applied for the analysis of functional protein complexes as well as of whole viruses and virus fragments [23-26].

Human rhinoviruses (HRVs), the main causative agent of the common cold, are already well characterized many aspects [27,28]. They are composed of four different proteins with 60 copies of each making up the icosahedral shell that encases the genomic RNA. As derived from the x-ray ccordinates of structural models solved at a resolution of about 0.3 nm, these particles exhibit a diameter of abut 30 nm[29]. From the analytical point of view the viral particle can be considered a big non-covalent protein complex that has already been analysed with GEMMA [24]. The symmetry of these viruses implies that 60 identical sites are present on the surface. Using human rhinovirus serotype 2 (HRV2) as a model, the formation of stoichiometric complexes with a neutralising monoclonal antibody (directed towards the viral surface) as well as with different recombinant soluble receptor molecules (derived from the human very-low density lipoprotein receptor, VLDLR) have been studied by capillary electrophoresis. [30-32].

In the present work we demonstrate the utility of nESI-GEMMA for he analysis of stoichiometric complexes between HRV2 and the monoclonal antibody 8F5. The same technique is also shown to allow the analysis of complexes between HRV2 and a recombinant soluble very-low density lipoprotein receptor fused to maltose binding protein (MBP-V33333) that attaches at lower ratio and is smaller than the antibody. To our knownledge, our experimental approach is the first of its kind.
The results confirm that the measurement of molecular assemblies into the 10 MDa range is possible with nESI-GEMMA allowing to resolve the complexes from the constituents and thus yielding the respective stoichiometries.

Materials and Methods

GEMMA instrument

The GEMMA system (Fig. 6.1) consists of a nano-electrospray unit, a nano-differential mobility analyzer (nDMA) and an ultrafine condensation particle counter (uCPC) as detector (all parts from TSI Inc, Shoreview, MN, USA). The nano-ESI generated multiple charged particles are charge reduced in a bipolar air environment produced by alpha-radiation from a Po-210 radioactive source[22,23]. This charge-reduction process results in neutral and only singly charged on the nanoparticles. The presence of multiply charged particles would generate interference signals and complicate the interpretation of the measured spectra. The operating particle size range of the particular combination of components in this system is between 3 nm (limited by the particle detection with the uCPC) and 65 nm (the upper scan limit of the nDMA when using maximum sheath flow for maximum nDMA resolution). The nDMA was operated with negative high voltage polarity, thus analysing the positively charged fraction of the generated aerosol particles. The detection limit of the complete nESI-GEMMA system in terms of particle concentration is 1 singly charged particle / cm³. However, due to the limited efficiency of the charging process [33] ,virus, virus-mAB and virus-receptor complex concentrations have to be of at least 10.000 particles / cm³ to obtain appropriate particle count statistics across the whole sizing/scanning range within a reasonable time frame (120 s per scan). Ten scans were averaged for each final spectrum.

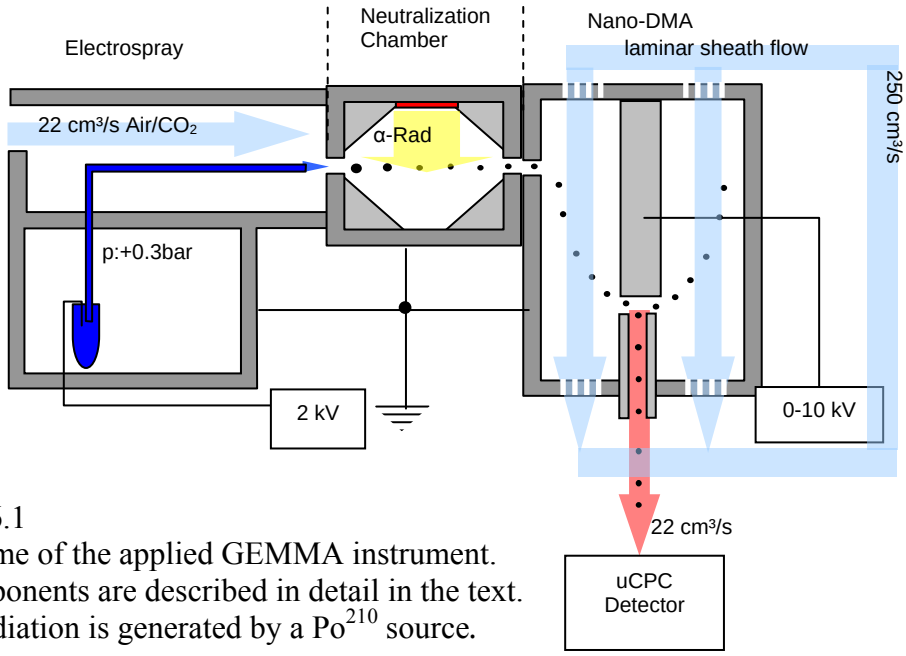

Fig. 6.1
Scheme of the applied GEMMA instrument. Components are described in detail in the text. α-Radiation is generated by a Po^{210} source.

Nanoelectrospray ionization conditions

For all measurements, the settings of nano ESI, buffer concentrations, and solution conductivity were identical. Samples were electrosprayed in 20 mM ammonium acetate buffer (pH 7.4). For this solvent system and spray-chamber design we found that a stable cone-jet mode operation was obtained at 2 kV and 0.3 L/min CO_2 (Air Liquide N45) / 1L/min compressed air (Air Liquide, Synthetic Air 5.0). A pressure difference of 4 psi between sample and spray chamber was applied, which resulted in a sample solution flow of 67 nL/min through the fused silica capillary (25 µm inner diameter and 160 µm outer diameter, uncoated; supplied from TSI Inc.). The primary generated droplet size, which is determined by the conductivity of the solvent system and the sample flow through the capillary as well as the inner diameter of the capillary was 150 nm, corresponding to a flow of 2×10^{11} droplets per minute or about 1.7×10^{8} droplets per cm³. The electrospray process was operated in the positive ion mode, which means that droplets with a high initial number of positive charges were produced. Specimen concentrations were kept below 0.1 nmol / µL to limit the probability that more than one molecule/virus particle is contained in an individual sprayed droplet.

Sample preparation

Prior to GEMMA analysis, it is necessary to remove all non-volatile components (e.g. sodium phosphate or detergents) which are different from the analyte of interest. The samples were purified and desalted by centrifugal ultrafiltration in Centricon tubes (Nanosept) with a 100 kDa lower-cut off membrane (in case of HRV2) and with a 10 kDa cut-off membrane (in case of the antibodies and receptor). After washing twice with double-distilled water, they were resuspended in 20 mM ammonium acetate buffer (pH 7.4). Purified virus samples were analyzed directly (for quality control of starting material) and mixed either with monoclonal antibody 8F5 (16) or with an unspecific mAB (human plasma derived, provided by Octapharma Inc.), at molar ratios between 1:30 and 1:150 and incubated for 2 h at RT prior to analysis. The recombinant concatemeric pentamer of repeat 3 (V3) of the human very-low density lipoprotein receptor (VLDLR) fused to maltose binding protein (MBP-V33333; [31]) was mixed with HRV2 at a 30:1 molar ratio and incubated for 1 hour at RT. MBP-V33333 was prepared and purified as described [15,31].

Results and Discussion

Analysis of complexes between HRV2 and monoclonal antibody 8F5

In the first series of experiments, we assessed the attachment of a monoclonal antibody (mAB) 8F5 that exhibits bidentate binding properties and whose attachment geometry has been extensively studied by X-ray crystallography and electron cryo-microscopy [27,28,34-37]. The mAB 8F5 binds to the antigenic loop in the capsid protein VP2 over the two-fold axis of icosahedral symmetry; both its Fv-arms attach to the same virion, therefore, no aggregation occurs. As previously shown by cryo-EM[27] a maximum number of 30 antibodies can attach to the surface of one virus particle. A scheme of the symmetry as well as the position of the binding site can be found in Fig. 6.2 A. These binding sites should theoretically be increasingly saturated with the mAB 8F5 with increasing mAB concentration and thus lead to an increase of the diameter of the detected virus particle until all binding sites are saturated (Fig. 6.2 B and C). The addition of the unspecific antibody to the virus should not lead to a binding of an antibody and thus an increase of the size of the virus particle (Fig.6.2).

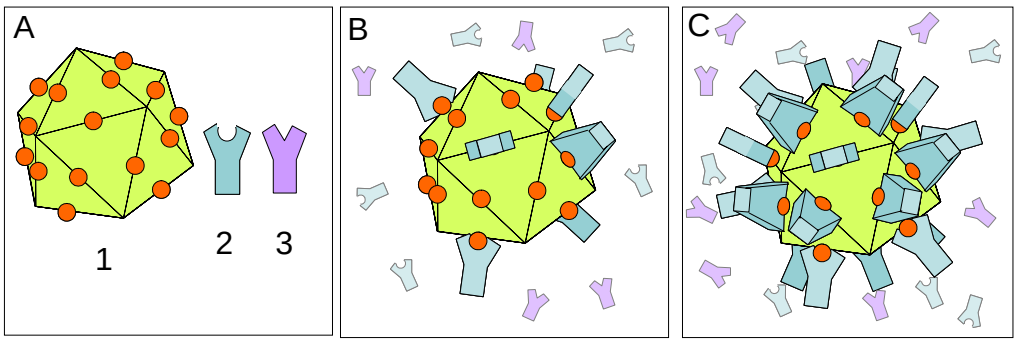

Fig. 6.2

A) 1: free HRV particle with icosahedral symmetry, red circles indicate the binding sites for the antibody; 2: mAB 8F5; 3: non-specific AB

B) HRV particle in low concentrated antibody solution; the binding sites are only partly covered with the specific binding mAB

C) HRV particle in highly concentrated antibody solution; all binding sites are saturated with the specific mAB

nESI-GEMMA analysis of the virus showed a relatively broad peak at 29.8 nm with a weakly structured trailing edge at EMD values up to 35 nm (Fig 6.3A). It is likely that these latter originates from subviral A- or B-particles. These are the product of conformational modifications of the virus occurring *in vivo* during the infection route but also *in vitro* upron heating or exposure to low pH[38,39].

Since these particles are intermediates of disassembly, it is likely that they also occur upon exposure of the virus to physical stress, as might be the case during nESI-GEMMA analysis. A-particles lack the innermost capsid protein VP4 and B-particles, in addition, lack the genomic RNA and are thus empty. However, although their molecular mass is less than that of native virus by roughly 5% (A-particles) and 30% (B-particles) their diameter is increased by about 4%[40]. Since it is rather the diameter than the molecular mass that is measured by nESI-GEMMA, it is possible that the shoulders at the higher EMD correspond to subviral particles.

As can be seen in Fig. 6.3B, the EMD of mAB 8F5 is 8.8 nm. For a comparison and control purposes, a non-specific isotype-matched antibody was also included into the analysis and all experiments were conducted identical with both antibodies with respect to incubation time, temperature and concentration ratios. The spectra of the two antibodies are practically identical (compare Fig. 6.3B and C).

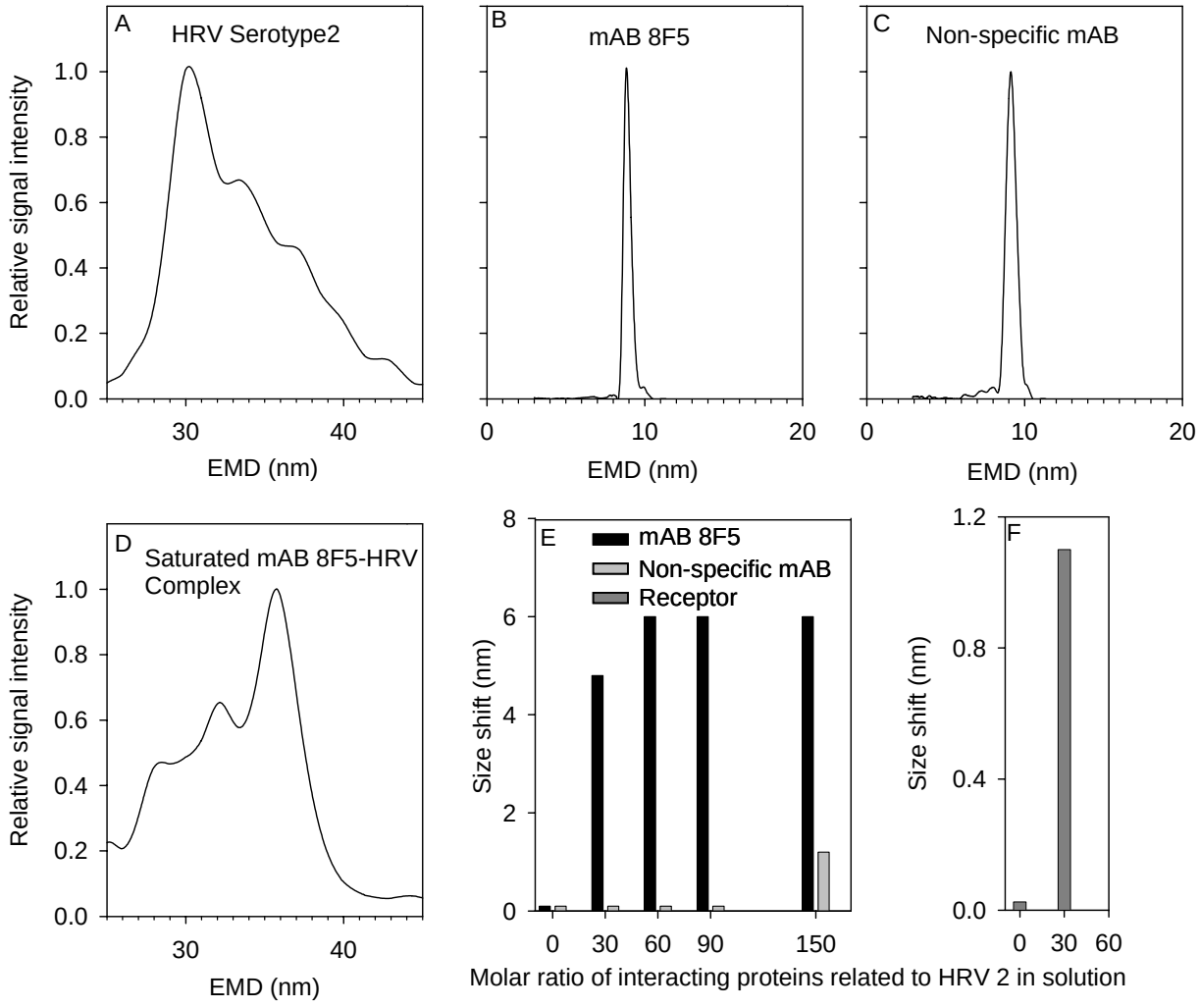

Fig. 6.3 GEMMA analysis of
A) HRV 2; B) monoclonal abtibody 8F5; C) non specific Antibody
D) Saturated HRV2-mAB 8F5 complex
E) and F) show the size shift that occurred at different molar ratios between HRV 2 and its three complex partners mAB-8F5, the non specific mAB and the artificial receptor MbP-V33333

In the second series of experiments the virus was incubated with mAB 8F5 at different molar ratios and the products were analyzed by nESI-GEMMA. The spectrum of the virus/antibody complex at saturation (ratio of virus to antibody 1:90; compare to Fig. 6.3E) is presented in Fig. 6.3D and the size shifts observed at different virus to antibody ratios are depicted in Fig. 6.3E in form of a bar diagram. At the lowest HRV2 to mAB ratio (1:30) the size increased by 4.5 nm when compared to free HRV2.

This difference further increased to 5.8 nm upon augmenting the ratio between the specific mAB and HRV2; but no further change of the EMD was seen on addition of more antibody indicating saturation (Fig. 6.2C).

The diagram shows a clear shift of peak towards larger EMDs when compared with the non-treated virus as a function of increased amount of antibodies (Fig. 6.3E). Comparison of the spectra of free HRV2 and antibody-saturated HRV2 indicates that some material of about the same size as the virus does not interact with the IgG. This might be virus whose antigenic epitopes have been denatured, other components remaining from cell culture (see above), or subviral particles; 8F5 is highly specific for native virus and does not bind subviral particles[41]. The occurrence of such material was also corroborated by CE experiments. The reference experiment in which the HRV2 was incubated with increasing amounts of a non-specific antibody showed no size shift of the virus peak except for a small increase in the solution with the highest amount of IgG added (Fig. 6.3E). This shift might be either caused by unspecific attachment of the IgG at high concentrations or by trapping of the antibody together with the virus within the same droplet during the ESI process.

The analysis of complexes of human rhinovirus and a recombinant soluble receptor.

The successful analysis of the attachment of a virus-specific monoclonal antibody to HRV2 promted us to ask, whether binding of a soluble receptor derivative to the virus could also be assessed by nESI-GEMMA. HRV2, as other minor receptor group human rhinovirus serotypes, attaches to the host cell via LDLR, VLDLR, and LDLR-related protein (LRP) [42,43]. These receptors are mosaic proteins with a characteristic ligand-binding domain composed of various numbers of modules with high sequence similarity. VLDLR possesses eight such repeats with some of them binding simultaneously to symmetry-related sites around the vertex of the viral icosahedron. The soluble artificial concatemer of repeat number 3 (V3), genetically fused to maltose binding protein (MBP-V33333), has been used previously to determine affinity, geometry, and stoichiometry of its attachment to the virus by various means [15,44-46]. Individual modules bind to exposed amino acid resides from the BC, DE, and HI loops of the capsid protein VP1 of HRV2. Five identical binding sites are arranged in the form of a star-shaped dome or mesa at each of the five-fold axes of the icosahedral protein shell of the virus.

The presence of five receptor modules in MBP-V33333 allows for multimodular attachment and most likely all five receptor repeats are bound simultaneously to each of the five binding sites at the vertex resulting in attachment of twelve copies of the receptor per virion [15].

This geometry translates into very high binding avidity [15]. From electron cryo-microscopy image reconstruction [45] and X-ray crystallography [47] it is known that the saturated HRV2/ MPB-V33333 complex is highly symmetrical and spherical since the receptor contributes only marginally to the diameter of the complex. We thus decided to investigate whether nESI-GEMMA was able to resolve complexes between virus and this particular receptor derivative as well. Since only 12 molecules can attach to the virus surface, a size shift by far smaller than in the previous setup was expected and would drive the system to its resolution limits.

First, the spectrum of the recombinant receptor was recorded. Its shape did not differ from the spectra of the two antibodies except that the monomer peak appeared at 7.2 nm (not shown). The size shift derived from comparison of the spectra of free virus and virus incubated with MBP-V33333 was of 1.1 nm (Fig. 6.3F). Taking into account that i) only 12 receptor molecules are able to attach to the virus ii) the mass difference between free virus and virus complexed to the receptor is only about 10%, and iii) that the mass correlates to the third power with the size (EMD), this was the maximum of size shift expected in this experiment.

Correlation of the electrical mobility diameter and the stoichiometry of the HRV2 / IgG and the HRV2 / MBP-V33333complexes.

As can be derived from Fig. 6.2 A-C, the number of attached antibodies respectively receptor molecules to the virus particles leads to an increase of the diameter of the detected virus particle. For the calculation of the number of attached mAB 8F5 respectively MbP-V33333 molecules some assumptions have to be made.

1) The electrical mobility diameter (EMD) is identical with the geometrical mean diameter for singly charged particles. This assumption is valid for spherical particles based on a number of comparisons between particle diameters obtained with the DMA and other methods such as electron microscopy and light scattering.

2) The volume of the complex is the sum of the volume of free HRV2 and of the attached molecules (i.e. IgG or receptor). This contention is valid as long as no conformational changes occur that might alter the volume and thus the density of the virus or the antibody (receptor) during the formation of the complex.

3) All aerosol particles in this study possess a spherical shape (see also Fig. 6.2). Hence the assumption that the area-equivalent mobility diameter, as determined by nESI-GEMMA, is identical with the volume equivalent diameter, is permissible [48]. This assumption is important in order to correlate the mobility diameter with a volume and, together with assumption 2) a mass, which was shown to be valid for various spherical proteins in a mass range between 2 and 2000 kDa [24].

Under these assumptions the diameter of the HRV2 / IgG complexes as well as of the HRV2 / MBP-V33333 complexes of various compositions can be calculated with the simple equation

(1) $EMD_{HRV2:nIgG} = \sqrt[3]{EMD_{HRV2}^3 + n * EMD_{IgG}^3}$

or, when transformed to determine the composition of a complex with a given experimentally determined diameter (2):

(2) $n_{IgG} = \frac{EMD_{HRV2:n*IgG}^3 - EMD^3{}_{HRV2}}{EMD_{IgG}^3}$

Considering the antibody, the EMD of the virus complexed with mAB 8F5 under non-saturating conditions (Fig. 6.2E) agrees with 20 antibodies bound per virion. However, the maximum EMD obtained with mAB 8F5 when added in excess corresponds to 28 ± 4 antibodies per virion according to the calculation with formula (2). This agrees very well with the 30 binding sites for this antibody as determined previously by electron cryo-microscopy [32].

When applying these formulas to the size shift observed upon binding of MBP-V33333 to HRV2, an average number of about 8 receptor molecules attached to the virus surface were obtained. However, because of the low mass of the receptor and the diameter resolution of the nESI-GEMMA of about 0.5 nm in the size range of this virus, the result is correct within approximately ± 5 receptor molecules.

Although low, this resolution allows a differentiation between the possible attachment of 60 (all symmetry-related sites occupied), 30 (simultaneous binding to two sites related by the two-fold symmetry, like in the case of mAB 8F5), 24 (simultaneous attachment to two sites related by the five-fold symmetry, as assumed for MBP-V33), and MBP-V23[47], finally, to the 12 vertices of the icosahedron. The results obtained thus agrees with that of capillary electrophoresis [15,31] and that derived from X-ray crystallography data [47] .

Our results clearly demonstrate the ability of the nESI-GEMMA methodology to characterize protein complexes, especially in a mass range not accessible to conventional mass spectrometry. It is of note, that,if the components of the complex possess a similar mass and size and do not differ by as much as HRV2 and mAB 8F5 (about 2 orders of magnitude), the nESI-GEMMA system can determine the composition of a complex with much higher precision than this was possible our present studies. The time frame to obtain one spectrum is currently in of the order of 60 s. allowing for the characterization of the dynamics of protein complex formation *in situ* which is an object of our future studies

Acknowledgements

This research was supported by the Austrian Science Foundation Grants 16185 (to W.W. S.), # 15008 (to G.A.) and # 17516 (to D.B.). We thank Irene Goesler for preparing HRV2 samples.

References

(1) Toonen, R. F. G.; Verhage, M. *Trends Cell Biol.* **2003**, *13*, 177-185.
(2) Lisby, M.; Rothstein, R. *Curr. Opin. Cell Biol.* **2004**, *16*, 328-334.
(3) Allemann, R. K.; Egli, M. *Chem. Biol.* **1997**, *4*, 643-650.
(4) Dahlbäck, B. *Lancet* **2000**, *355*, 1627-1632.
(5) Marianayagam, N. J.; Sunde, M.; Matthews, J. M. *Trends Biochem. Sci.* **2004**, *29*, 618-625.
(6) Schreiber, G. *Curr Opin. Struct. Biol.* **2002**, *12*, 41-47.
(7) Ruotolo, B. T.; Giles, K.; Campuzano, I.; Sandercock, A. M.; Bateman, R. H.; Robinson, C. V. *Science Reports* **2005**, *310*, 1658-1660.
(8) Zehl, M.; Allmaier, G. *Anal. Chem.* **2005**, *77*, 103-110.
(9) Tao, Y.; Zhang, W. *Curr. Opin. Struct. Biol.* **2000**, *10*, 616-622.
(10) Yang, Y.; Wang, H.; Erie, D. A. *Methods* **2003**, *29*, 175-187.
(11) Viani, M. B.; Pietrasanta, L. I.; Thompson, J. B.; Chand, A.; Gebeshuber, I. C.; Kindt, J. H.; Richter, M.; Hansma, H. G.; Hansma, P. K. *Nat. Struct. Biol.* **2000**, *7*, 644-647.
(12) Kremser, L.; Blaas, D.; Kenndler, E. *Electrophoresis* **2004**, *25*, 2282-2291.
(13) Lykmeda, J. *Fundamentals of Interface and Colloid Science*; Academic Press: San Diego, 1995.
(14) Grossman, P. D.; Soane, D. S. *Anal. Chem.* **1990**, *62*, 1592-1596.
(15) Konecsni, T.; Kremser, L.; Snyers, L.; Rankl, C.; Kilár, F.; Kenndler, E.; Blaas, D. *FEBS Lett.* **2004**, *568*, 99-104.
(16) Gross, J.; Strupat, K. *Trends Anal. Chem.* **1998**, *17*, 470-484.
(17) Heck, A. J. R.; Heuvel, R. H. H. v. d. *Mass Spectrom. Rev.* **2004**, *23*, 368-389.
(18) Moniatte, M.; C. Lesieur; Vecsey-Semjen, B.; Buckley, J. T.; Pattus, F.; van der Goot, F. G.; van Dorsselaer, G. *Int. J. Mass Spectrom. Ion Process.* **1997**, *169/170*, 179-199.
(19) Veenstra, T. D. *Biophys. Chem.* **1999**, *79*, 63-79.
(20) Loo, J. A. *Int. J. Mass Spectrom.* **2000**, *200*, 175-186.
(21) Thomas, J. J.; Bothner, B.; Traina, J.; Benner, W. H.; Siuzdak, G. *Spectroscopy* **2004**, *18*, 31-36.
(22) Liu, B. Y. H.; Pui, D. Y. H. *J. Colloid Interface Sci.* **1974**, *74*, 155-171.
(23) Hogan, C. J.; Kettleson, E. M.; Ramaswami, B.; Chen, D.-R.; Biswas, P. *Anal. Chem.* **2006**, *28*, 844-852.
(24) Bacher, G.; Szymanski, W. W.; Kaufman, S. L.; Zöllner, P.; Blaas, D.; Allmaier, G. *J. Mass Spectrom.* **2001**, *36*, 1038-1052.
(25) Wick, C. H.; McCubbin, P. E. *Toxicol. Meth.* **1999**, *9*, 245-252.
(26) Loo, J. A.; Berhane, B.; Kaddis, C. S.; Wooding, K. M.; Xie, Y.; Kaufman, S. L.; Chernushevich, I. V. *J. Am. Soc. Mass Spectrom.* **2005**, *16*, 998-1008.
(27) Hewat, E. A.; Blaas, D. *The EMBO Journal* **1996**, *15*, 1515-1523.
(28) Tormo, J.; Fita, I.; Kanzler, O.; Blaas, D. *J. Biol. Chem.* **1990**, *265*, 16799-16800.
(29) Verdaguer, N.; Blaas, D.; Fita, I. *J.Mol. Biol.* **2000**, *300*, 1179-1164.
(30) Okun, V. M.; Ronacher, B.; Blaas, D.; Kenndler, E. *Anal. Chem.* **2000**, *72*, 4634-4639.
(31) Okun, V. M.; Moser, R.; Ronacher, B.; Kendler, E.; Blaas, D. *J. Biol. Chem.* **2001**, *276*, 1157-1062.
(32) Okun, V. M.; Moser, R.; Blaas, D.; Kenndler, E. *Anal. Chem.* **2001**, *73*, 3900-3906.

(33) Reischl, G. P.; Makela, J. M.; Karch, R.; Necid, J. *J. Aerosol Sci.* **1996**, *27*, 931-949.
(34) Tormo, J.; Stadler, E.; Skern, T.; Auer, H.; Kanzler, O.; Betzel, C.; Blaas, D.; Fita, I. *Protein Sci.* **1992**, *1*, 1154-1161.
(35) Tormo, J.; Centeno, N. B.; Fontana, E.; Bubendorfer, T.; Fita, I.; Blaas, D. *Protein Struct. Funct. Genet.* **1995**, *23*.
(36) Verdaguer, N.; Mateu, M. G.; Bravo, J.; Tormo, J.; Giralt, E.; Andreu, D.; Domingo, E.; Fita, I. *Protein Struct. Funct. Genet.* **1994**, *18*, 201-203.
(37) Tormo, J.; Blaas, D.; Parry, N. R.; Rowlands, D.; Stuart, D.; Fita, I. *The EMBO Journal* **1994**, *13*, 2247-2256.
(38) Holm, K. L.; Noble-Harvey, J. *J. Virol.* **1973**, *12*, 819-826.
(39) Korant, B. D.; Lonberg-Holm, K.; Noble, J.; Stasny, J. T. *Virology* **1972**, *48*, 71-86.
(40) Hewat, E. A.; Neumann, E.; Blaas, D. *Mol. Cell* **2002**, *10*, 317-326.
(41) Skern, T.; Neubauer, C.; Frasel, L.; Grundler, P.; Sommergruber, W.; Zorn, M.; Kuechler, E.; Blaas, D. *J. Gen. Virol.* **1987**, *62*, 315-323.
(42) Hofer, F.; Grünberger, M.; Kowalski, H.; Machat, H.; Hüttinger, M.; Küchler, E.; Blaas, D. *Proc. Natl. Acad. Sci.* **1994**, *91*, 1839-1842.
(43) Marlovits, T. C.; Abrahamsberg, C.; Blaas, D. *J. Virol.* **1998**, *72*, 10246-10250.
(44) Moser, R.; Snyers, L.; Wruss, J.; Angulo, J.; Peters, H.; Peters, T.; Blaas, D. *Virology* **2005**, *338*, 259-269.
(45) Neumann, E.; Moser, R.; Snyers, L.; Blaas, D.; Hewat, E. A. *J. Virol.* **2003**, *77*.
(46) Hewat, E. A.; Neumann, E.; Conway, J. F.; Moser, R.; Ronacher, B.; Marlovits, T. C.; Blaas, D. *The EMBO Journal* **2000**, *19*, 6317-6325.
(47) Verdaguer, N.; Fita, I.; Reithmayer, M.; Moser, R.; Blaas, D. *Nat. Struct. Biol.* **2004**, *11*, 429-434.
(48) Lall, A. A.; Friedlander, S. K. *J. Aerosol Sci.* **2006**, *37*, 260-271.

Nanoletters for submission (2007)

7. Characterization and selective sampling of nano-sized airborne particles with the parallel differential mobility analyzer (PDMA) and comparison with transmission electron microscopy (TEM)

Christian Laschober[1,2], Georg P. Reischl[1], Paul Messner[3] Günter Allmaier[2] and Wladyslaw W. Szymanski*[1]*

*Corresponding Authors

University of Vienna, Faculty of Physics, Boltzmanngasse 5, A-1090 Vienna

e9727028@stud3.tuwien.ac.at, wladyslaw.szymanski@univie.ac.at

[1] University of Vienna, Faculty of Physics

[2] Vienna University of Technology, Institute of Chemical Technology and Analytics

[3] University of Natural Resources and Applied Life Sciences, Vienna, Center for Nanobiotechnology

TABLE OF CONTENTS GRAPHIC:

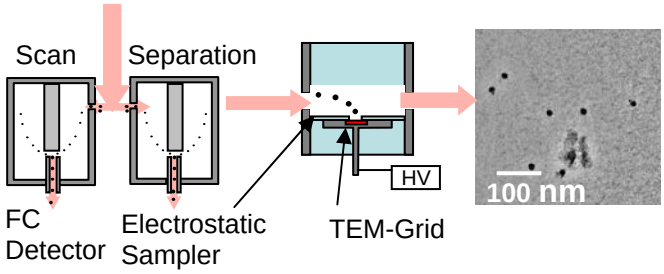

ABSTRACT:

Characterization of nanosized materials gains relevance due to the growing importance of nanoscience and nanotechnology. We present results obtained with a Parallel-Differential-Mobility-Analyzer (PDMA), a device that provides means for real-time characterization and selective enrichment of airborne nanoparticles in a size range between 1 and 100 nm. To verify the performance of the PDMA, silica nanoparticles were size classified and collected. Subsequent transmission-electron-microscopy confirmed the feasibility of the PDMA as nano-particle characterisation and enrichment tool.

MANUSCRIPT TEXT

Differential mobility analysis (DMA) is a method to classify sizes of airborne particles under ambient pressure conditions according to their electrical mobility diameter. This method was initially designed to characterize aerosol in the micrometer and submicrometer size range[1]. In the recent decade various designs of mobility analyzers were developed and adapted to extend this method into the single digit nanometer range[2-6]. It has been recently demonstrated that the working range of theses new analyzers matches with the kDA to high MDA mass range[7-9] . This technique, combined with a soft method for aerosol generation from solution, such as nano-Electrospray[10-13], has been utilized for the characterization of proteins[7], protein complexes[7,14], DNA [15], polymers[8,16,17], bacteriophages[18], viruses and virus fragments[7,19] and inorganic particles[20] according to their size.

In above mentioned investigations, the size analysis –in a way somewhat similar to mass spectrometry- has allowed to draw conclusions about the abundance of protein complexes and agglomerates in the analyzed solution, the polydispersity of particles and polymers, the degradation of viruses as well as the determination of the molecular mass of high molecular mass components with proper calibration. However, in these examples all characterized nanoparticles were generated from components of known origin and composition. When completely unknown components appear in the size spectrum, or when aerosols of unknown composition are analyzed, size spectra from a differential mobility analyzer (DMA) alone are frequently insufficient for satisfactory analysis and data interpretation. As one substantial feature of DMAs when compared to mass spectrometry is that are operated under ambient pressure the investigated aerosols are intact after sizing which opens a specific opportunity for the DMA technique.

Based on this rationale, a PDMA (Fig. 7.1) was designed enabling simultaneous recording of the size distribution of particles in question and selection of a specific size fraction for further purposes.

Here we discuss the controlled generation of an aerosol from suspended inorganic silica particles of disperse diameters and their application on the PDMA. Different size fractions should be selected for sampling on a microscopic target suited for transmission electron microscopy (TEM). The TEM based size analysis of the silica stock solution and the sampled size fractions are used as quality criterion for the performance of the PDMA. Reasons for using nanosized silica particles for the investigation of the PDMA features were their availability in different sizes making them an ideal test example in the group of inorganic nanosized particles whose importance as support substrate for biochemical, catalytical and commercial applications is growing rapidly[21-23].

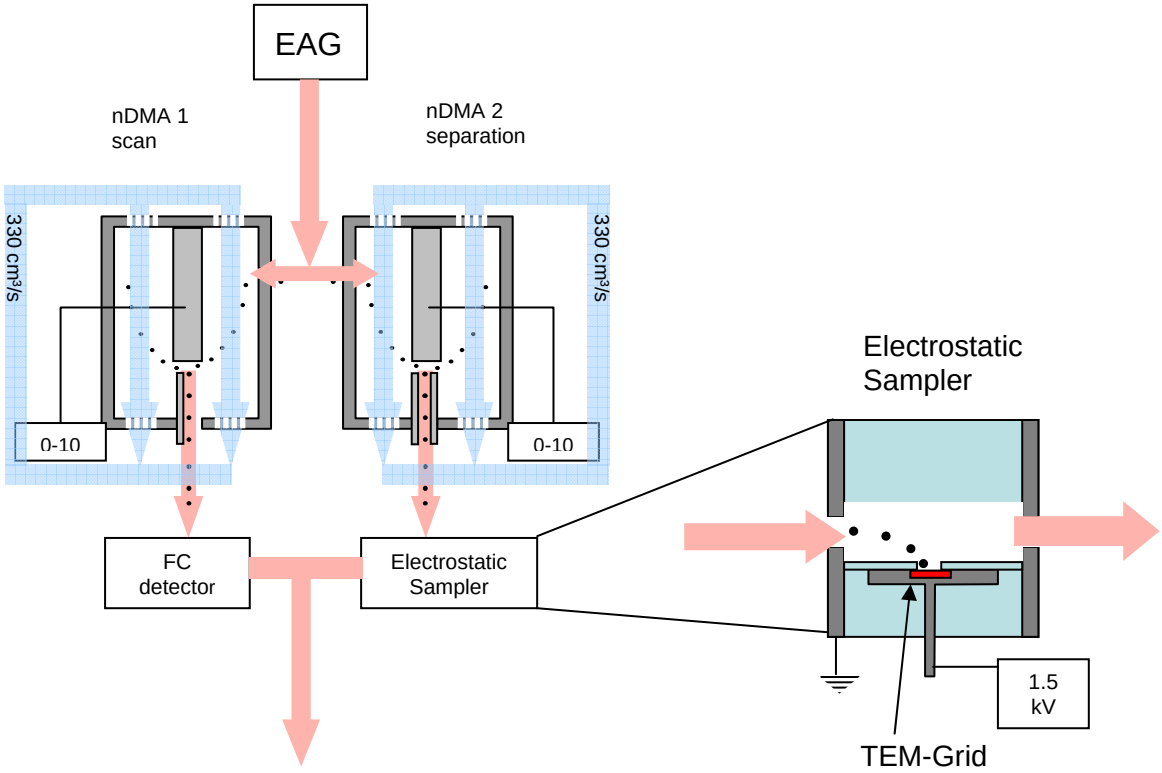

Fig. 7.1 Scheme of the experimental setup

From commercial available highly concentrated silica particle suspensions, dilute solutions (20-100 µg/mL) in a 20 mM ammonium acetate buffer were prepared. By electrospraying[11,12] of this solutions with an electrospray aerosol generator (EAG, TSI Inc.) in a stable cone-jet mode[24,25], controlled generation of silica nano-aerosols was achieved. The EAG generates highly charged droplets, which are then subsequently dried and exposed to a bipolar ion environment produced by a Po^{210} α-radiation source. This process results in charge conditioned nano-particles with neutral and mainly singly negatively and positively charge [26-28]. Following the charge conditioning process, the particles enter the PDMA, where they move on trajectories determined by laminar sheath air flow and the electric field defined by the applied voltage (Fig. 7.1). Due to unique relationship between applied voltage and particle size for singly charged particles, scanning of the voltage in combination with a particle detector delivers size distribution of the nanoparticles in question[29,30].

The PDMA system described here is combined with an electrical aerosol detection device working on the Faraday cup principle[4]. Parallel with the scanning nDMA 1 which scans and delivers the size spectrum of the investigated particles, an identical separation unit nDMA 2 is in operation at one given voltage setting and used for sampling or enrichment of the selected size class of nano-particles, hence the acronym PDMA[31]. The most recent engineering solutions extended the lower detection limit of the PDMA system even below 1 nm in terms of the electrical mobility diameter. The prerequisite for this detection method is the necessity of a certain minimum number of charged particles (concentration) needed to achieve measurable electrical signal. The detection limit of this system is currently in the order of 10^2 charged particles per cm^3.

For sampling of a selected size fraction, an electrostatic sampler (Fig. 7.1) was designed. A high voltage source is imbedded into the insulating bottom of the electrostatic sampler and electrically connected with a TEM support grid. The HV polarity between the housing and the TEM support grid was matched to the polarity of the central electrode of the PDMA to achieve deflection of the oppositely charged particles perpendicular to the aerosol flow in direction of the TEM-grid. Sampling was performed within 30 minutes for all presented experiments. After sampling, the diameter of about 100 particles per analyzed particle fraction (stock solution and the two selected size fractions) was determined with a TEM in order to calculate their size distribution.

Image analysis of the silica particles suspended in the stock solution (Fig.7.3a) and the DMA size spectrum of the produced aerosol, which contains the whole population of the silica particles from this solution (Fig.7.2) show very satisfactory agreement of measured size distributions. From this original aerosol, two size fractions centered at 14.5 and 20.7 nm were selected with the PDMA and subsequently collected with the electrostatic sampler on a TEM grid.

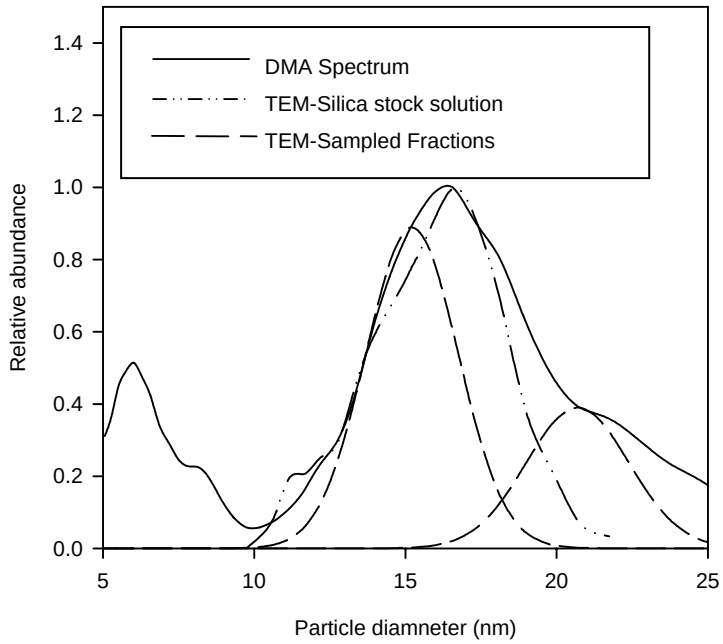

Fig. 7.2 Size spectra derived from TEM images of the stock solution and obtained with the PDMA

Comparison between the selected particle size (with nDMA2) and the size derived from TEM pictures show a difference of 0.7 nm in case of the smaller size fraction (Tab. 7.1). Examining the TEM picture of the 20.7 nm size fraction, a qualitative difference to the smaller size fraction can be noticed. In this size fraction, not only singular silica particles, but also deposited cluster particles consisting of two attached silica particles of smaller size can be found. The TEM-derived average diameter of the single particles is practically identical with the in the PDMA selected diameter.

The relative standard deviation of the in the TEM image observed particle diameter of the selected size fraction was about 15 % for both cases. This observed distribution width is caused on one hand by the resolution of the PDMA separation itself, which is determined by the ratio between sheath flow and aerosol flow through the mobility analyzer (Fig. 1; 10% in this case) and by additional broadening due to particle diffusion inside the DMA[3,4,32,33], which cannot be neglected for nano-aerosols, and on the other hand by an added uncertainty in the determination of the particle diameters in the TEM image analysis caused by fading contrast at the edges.

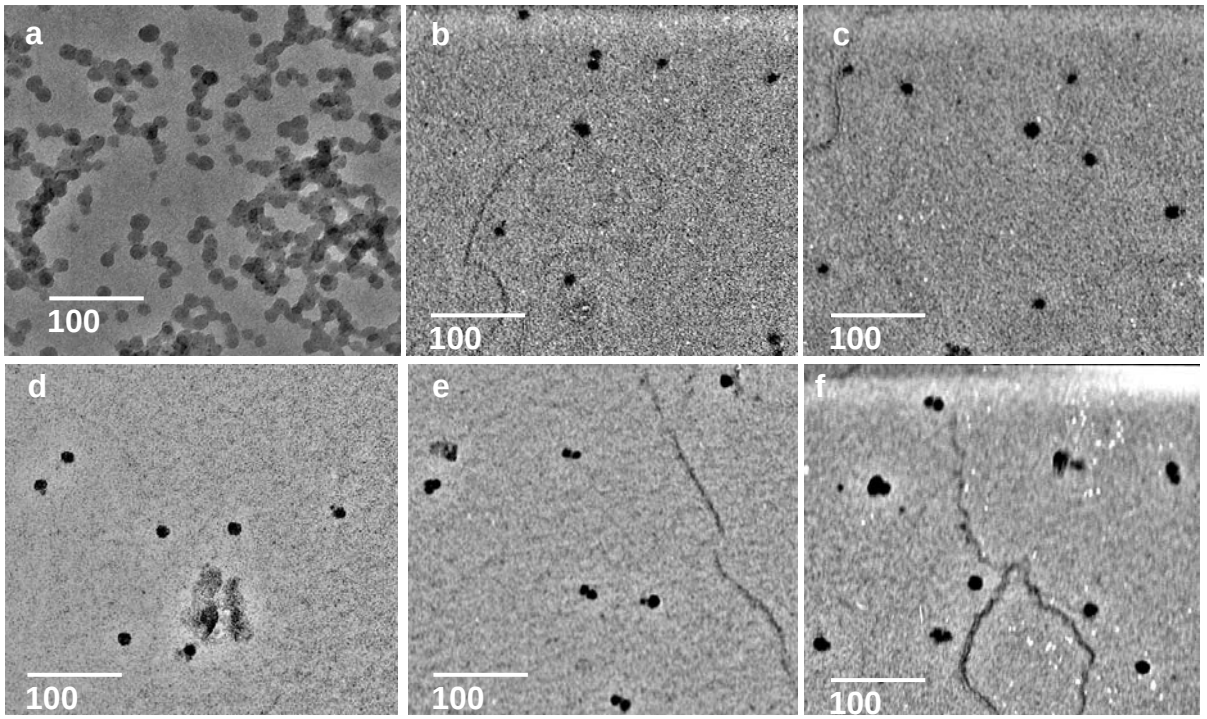

Fig. 7.3 Silica particle images, 400x400 nm
a: stock solution; b,c: 14.5 nm sampled fraction; d,e,f: 20.7 nm sampled fraction

The question arises how to address the particles consisting of two attached silica spheres (dimers). The DMA sizes particles according to the average electric mobility diameter, which is only equal to a geometric diameter in case of spherical particles. For the non-spherical dimer particles, two different diameters were calculated: the volume equivalent diameter (Diameter of a sphere of identical volume, ($D_V = \sqrt[3]{D_1^3 + D_2^3}$) and the area equivalent diameter (Diameter of a sphere with identical cross-sectional area, $D_A = \sqrt[2]{D_1^2 + D_2^2}$), and compared to the selected diameter during the sampling process.

As can be seen in Tab.7.1, the area equivalent diameter matches well the diameter of the selected size (D_P=20.7 nm), thus suggesting that non-spherical particles possess a certain non-stochastic orientation during the mobility analysis inside the PDMA. Otherwise, with free rotation of the dimer particles during mobility analysis, non-spherical particles would have been classified according to their average diameter rotated in all three directions in space, which would be likely the diameter of a sphere with corresponding volume.

Selected D_P nDMA2	Single Particle D_P	Dimer D_V	Dimer D_A
nm			
14.5	15.2 ± 2.0	-	-
20.7	20.7 ±2.9	18.2 ±1.7	20.3 ± 1.9

Tab. 7.1 PDMA-Selected diameters and from TEM image analysis derived diameters of silica particle fractions

D_V… Volume equivalent diameter
D_A…Area equivalent diameter

The presented experiments results show the feasibility of the PDMA system because it allows to parallel analyze the size distribution of a airborne nano-particles, and to select a specific nano-particle fraction for subsequent analytical purposes. The use of the electrostatic sampler also provides a possibility of visual analysis to gain insights into mobility issues of nano-particles. For the spherical singular silica particles the selected mobility diameter was identical with the geometrical diameter determined with TEM. For aggregates of two silica particles, the selected mobility diameter was nearly identical with the area equivalent diameter, indicating a preferential orientation of non-spherical particles during the mobility analysis. It is evident, that the PDMA with subsequent sampling system is a simple and reliable tool for the characterization, manipulation and enrichment of nanoparticles.

SUPPORTING INFORMATION

The silica nanoparticles used for preparation of the test aerosol, are commercially available in a 40% w/w 1% NaOH solution (Sigma-Aldrich; Ludox® HS-40 colloidal silica). This stock solution was diluted 1/1000 in a 20 mM ammonium acetate (Sigma Aldrich, p.a. grade) buffer solution adjusted to a pH value of 9, to ensure a negative charge of these particles in solution and to prevent these particles from aggregation. This has proven to provide stable particle generation with the EAG (TSI Mod. 3480).

For the solvent system used for this analytes, and this device we found that a stable cone-jet mode[24,25] operation was obtained at 2 kV and 0.3 L/min CO_2 (99.995%, Air Liquide N)/1L/min compressed air (99.999% synthetic air, Air Liquide). A pressure difference of 4 psi between sample and spray chamber was applied, which resulted in a sample solution flow of 67 nL/min through the fused silica capillary (25 µm inner diameter and 160 µm outer diameter, uncoated). The settings of the EAG, buffer concentrations, and solution conductivity were identical for all presented experiments. The primary generated droplet size, which is determined by the conductivity of the solvent system and the sample flow through the capillary as well as the inner diameter of the capillary was 150 nm, corresponding to a flow of 2×10^{11} droplets per minute or about 1.7×10^{8} droplets per cm^3.

The dimension of the TEM-support grid was 3mm in diameter, with a copper mesh grid base and a 20nm carbon film on top (Bal-Tec Inc. –No. S160). The high voltage (HV) applied to the electrostatic sampler was operated with +1.5kV.

Silica particles fractions were investigated in a Philips CM12 electron microscope (Philips, Eindhoven, The Netherlands). Silica particles generate enough contrast by themselves for TEM measurements, so no contrast enhancement through staining with uranyl acetate was required. All TEM pictures were contrast and brightness optimized for subsequent analysis.

References

(1) Liu, B. Y. H.; Pui, D. Y. H. *J. Colloid Interface Sci.* **1974**, *74*, 155-171.
(2) Chen, D.-R.; Pui, D. Y. H.; Hummes, D.; Fissan, H.; Quant, F. R.; Sem, G. J. *J. Aerosol Sci.* **1998**, *29*, 497-509.
(3) de la Mora, J. F. *Trends Anal. Chem.* **1998**, *17*, 328-339.
(4) Reischl, G. P.; Makela, J. M.; Necid, J. *Aerosol Sci. Technol.* **1997**, *27*, 651-672.
(5) Zhang, S.-H.; Flagan, R. C. *J. Aerosol Sci.* **1996**, *27*, 1179-1200.
(6) Fissan, H.; Pöcher, A.; Neumann, S.; Boulaudc, D.; Pourprix, M. *J. Aerosol Sci.* **1998**, *29*, 289-293.
(7) Bacher, G.; Szymanski, W. W.; Kaufman, S. L.; Zöllner, P.; Blaas, D.; Allmaier, G. .*J Mass Spectrom.* **2001**, *36*, 1038-1052.
(8) Saucy, D. A.; Ude, S.; Lenggoro, I. W.; de la Mora, J. F. *Anal. Chem.* **2004**, *76*, 1045-1053.
(9) Ku, B. K.; de la Mora, J. F. *Anal. Chem.* **2004**, *76*, 814-822.
(10) Veenstra, T. D. *Biophys. J.* **1999**, *79*, 63-79.
(11) Wilm, M.; Mann, M. *Anal. Chem.* **1996**, *68*, 1-8.
(12) Juraschek, R.; Dülcks, T.; Karas, M. *J. Am. Soc. Mass Spectrom.* **1999**, *10*, 300-308.
(13) Schmidt, A.; Kras, M. *J. Am. Soc. Mass Spectrom.* **2003**, *14*, 492-500.
(14) Loo, J. A.; Berhane, B.; Kaddis, C. S.; Wooding, K. M.; Xie, Y.; Kaufman, S. L.; Chernushevich, I. V. *J. Am. Soc. Mass Spectrom.* **2005**, *16*, 998-1008.
(15) Mouradian, S.; Skogen, J. W.; Dorman, F. D.; Zarrin, F.; Kaufman, S. L.; Smith, L. M. *Anal. Chem.* **1997**, *69*, 919-925.
(16) In *http://www.tsi.com/documents/CHEMC-006-Water-solublePEGPolymer.pdf*; TSI Inc.: Minneapolis, MN.
(17) In *http://www.tsi.com/appnotes/images/gemma-starburst.gif*; TSI Inc.: Minneapolis, MN.
(18) Wick, C. H.; McCubbin, P. E. *Toxicol. Meth.* **1999**, *9*, 245-252.
(19) Hogan, C. J.; Kettleson, E. M.; Ramaswami, B.; Chen, D.-R.; Biswas, P. *Anal. Chem.* **2006**, *28*, 844-852.
(20) Laschober, C.; Kaufman, S. L.; Reischl, G.; Allmaier, G.; Szymanski, W. W. *J. Nanosci. Nanotechn.* **2006**, *6*, 1474-1481.
(21) Salata, O. V. *J. Nanobiotechn.* **2004**, *2*.
(22) Mazzola, L. *Nature Biotechnology* **2003**, *21*, 1137-1143.
(23) Luther, W. *Future technology* **2004**, *54*, 1-112.
(24) Cloupeau, M.; Prunet-Foch, B. *J. ELectrostat.* **1990**, *25*, 165-184.
(25) M. Cloupeau ; Prunet-Foch, B. *J. Electrostat.* **1989**, *22*, 135-159.
(26) Hussin, A., Scheibel, H. G., Backer, K. H., & Porstendorfer, J. *J. Aerosol Sci.* **1983**, *14*, 671-677.
(27) Reischl, G. P.; Makela, J. M.; Karch, R.; Necid, J. *J. Aerosol Sci.* **1996**, *27*, 931-949.
(28) Fuchs, N. A. *Geofis. Pura Appl* **1963**, *56*, 185-193.
(29) Reischl, G. P. *Aerosol Sci. Technol.* **1991**, *14*, 5-24.
(30) Liu, B. Y. H.; Whitby, K. T.; Pui, D. Y. H. *APCAJ* **1974**, *24*, 1067-1072.
(31) Allmaier, G.; Laschober, C.; Reischl, G. P.; Szymanski, W. W.: Austrian pat. No A1327 (2005) pending.
(32) Stolzenburg, M. R.; University of Minnesota: Minneapolis, MN, 1988.
(33) Chen, D.-R.; Pui, D. Y. H. *J. Aerosol Sci.* **1997**, *28*, 985-1004.

Conclusions

Experiments performed within this PhD thesis made it possible to further optimize the ES-DMA method in terms of sensitivity, to determine stability and comparability of results of different DMA instruments, and to apply this method to analytical purposes specially suited for its unique features like high mass range (from KiloDa to MegaDa and up to GigaDa), preservation of non-covalent bonds and operation under atmospheric pressure.

A corona based charging device designed to replace the commonly used, radioactivity based bipolar diffusion chargers for the production of singly charged particles/molecules as required by differential mobility analysis (DMA) was implemented and characterized. Reason for the development of this corona-charger is the poor efficiency of these bipolar diffusion chargers, with a ~1% yield of singly charged particles in the nm size regime, as well as their limited lifetime and the fact that their working principle offers no possibility of controlling and further optimizing the charging process. The efficiency of the new corona based instrument in the production of singly charged particles was found to be 3-4 fold higher compared to a bipolar charger. Furthermore is the yield of these charged particles dependant on the specific operation parameters of the corona charger, which offers an additional way of controlling the charging process and thus leads to a possibility for a further optimization.

For investigation of stability and comparability of DMA within different instruments, identical protein samples in the size range between 3 and 15 nm were applied to several DMA systems. Results show high stability (0,1 % variation or pecision) of the measured diameter values within a series of size spectra with each DMA and confirms the ability of these instruments for the characterisation and analysis of nano-sized biological, inorganic and polymeric material. But the fact that all DMA systems even though operated under optimal and nearly identical working conditions showed consistently a sizing disagreement of up to 15%, indicates that not all parameters which influence the size analysis can be controlled (or are known) to a level at which differences between various DMAs would be below 5%.

Wherever these differences root – in the exact value of the of the sheath gas flow, in discrepancies between geometrical and effective separation length or in an not completely corrected time delay between setting of the DMA and particle detection – the result clearly lead to the conclusion that for qualitative analysis of nanoparticles, a harmonized calibration of such systems with size or mass standards is inevitable.

Polyamido-amine (PAMAM) dendrimers were investigated as possible calibrants, because they are commercially available, cover a size range from 3 to 15 nm (approx. moleculara weight of 1 MegaDa) and because of their theoretically uniformity. ES-DMA and MALDI mass spectrometric characterization of the PAMAM dendrimers was conducted to determine the uniformity of the different dendrimer generations. Results of the dendrimer diameters showed excellent agreement between DMA results and results from literature derived with atomic force microscopy, transmission electron microscopy (TEM), X-ray and neutron scattering. MALDI time-of-flight mass spectrometry revealed that the difference between measured and by ideal polymer growth predicted dendrimer molecular mass increased with increasing dendrimer generation, with 40% discrepancy in the values of obtained and theoretically calculated molecular mass for the largest dendrimer generation (n = 10). Calculation of the particle densities from experimental values resulted in constant values for dendrimers upon a certain size, suggesting that dense packing at the outer shells of the dendrimer particles prevents a full saturation of branching spots during synthesis and thus results in lower particle molecular masses than predicted by ideal dendrimer growth.

In another series of experiments it has been demonstrated, that it was possible to analyze intact rhinovirus-antibody complexes in the range of 8 to 12 MegaDa. Mass; a mass range that is not accessible to conventional state-of-the-art mass spectrometry. It was furthermore possible to calculate the average number of antibodies attached non-covalently to the virus from the observed size difference between the free virus particle and the virus particle saturated with attaching antibodies, resulting in a number of 28 ± 4 biospecific antibodies noncovalently bound to the virus particle. This value is practically identical with the theoretical number of 30, which is determined by virus symmetry and position of antibody binding sites.

As ES-DMA systems operate under atmospheric pressure and particles remain intact after analysis, this method offers also opportunity for micropreparative application like enrichment or sampling of virus particles or inorganic nanoparticles. For this reason a parallel-DMA (PDMA) and an electrostatic sampler were designed and constructed within this PhD thesis. Nanometer sized silica particles were in an experiment analyzed with the PDMA and a size fractions around 14.5 nm and 20.7 nm diameter were selected for sampling on a electronmicroscopic grid. TEM images of the sampled size fractions were analyzed and the so received size distribution of the sampled fractions compared to the particle size selected through PDMA settings. Particle sizes determined by TEM and selected in the PDMA showed excellent agreement and confirmed the feasibility of the PDMA setup for sampling and specific enrichment of nanometer sized particle.

Curriculum Vitae

Name:	**Christian Laschober**
Date of birth:	3.7.1979
Adress:	Neilreichgasse 20/9
	A-1100 Vienna
Nationality:	Austrian

Education :

15.10.2003	Start of the PhD Thesis on the analysis of Bio- and Nanoaerosols within a cooperation project between the Faculty of Phyics (Prof W.W. Szymanski, University of Vienna) and the Institute for Chemical Analysis and Technology (Prof. G. Allmaier, Vienna University of Technology)
16.5.2003	Master Degree in Technical Chemistry with distinction
June 2002- March 2003	Diploma Thesis „Palladuim- a possible tracer for traffic emissions“
2001-2003	Second section of the study with special focus on analytical chemistry
26.3.2001	Finish of the first study section with distinction
1.3.1998	Inscription at the Vienna University of Technology for the Study in Technical Chemistry
6.6.1997	Finishing Matura with distinction
1989-1997	Realymnasium Oberschützen (focus on physics and biology)
1985-1989	Elementary School Oberwart, Austria

Work Experience:

Oktober 2003 – June 2006	Project Assistent, Faculty of Physics, Prof. Szymanski, University of Vienna
July, August 2000	Neuber, Guntramsdorf, Red Bull Components
July 1999	Baxter Immuno AG, Production of Sterile Components
July 1998	Beiersdorfer Vienna,
1.7.1997-28.2.1998	Military service
July, August 1996	Kitchen, home for old people, Oberwart

Presentations and Publications:

2007	Publication	Submitted to *Macromolecules*	"Determination of molecular weight, particle size and density of high number generation PAMAM dendrimers using MALDI-TOF-MS and nES-GEMMA"
2007	Publication	Submitted to *Experimental Nanoscience*	"Comparison of the mobility analysis of globular proteins with different nano-differential mobility instruments (nDMAs)"
2006	Publication	Submitted to *Nanoletters*	"Characterization of nano-sized airborne particles and viruses with the parallel differential mobility analyzer (PDMA) and comparison with transmission electron microscopy (TEM)"
2006	Publication	Submitted to *Biotechniques*	"Gas Phase Electrophoretic Molecular Mobility Analysis of Size and Stoichiometry of Complexes of a Common Cold Virus with Antibodies"
8.11.& 13.11.2006	Oral Presentation	Seminar in Aerosol Physics, University of Vienna	„Investigation of Bio-and Nanoaeriosols- Highlight of a PhD Thesis"
10.6. 2006	Oral presentation	Annual meeting of the Austrian Society for Analytical Chemistry, Graz	„Charakterisierung von PAMAM (Poly(amido-amin)) Dendrimeren mit nESI GEMMA (Gas-Phase Electrophoretic Mobility Macromolecular Analyzer) und MALDI (Matrix-Assisted Laser Desorption Ionisation) Linear-flugzeitmassenspektrometrie"

2006	Publication	*Journal of nanoscience and nanotechnology* 6(5), 1474-81	"Comparison between an unipolar corona charger and a polonium-based bipolar neutralizer for the analysis of nanosized particles and biopolymers"
29.5. 2006	Poster	54th Annual Conference of the ASMS, Seattle, WA, US	"Nano-ESI Gas-phase Electrophoretic Mobility Analysis (GEMMA) of an Intact Specific Human Rhinovirus (HRV)-Monoclonal Antibody (mAB) Complex "
2005	Oral presentation	Seminar „modern Analytical Chemistry" Vienna University of Technology	" Nano-ESI-GEMMA: Instrumentation and new applications"
16.11.2005	Oral presentation	Seminar in Aerosolphysics University of Vienna	"Investigation of Bio- and Nanoaerosols"
10.5. 05	Oral presentation	Seminar in Aerosolphysics University of Vienna	" Calibration of nDMAs"
2004	Accepted Publication	*‚Atmospheric Environment* 38(14), 2187-2195	"Real world emissions of inorganic aerosol constituents in the Kaisermühlentunnel " -Accepted paper in Environemental science and Technology
7.9.2004	Poster	European Aerosol Conference, Budapest	"Comparison between corona and diffusion charging for nanosized biomolecules"-
2.6. 2004	Oral presentation	Seminar Aerosolphysics University of Vienna	"Analysis of Bio and Nanoaerosols"
17.6.2003	Oral Presentation	3rd Artefacta meeting TU München	„Determination of Palladium in airborne particulate matter"
5. 2003	Oral Presentation	Seminar „modern Analytical Chemistry" Vienna University of Technology	„Platin- a possible tracer for traffic emissions"
14.01.03	Oral Presentation	Seminar „Atmospheric Chemistry", Vienna University of Technology	„Platingruppenmetalle im urbanen Aerosol"

Skills and Competences:

foreign languages: English (skilled); French (basic knownledge),

EDV: MS-Office, MS-Windows, SigmaPlot, Origin, CorelDraw, Adobe Acrobat (skilled)

Instrumentation: GC-MS, LC-MS, differential mobility analysis, nano-electrospray, particle sampling, GF-AAS, BC/OC analysis (skilled); MALDI-MS, SIMS (medium knowledge)

Other: Scientific presentations, teaching (private lessons) in chemistry, physics and mathematics

References:

Univ-Prof. Dr. Wladyslaw .W. Szymanski,
University of Vienna,
wladyslaw.szymanski@univie.ac.at,
+43-1-4277-51109

Univ. Prof. Dr. Günter Allmaier
Vienna University of Technology
guenter.allmaier+e164@tuwien.ac.at
+43-1-58801-15160

Univ. Ass. Dr. Andreas Limbeck
Vienna University of Technology
andreas.limbeck+e164@tuwien.ac.at
+43-1-58801-15180